2015-01-01

Depositional Facies And Interpretation Of Salt-Sediment Interaction In The Lower Triassic Moenkopi Formation Adjacent To The Castle Valley Salt Wall, Paradox Basin, Utah

Ann Marie Foster

DEPOSITIONAL FACIES AND INTERPRETATION OF SALT-SEDIMENT INTERACTION IN THE LOWER TRIASSIC MOENKOPI FORMATION ADJACENT TO THE CASTLE VALLEY SALT WALL, PARADOX BASIN, UTAH

ANN M. FOSTER

Department of Geological Sciences

APPROVED:

Katherine Giles, Ph.D., Chair

Richard Langford, Ph.D.

Gregory Mack, Ph.D.

Charles Ambler, Ph.D.
Dean of the Graduate School

DEPOSITIONAL FACIES AND INTERPRETATION OF SALT-SEDIMENT INTERACTION IN THE LOWER TRIASSIC MOENKOPI FORMATION ADJACENT TO THE CASTLE VALLEY SALT WALL, PARADOX BASIN, UTAH

by

ANN M. FOSTER, B.S.

THESIS

Presented to the Faculty of the Graduate School of

The University of Texas at El Paso

in Partial Fulfillment

of the Requirements

for the Degree of

MASTER OF SCIENCE

Department of Geological Sciences

THE UNIVERSITY OF TEXAS AT EL PASO

May 2015

ACKNOWLEDGEMENTS

First, even though words of thanks are inadequate to express my gratitude, I would like to thank Kate Giles for not only taking on this project as I could not have been completed without her, but for her support and patience. I am also appreciative of support by Nila Matsler and Greg Mack. I would also like to thank the Department of Geological Sciences at UTEP for allowing the opportunity to complete this project.

Several instructors from Santa Barbara City College inspired my love for geology and I will be forever thankful for their enthusiasm, encouragement, support, quality instruction and friendship. They are Jan Schultz, Karl Halbach, Bob Gray, Jan Dependahl and Jeff Meyer. Additionally, I would like to thank instructors from Sonoma State University, Rolfe Erickson, Tom Anderson, Walt Venum and Matt James, for the excellent education that I received.

I would also like to thank those that assisted me in the field, Ron Foster, Darcey Hughes, Jesse Burrows and Kristel Lovelady, for willingly climbing up steep, crumbly slopes in all weather conditions, getting completely covered in red dirt and still speaking to me afterward!

My parents, Tom and Colby Kline, provided not only financial support through much of this project, they also provided much needed emotional support.

Lastly, I want to personally thank my husband Ron Foster for his unwavering love and support throughout this entire process. Without his encouragement I would have given up many times and I am grateful he helped to push me through the toughest times.

ABSTRACT

Stratigraphic, sedimentologic and compositional data collected from the Triassic Moenkopi Formation adjacent to the Castle Valley salt anticline, Paradox Basin, Utah indicate passive diapirism of the salt wall with well-developed topography and exposed salt during the Early Triassic. Moenkopi strata thin to 150m on to the Castle Valley salt anticline and thicken to an estimated 275m away from it, indicating control of sedimentation by salt-generated topography. The distribution of nine terrestrial facies assemblages within Moenkopi Formation strata on the margins of Castle Valley Salt Wall, in combination with identification of three halokinetic sequences interpreted from stratal architecture adjacent to the salt wall, further support this assertion.

Nine terrestrial facies were recognized within the Moenkopi Formation in the study area: 1) channel-form sandstone and organized conglomerate (axial fluvial), 2) thinly-interbedded siltstone and fine-grained sandstone (fluvial overbank), 3) tabular-lenticular siltstone and sandstone sheets (unconfined channels and sheet floods), 4) structureless to weakly-bedded sandstone (distal wadi fan), 5) disorganized conglomerate (debris flow from exposed diapir), 6) well-sorted, well-rounded sandstone (eolian sand sheets), 7) gypsic sandstone (eolian sand), 8) gypsic paleosols and 9) calcic paleosols .

The location and distribution of axial channel facies, in addition to paleocurrents that are generally parallel to the northwest trending long axis of the salt wall, suggest that large drainage systems were controlled by salt diapir topography. At the northwest termination of Castle Valley, the salt wall bends abruptly to the north, where paleocurrents also shifted to the north.

Local gypsum sheet sandstones and thin debris-flow beds containing reworked clasts of gypsum and carbonate “caprock” derived from the diapiric Paradox Formation of Pennsylvanian age provide evidence for significant topography and exposed evaporite during Moenkopi deposition. The salt diapir itself is therefore interpreted to have provided the sulfate source for both gypsic paleosols and gypsic sandstone sheets in the Moenkopi. The world's oldest documented gypsic paleosols are found in

overbank strata interbedded with high width/depth ratio sandstone bodies deposited by ephemeral rivers. In combination, these features indicate arid to semi-arid, wadi environments for the lower three Moenkopi Formation members (Tenderfoot, Ali Baba and Sewemup). The uppermost Pariott Member lacks gypsum and contains calcic paleosols, indicating a change to a semi-arid climate. This data in combination with facies differences between the uppermost member and the lower three members suggest that the Pariott Member should not be assigned to the Moenkopi Formation and should either be included in the Chinle Formation strata or reassigned to formation status.

Each member is characterized by distinct facies associations, facies-association distributions and stratal geometries. As such, each of the four members represents a stage of salt-sediment deposition with corresponding wedge and hook halokinetic sequences (HS) identified. The HS comprise three composite halokinetic sequences (CHS): a 1) northeast flank of wedge HS that build into a tapered CHS, 2) a western Red Hills series of wedge HS that build into a tapered CHS and 3) an eastern Red Hills series of hook HS that build into tabular CHS. Wedge HS indicate that sediment accumulation rates were greater than diapiric rise rates to the northeast and to the west-southwest of the salt wall. The hook HS on the east side of the weld, where abrupt facies changes occur and strata thickens away significantly, indicates the area experienced higher diapiric rise rate than sediment accumulation, most likely due to deflation related to a sharp bend in the salt wall.

TABLE OF CONTENTS

LIST OF TABLES

LIST OF FIGURES

Chapter 1

INTRODUCTION

Ever since John N. Newcomb's 1859 expedition (Newberry, 1861), excellent rock exposures within the Paradox Basin of southeast Utah and southwest Colorado have provided geologists with a window to the past and the pursuit of coal, uranium and petroleum in the basin has advanced the understanding of the geologic history of this province. A series of linear, northwest trending valleys cored by Paradox Formation evaporites within the northeast part of the basin are collectively referred to as the salt anticline region (SAR) (Fig. 1.1) (Prommel, 1923; Shoemaker and Newman, 1959; Stewart, 1969; Blakey and Gubitosa, 1984; Bromley, 1991; Doelling and Ross, 1998; Miall and Arush, 2001; Matthews et al., 2004; Trudgill et al., 2004). Strata within this area generally thin adjacent to salt anticlines and thicken away from them, indicating control of sedimentation by salt-generated topography during passive diapirism (Jones, 1959; Cater & Elston, 1963, Doelling and Ross, 1998; Lawton and Buck, 2006). Because of this relationship, this area provides an excellent opportunity to study salt-sediment interaction in a variety of depositional systems as a potential outcrop analog to petroleum-bearing salt basins such as the Gulf of Mexico and North Sea and for improving predictive models, especially sub-seismic scale facies-geometries and distribution. The well-exposed Triassic Moenkopi Formation within the SAR provides an excellent opportunity to understand the facies architecture, associated depositional environments and sub-seismic scale geometries of nonmarine strata deposited adjacent to passively rising salt walls.

This study documents depositional facies and sub-seismic scale stratal geometries within the terrestrial Triassic Moenkopi Formation flanking the Castle Valley salt wall. Results from this study show that the Castle Valley Salt Wall was passively rising during the early Triassic, created topographic relief that controlled the drainage pattern of Moenkopi Fluvial systems and provided a source of gypsum to surrounding sediments.

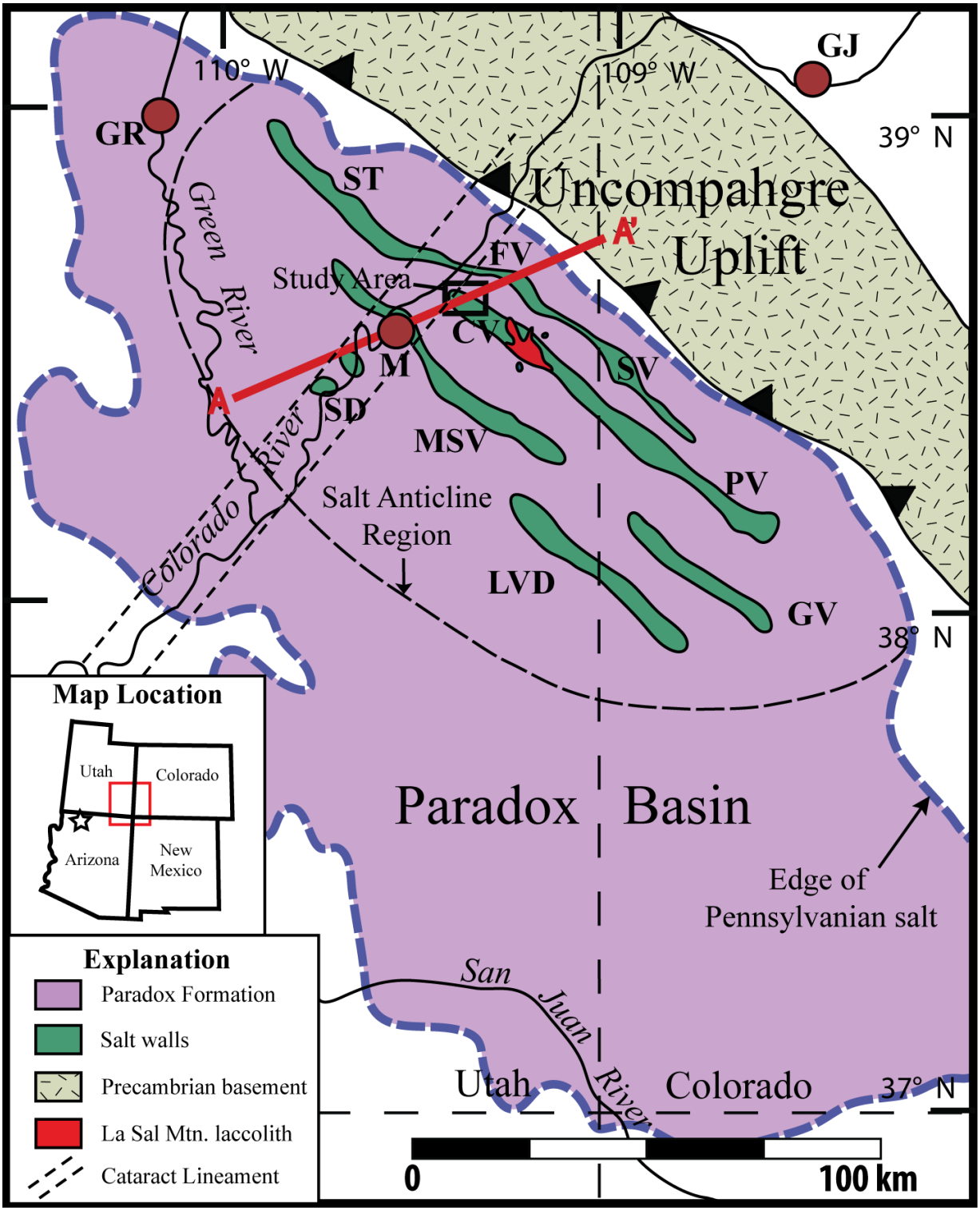

Figure 1.1: Location map of salt anticline province within the Paradox Basin. Salt walls: CV, Castle Valley; FV, Fisher Valley; GV, Gypsum Valley; LVD, Lisbon Valley-Dolores; MSV, Moab-Spanish Valley; PV, Paradox Valley; SD, Schafer Dome; ST, Salt Valley; Sinbad Valley. Communities near study area: M, Moab; GR, Green River; GJ, Grand Junction. Extent of salt is from Condon (1997); distribution of salt walls is after Shoemaker et al. (1958). Star in map location insert is Moenkopi Fm. type locality. Cataract Lineament from Stevenson and Baars (1986). Inset rectangle at northwest end of Castle Valley indicates study area. Red line A to A' is cross section of Figure 1.3.

1.1 Geologic Setting of the Paradox Basin

The Paradox Basin (Figs. 1.1 and 1.2) is an asymmetric intracratonic foreland basin (Kelley, 1958; Doelling, 1988) that formed during the Middle Pennsylvanian Ancestral Rocky Mountain (ARM) orogenic event as a flexural response to the tectonic loading by the basement-cored Uncompahgre uplift (White and Jacobson, 1983; Huntoon et al., 2002; Barbeau, 2003). The basin was originally interpreted as a pull-apart basin (Stevenson and Baars, 1986) and more recently as an intracontinental flexural basin (Barbeau, 2003). The basin subsided rapidly during Pennsylvanian time while being filled with ~ 2500m of cyclically deposited dolostone, evaporite and shale in the foredeep part of the basin and equivalent biohermal carbonates in the distal forebulge/backbulge margin of the basin (Fig. 1.2) (Hite, 1968; Peterson and Hite, 1969; Baars and Stevenson, 1981; Condon, 1997; Trudgill, 2010). These basin-fill units are collectively assigned to the Paradox Formation.

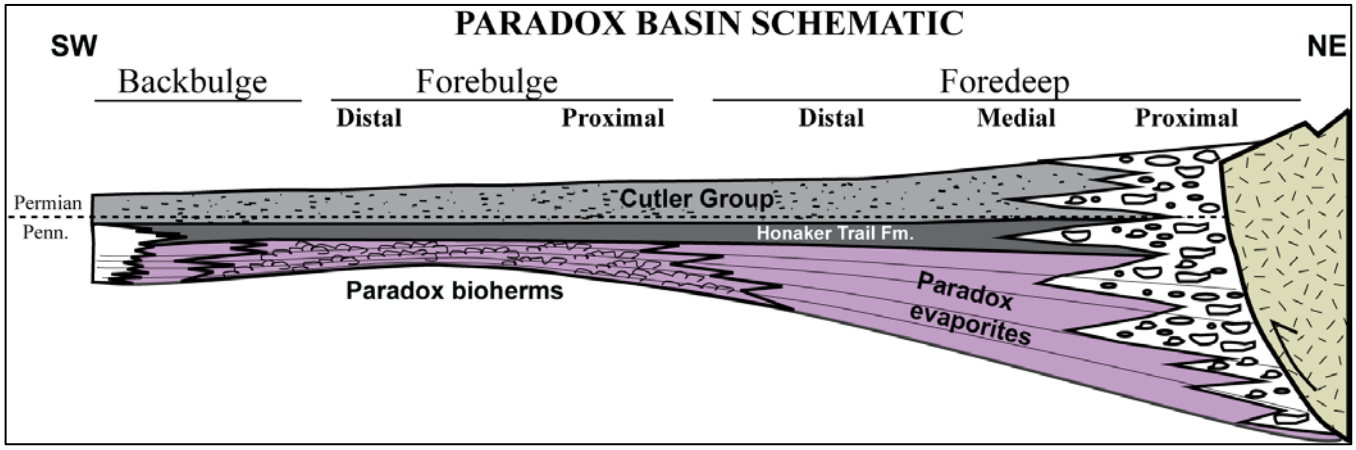

Figure 1.2: Pennsylvanian-Permian tripartite division of the Paradox Basin strata into foredeep, forebulge and backbulge. Modified from Barbeau (2003) and Trudgill and Paz (2009).

The geographic extent of Paradox Formation evaporitic facies are used to define the limits of the basin (Condon, 1997). Marine transgression of the basin resulted in deposition of interbedded marine limestone and sandstone of the Honaker Trail Formation. During the latest Pennsylvanian and Early Permian, a southwestward prograding alluvial wedge (Cutler Group) was shed from the Uncompahgre highlands (e.g. Mack and Rasmussen, 1984; Barbeau, 2003) and interfingered southwestward with the

evaporitic and marine facies of the Paradox and Honaker Trail formations in the proximal and medial parts of the basin (Fig. 1.2) (Barbeau, 2003; Trudgill and Paz, 2009). The clastic wedge generated differential loading of Paradox evaporite and is thought to have triggered diapiric rise of the underlying Paradox Formation evaporites (Trudgill and Paz, 2009).

Paradox salt diapirism formed a series of northwest-trending, elongate salt walls (Fig. 1.1) and salt pillows (Doelling et al., 2002; Trudgill et al., 2004, Trudgill 2010). The salt walls formed over northwest-trending basement faults that cut to the Mississippian level (Fig. 1.3) (Stevenson and Baars, 1986; Trudgill, 2010). The position and orientation of preexisting basement faults below several salt structures are interpreted to have controlled the location and NW-SE orientation of the salt walls (Case and Joesting, 1973; Szabo and Wengerd, 1975; Baars and Stevenson, 1981; Friedman et al., 1994; Trudgill, 2010). NE-SW trending basement faults partially controlled evaporite thickness and distribution, producing abrupt terminations of salt walls (Trudgill, 2010). Salt-withdrawal mini-basins developed adjacent to salt walls and subsequently influenced sediment dispersal and facies architecture with stratigraphic trends characterized by thinning and localized absence of units adjacent to salt

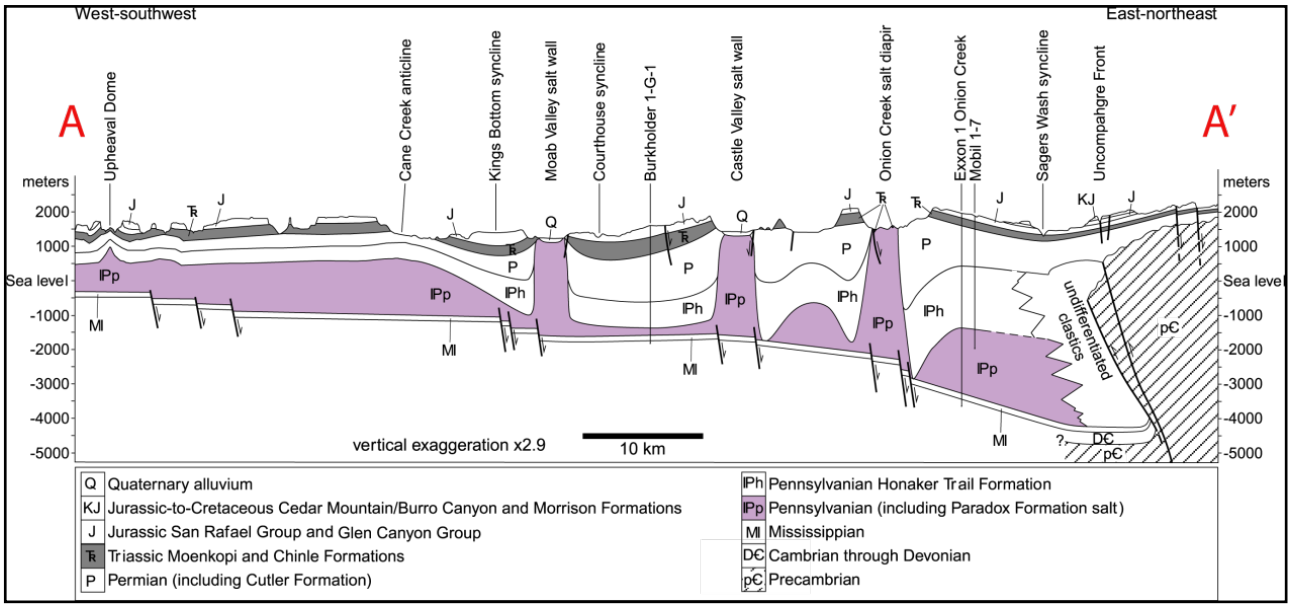

Figure 1.3: Regional structural cross-section of northeastern Paradox Basin showing positions of basement faults to major salt walls and generalized strata architecture adjacent to them. Modified from Trudgill (2004) and Mathews et al. (2007).

structures, depositional facies variations and pronounced local angular unconformities (Prommel, 1923; Shoemaker and Newman, 1959; Stewart, 1969; Stewart et al., 1972; Blakey and Gubitosa, 1984; Bromley, 1991; Hazel, 1994; Doelling and Ross, 1998; Miall and Arush, 2001; Doelling 2001; Doelling, 2002; Doelling et al., 2002; Matthews et al., 2004; Trudgill et al., 2004; Banbury, 2005; Lawton and Buck, 2006).

Passive diapirism progressed for at least 75 Ma, with greatest activity during Pennsylvanian-Triassic time while the Paradox Basin was a major locus of siliciclastic deposition (Bromly, 1991; Tyler and Etheridge, 1993; Huntoon et al., 2002). Minor diapiric activity lasted through the earliest Jurassic (Trudgill et al., 2004). The Jurassic Navajo Sandstone is the youngest strata to exhibit thinning over salt structures (Fig. 1.4) and marks the end of passive salt diapirism in the basin (Trudgill, 2010). The overlying Carmel Formation does not exhibit thinning and records the onset of deposition not influenced by local salt movement (Trudgill, 2010).

Salt structures were later slightly shortened during the Paleogene Laramide orogenic event (Grout and Verbeek, 1997; Trudgill et al., 2004). During Neogene uplift of the Colorado Plateau over 3 km of sediment was stripped from the northeastern Paradox Basin (Nuccio and Condon, 1996). Following erosion of overburden on the Colorado Plateau, the salt-cored structures that are restricted to the Paradox fold and fault belt physiographic province (Kelley, 1958; Doelling, 1988) experienced localized dissolution and collapse of overlying sediment (Jones, 1959; Doelling and Ross, 1998), exposing Pennsylvanian-Jurassic growth strata along the valley walls.

1.2 Moenkopi Formation Regional Stratigraphy

Ward (1901) applied the name “Moencopie beds” for strata exposed at the mouth of Moencopie Wash, located approximately two miles northwest of the present community of Cameron, Arizona (Fig. 1.1). Gregory (1916) revised the spelling to Moenkopi, and replaced the original type section with a more complete section of Moenkopi about five miles northwest of Cameron within the walls of the Little

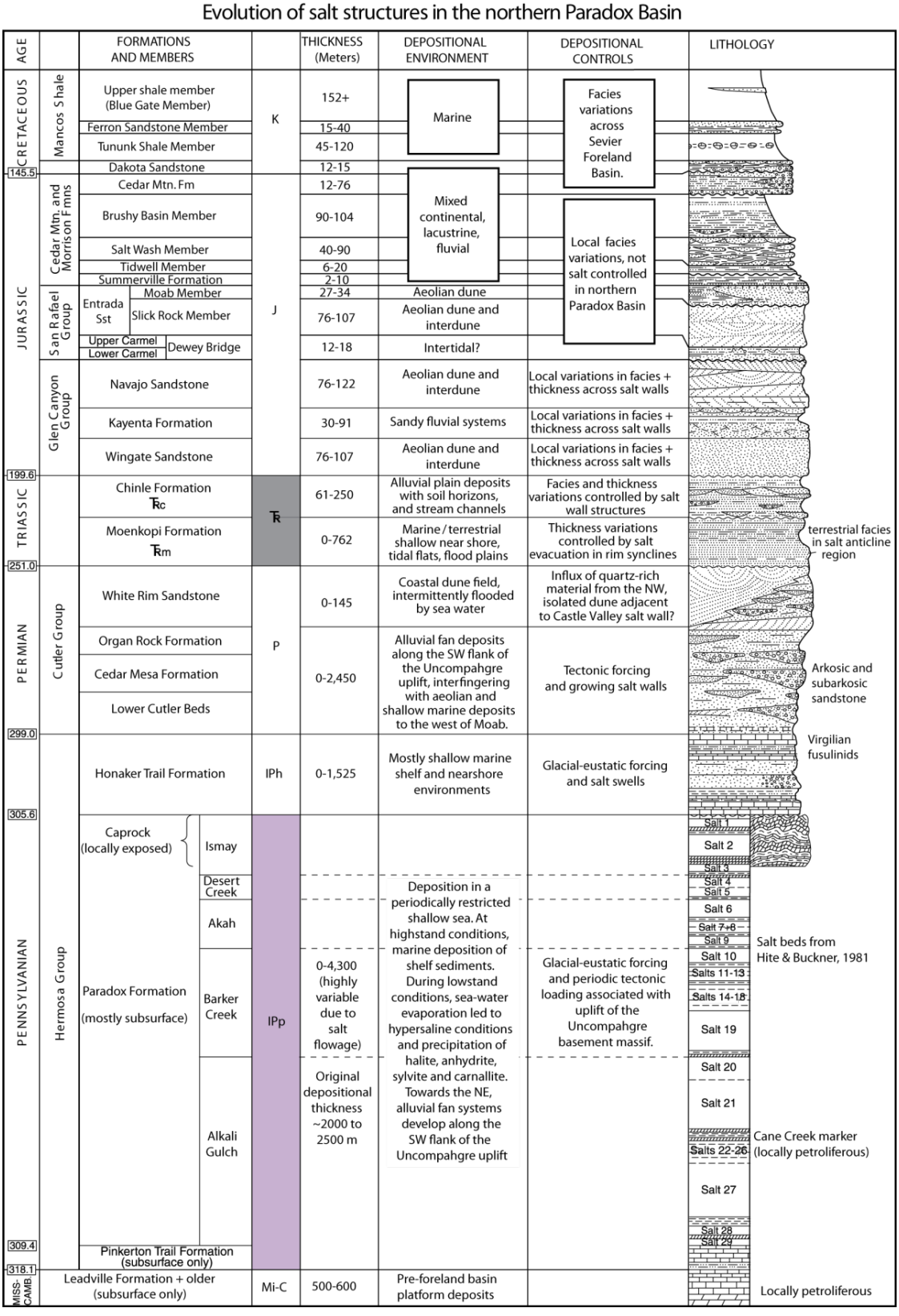

Figure 1.4: Stratigraphic column of northern Paradox Basin showing symbols and colors used in cross section A-A', ranges of thickness, depositional controls and lithology. Modified from Doelling (2001) and Trudgill (2010).

Colorado River Gorge (Gregory, 1917). Since then, many investigators have studied the deposition of this Lower to possibly Middle Triassic formation that crops out across much of the southwestern United States (e.g., Longwell et al., 1923; Baker et al., 1927; Baker and Reeside, 1929; Dane, 1935; Wengerd, 1950; McKee, 1954; Shoemaker and Newman, 1959; Cadigan, 1971;; Blakey, 1973; Molenaar, 1981). Baker et al. (1927), Dane (1935) and Shoemaker and Newman (1959) provided foundational studies and most recently work by Lawton and Buck (2006), Shock (2012) and Banham and Mountney (2013) have improved understanding of the Moenkopi Formation strata in the region with the aid of recent halokinetic models (Giles and Lawton, 2007; Giles and Rowan, 2012). The Moenkopi Formation thickens from a pinchout boundary near the modern Uncompahgre Plateau to over 700m in western Utah and eastern Nevada (Huntoon et al., 2002). In the northwestern part of the Paradox Basin, the Moenkopi Formation was deposited on Permian or older rocks along the Tr-1 unconformity and primarily represents a marine regression, consisting of over 215 m of mostly shallow marine and subordinate tidal and fluvial sediments (Fig. 1.5) (Blakey, 1974).

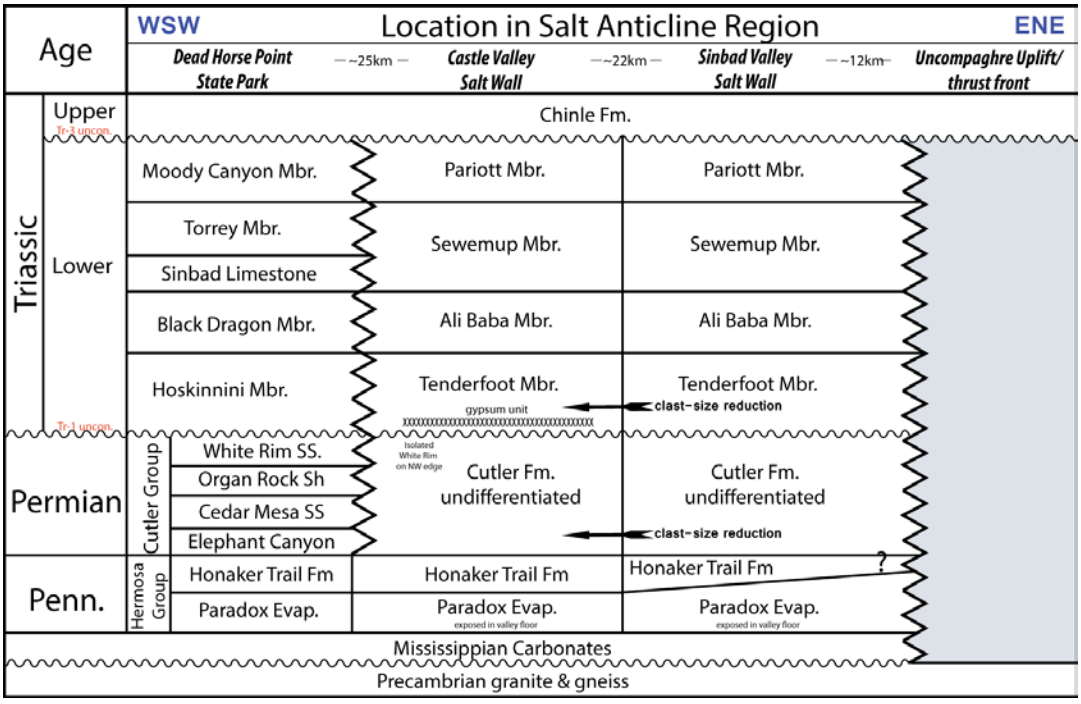

Figure 1.5: Generalized Moenkopi stratigraphic correlation chart within the Salt Anticline region. Stratigraphy compiled from Blakey (1974), Baars (2000), Barbeau (2003) and Lawton & Buck (2006). Not meant to be to scale.

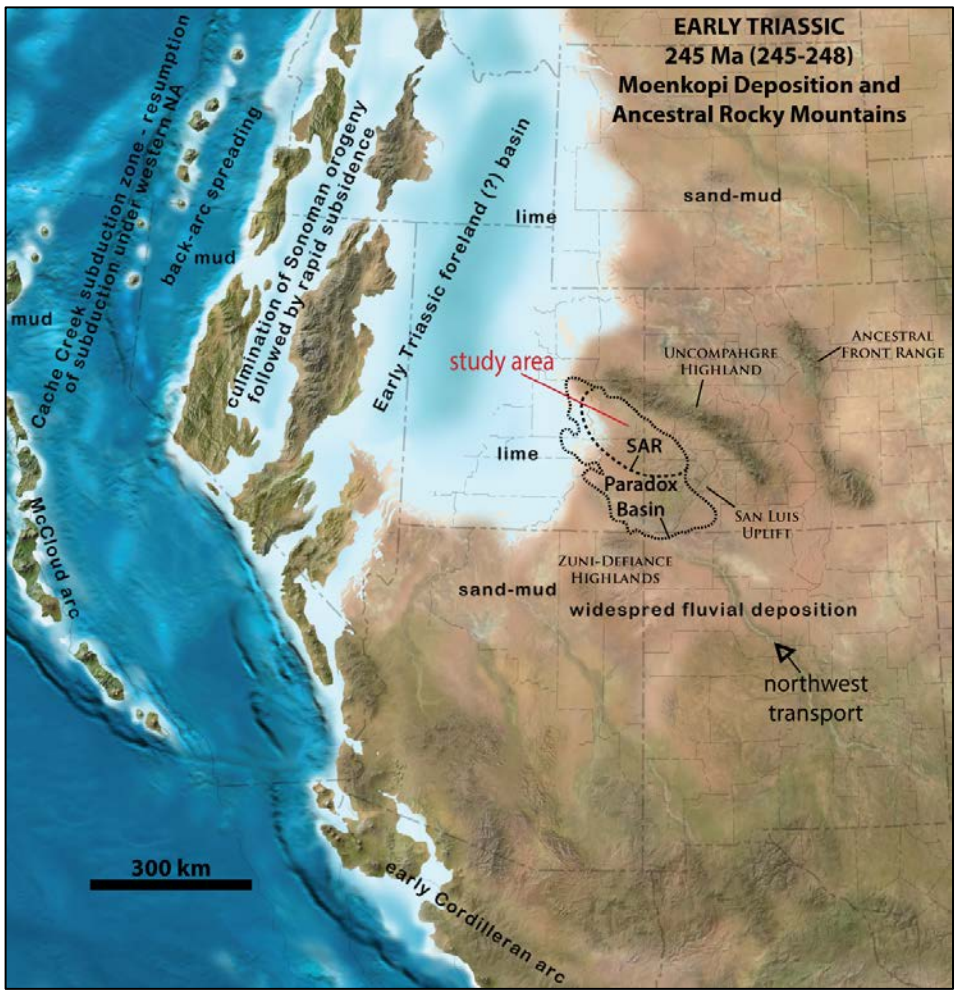

Figure 1.6: Paleogeographic map of the southwestern part of the United States during Early Triassic time. This interpretation shows the Salt Anticline Region (SAR) within the Paradox Basin, the Ancestral Rocky Mountain highlands, northwestward fluvial transport of Moenkopi Formation sediment and regressing coastline to the west/northwest. Modified from Blakey and Ranney (2008).

In the SAR, there is as much as 760 m of mostly arid, ephemeral fluvial sediments that flowed northwestward ~100-300 km across the basin following the regressing coastline (Fig. 1.6) (Stewart et al., 1972; Blakey, 1973; Blakey and Ranney, 2008). The provenance of Moenkopi sediments in the SAR was primarily the Uncompahgre Highland to the northeast and San Luis Highland to the southeast, where large catchments incised into exposed Precambrian basement rocks, which likely fed the low relief ephemeral fluvial systems (Cadigan and Stewart, 1971; Barbeau, 2003; Banham and Mountney, 2013). The Moenkopi Formation is unconformably overlain by the Upper Triassic Chinle Formation throughout the southwest United States along the Tr-3 unconformity. The Moenkopi Formation

increases in thickness from northeast to southwest in the SAR and deposits are locally absent in Gypsum Valley and most of the Lisbon Valley-Dolores Anticline salt wall, likely due to later regional erosion (Shoemaker and Newman, 1959; Molenaar, 1981; Trudgill, 2011; Banham and Mountney, 2013).

Many members with distinctive lithologies comprise the Moenkopi Formation, none of which extend throughout the entire Moenkopi depositional area (Blakey and Gubitosa, 1984). Shoemaker and Newman (1959) were the first to describe in detail the intertonguing coarse- and fine-grained fluvial facies of the Moenkopi in the SAR and divided the rocks into four members, which are the focus of this study. In ascending order, the members are the: 1) Tenderfoot, 2) Ali Baba, 3) Sewemup, and 4) Pariott (Shoemaker and Newman, 1959).

The Tenderfoot Member, named for Tenderfoot Mesa, Colorado, overlies the Cutler and Paradox formations with angular unconformity of a few to several degrees over much of the region and nearly 90° locally near anticlines (Shoemaker and Newman, 1959; Lawton and Buck, 2006; Banham and Mountney, 2013). The Tenderfoot Member is characterized by predominantly massive beds of orange-brown to dark brown, angular to sub-rounded, argillaceous and silty, poorly-sorted, very fine to very coarse-grained arkosic sandstone (Shoemaker and Newman, 1959; Banham and Mountney, 2013). It extends from 1-3kms further to the northeast than the other Moenkopi members. The Tenderfoot ranges from a zero-thickness pinchout (due to both onlap onto underlying units and erosional removal during deposition of the overlying Chinle Formation) to a maximum thickness of 89 m to the southwest (Shoemaker and Newman, 1959). A white to light gray bed of gypsum ~ 2m thick is present in the lower part of the Tenderfoot throughout much of the region, providing a distinctive marker bed within primarily reddish-colored sediments.

The Ali Baba Member is named for the Ali Baba Ridge in Sinbad Valley where it exhibits internal angular unconformities. The member is characterized by interstratified, multi-lateral and multi-storied, amalgamated, medium- to coarse-grained, red-brown to purple-brown arkosic conglomeritic sandstone and dark-brown fissile siltstone (Shoemaker and Newman, 1959, Banham and Mountney, 2013). Representing the coarsest grained Moenkopi member of significant thickness throughout most of the SAR (Banham and Mountney, 2013), it unconformably overlies the Tenderfoot Member. In the Sinbad, Paradox and Fisher valleys the unconformity is distinctly angular (several degrees), whereas in Moab Valley the contact is concordant (Shoemaker and Newman, 1959). Thickness of the Ali Baba Member ranges from zero to approximately 90 m (Shoemaker and Newman, 1959). The presence of the Lower Triassic ammonoid *Meekoceras* in sandy shale (Dane, 1935) and within a thin limestone (Shoemaker and Newman, 1959) were reported in Moenkopi rocks in Salt Valley and therefore the Ali Baba Member was interpreted to be correlative to beds that conformably underlie the *Meekoceras*-bearing limestone bed (Shoemaker and Newman, 1959). However Lucas and others (1997) determined that these beds contained Early Cretaceous freshwater gastropods and ostrocods and belong in the Cedar Mountain Formation and do not correlate to the Moenkopi Formation. In the vicinity of Gateway, Colorado, ~26 km from Castle Valley, the Ali Baba is absent beneath the Chinle Formation. Southwest of Moab Valley, the Ali Baba Member and overlying Sewemup Member become indistinguishable (Shoemaker and Newman, 1959).

The Sewemup Member is named for Sewemup Mesa on the eastern flank of Sinbad Valley where it conformably overlies, and is partially interstratified with, the Ali Baba Member. The Sewemup Member is characterized by heterolithic siltstone and sandstone beds composed predominantly of thinly- to medium-bedded orange-brown to dark brown fissile siltstone with subordinate conglomeratic sandstone and gypsum beds. Thickness ranges from zero to 137 m (Shoemaker and Newman, 1959; Banham and Mountney, 2013). The member is eroded northeastward toward the Uncompahgre Plateau

and over salt anticlines beneath the Chinle Formation. Near Sinbad and Castle valleys, the Sewemup is overlain by the Pariott Member, the uppermost unit of the Moenkopi Formation in the region.

Shoemaker and Newman (1959) named the Pariott Member for Parriott Mesa on the northern end of Castle Valley. The name 'Pariott' is used here to honor the official stratigraphic nomenclature, despite the current cartographic convention of 'Parriott Mesa'. The Pariott Member is approximately 76-m thick in Sinbad Valley where it is characterized by interbedded red-brown to purple brown sandstone and orange-brown, red-brown and dark brown siltstone (Shoemaker and Newman, 1959; Banham and Mountney, 2013). The member abruptly thickens to over 100m beyond the northwest end of Castle Valley before dipping beneath the surface. The Pariott Member disconformably overlies the Sewemup but, due to limited exposures of the Pariott Member and overlying Chinle Formation, whether or not it represents a significant break in sedimentation remains unclear (Shoemaker and Newman, 1959). Despite this uncertainty, the Pariott Member was arbitrarily assigned to the Middle Triassic. The exposure of the contact between the Pariott Member and the overlying Chinle Formation is also limited and represents the Tr-3 unconformity (Pipiringos & O'Sullivan, 1978).

1.3 Castle Valley Salt Structure

Castle Valley (19 x 3 km) is a NW-SE-trending, breached salt-cored anticline (Figs. 1.1 and 1.7) within the SAR that formed as a product of salt dissolution of a breached salt wall (Castle Valley Salt Wall) and erosion of sediment (Jones, 1959; Doelling & Ross, 1998; Ross 1998; Lawton and Buck, 2006). The Castle Valley salt wall terminates abruptly on the northwest end at the northeast-trending Cataract Lineament (Stevenson and Baars, 1986) (Figs. 1.1 and 1.8), coincident with the Colorado River, near a listric secondary salt weld that juxtaposes steeply dipping Permian and Triassic strata (Lawton and Buck, 2006; Trudgill, 2010). Although the modern Castle Valley salt structure terminates on the southeast end at the La Sal Mountains (Fig. 1.1), it was formerly connected to the Paradox Valley salt wall prior to emplacement of the 27.9-25.1 Ma La Sal intrusive complex (Jones, 1959; Shoemaker

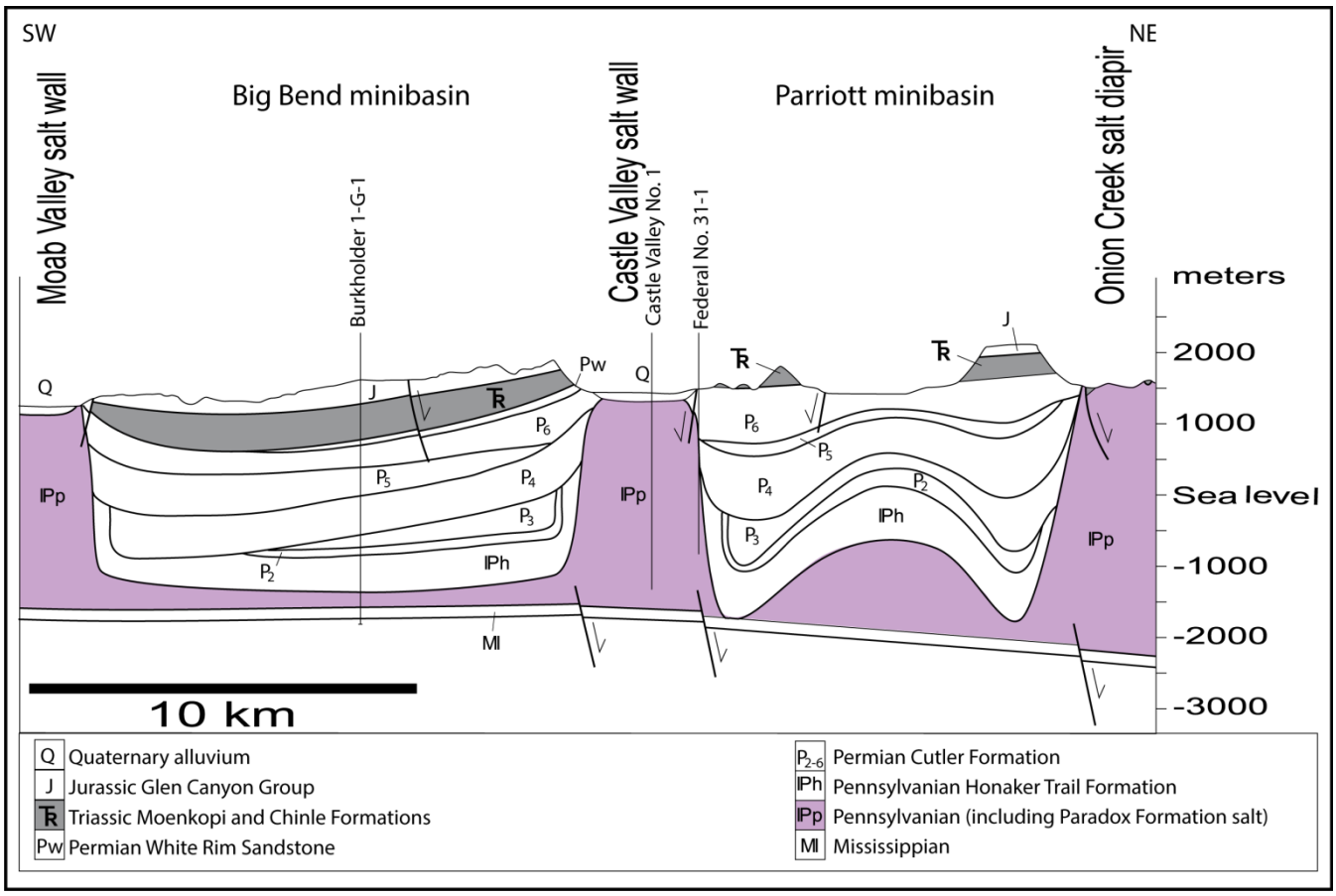

Figure 1.7: Part of structural cross-section along A-A' of Figures 1.1 and 1.4, across the Big Bend minibasin (Matthews, 2004), Castle Valley salt wall and Parriott minibasin (Banham and Mountney, 2013), showing steeper stratal architecture adjacent to salt walls during Pennsylvanian-Permian time and overlying shallower dips during Triassic and Jurassic times. Interpretations from Trudgill (2010) based on well (locations shown with respect to Castle Valley salt wall), gravity and seismic data.

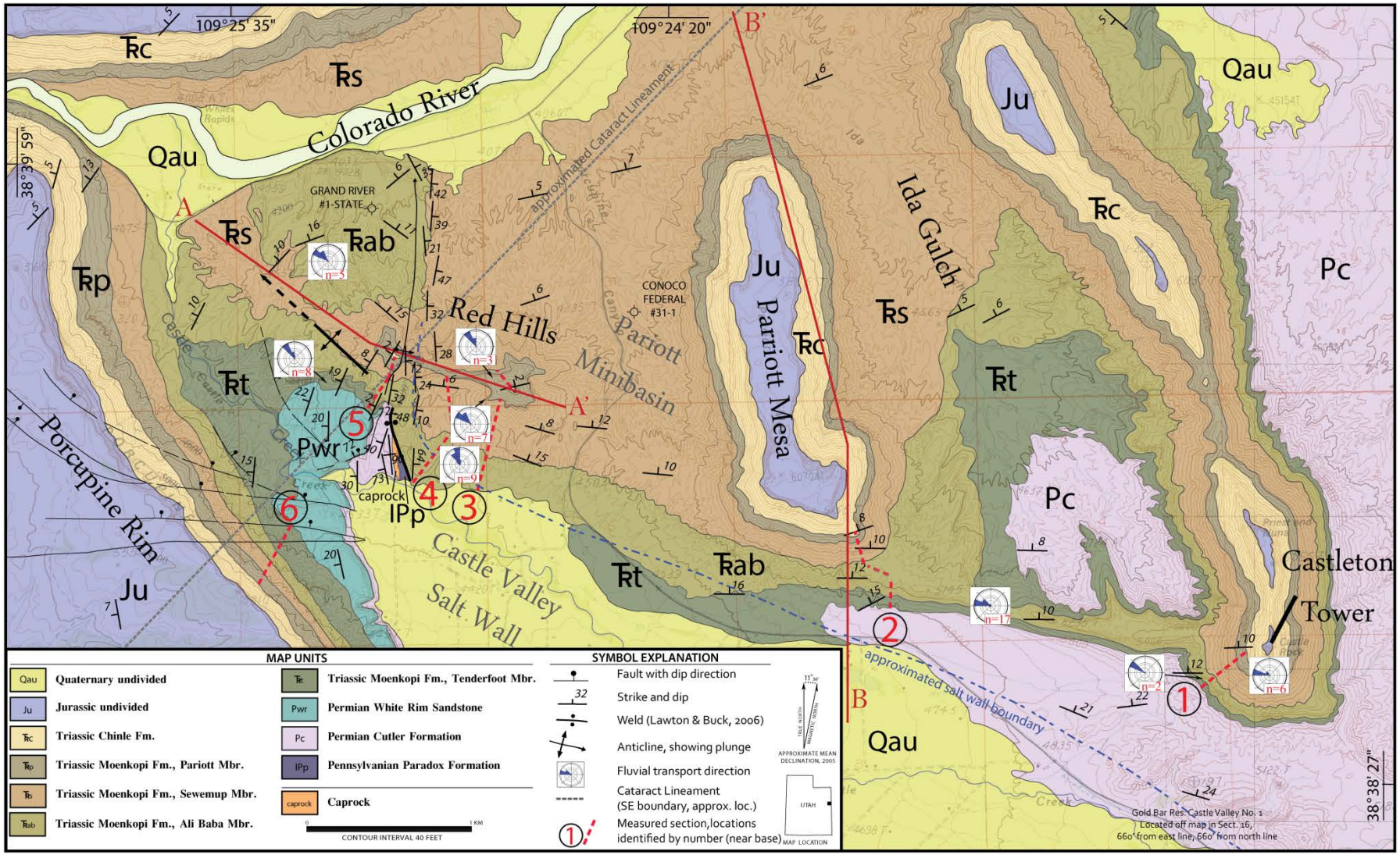

Figure 1.8: Geologic map (see Plate 1 for detail) of the northwest part of the Castle Valley salt wall showing Triassic Moenkopi members and locations of measured sections used in this study. Locations of Conoco Federal #31-1 and Grand River #1-State are shown on map, the Gold Bar Resources Castle Valley Unit #1 located off of mapped area. Faults along Porcupine Rim from Doelling and Ross (1998), weld from Lawton and Buck (2006), Cataract Lineament from Stevenson and Baars (1986) and Permian-Triassic caprock is from Shock (2012). Cross-sections through A-A' and B-B' are shown in Figures 4.3 and 4.

and Newman, 1959; Carter & Gualteri, 1965; Cater, 1970, Nelson, 1998). Paradox evaporite (mostly gypsum) is locally exposed in the Castle Valley floor (Lawton and Buck, 2006; Shock, 2012) and well data from the Gold Bar Resources Castle Valley Unit No. 1 in the east-central part of the valley (Fig. 1.7) indicates at least 3000m of salt is present from base of salt to top of exposed salt wall (Trudgill, 2010). Well data from the Grand River Oil & Gas Co. No. 1, located on the northeast flank of Castle Valley (Fig. 1.8), and regional gravity data also indicate steep salt wall flanks with more than 670 m of relief on the salt wall (Case et al., 1963; Case and Joesting, 1972; Doelling and Ross, 1998; Trudgill, 2010).

Permian, Triassic and Jurassic strata exposed along the margins of Castle Valley dip away from the salt wall toward the northeast and southwest. On the northern end, away from the northwestern welded termination of the salt wall (Doelling and Ross, 1998; Lawton and Buck, 2006; Trudgill, 2010), rocks of the Permian Cutler Formation have locally steep to overturned beds adjacent to the wall and decreasing dips away from the wall (Fig. 1.8). Triassic and Jurassic rocks dip less steeply adjacent to the salt wall than Permian strata, indicating decreased rates of Castle Valley salt wall growth (Lawton and Buck, 2006; Banham and Mountney, 2013).

Despite an overall symmetrical geometry of the Castle Valley salt structure (Case et al., 1963), surface outcrops exhibit stratigraphic asymmetry across the wall (Trudgill, 2010). A localized Permian eolian sandstone on the southwest side of the valley (Fig. 1.8), an equivalent to the White Rim Sandstone (Huntoon et al., 2002; Parr, 2012), is not present on the northeast side and ranges from approximately 300 feet at the northwest end of the valley to zero to the southeast over ~ 5 km due to angular truncation by the overlying Moenkopi Formation (Huntoon et. al, 2002).

1.4 Moenkopi Formation Adjacent to the Castle Valley Salt Wall

1.4.1 Transport Direction

Prior to Moenkopi deposition, in the minibasin on the northeast side of the Castle Valley salt wall, termed the Parriott minibasin by Banham and Mountney (2013), semi-arid, proximal fluvial-fan deposits of the Permian Cutler Group were transported and deposited in a generally southwesterly, direction, perpendicular to the salt wall (Mack and Rasmussen, 1984; Venus, 2012). This indicates that surface topography generated by the developing Castle Valley salt wall during deposition of the Cutler Group fluvial system was not significant enough to greatly influence paleoflow direction, as Cutler sedimentation rate exceeded the rate of diapiric uplift (Venus, 2012). The load of the Cutler sediments generated increased subsidence rates in the salt-withdrawal minibasins adjacent to the Castle Valley salt wall, resulting in a rim syncline that continued throughout Early Triassic Moenkopi Formation deposition (Trudgill, 2010; Banham and Mountney, 2013)

Dryland fluvial sediments of the Moenkopi Formation record transport direction changes from the Cutler Formation southwestward flow to a northwesterly (mean vector of 303°) flow in the Parriott minibasin, dominantly parallel to the Castle Valley salt wall (Fillmore, 2006; Banham and Mountney, 2013). Subsidence rates were greater in the Parriott minibasin than in the neighboring Fisher minibasin, on the northeast side of the Onion Creek salt wall. The overall rate of Moenkopi deposition was outpaced by the associated Castle Valley salt wall rise, resulting in a rim syncline on the northeast flank of the salt wall with 30m of stratal thickening (Banham and Mountney, 2013). The overlying Late Triassic Chinle Formation records continued parallel transport, punctuated by southwesterly transport of sediments in the upper part of the formation (Matthews et al., 2004).

1.4.2 Composition of the Salt Wall

Lawton and Buck (2006) documented gypsum- and dolostone clast-bearing growth strata within the Moenkopi Formation on the northeast flank and northwest termination of the Castle Valley salt wall.

There they documented a previously unrecognized listric secondary salt weld with (Fig. 1.8), which they mapped as Paradox Formation and dolostone referred to as ‘Lower Cutler beds’.

Exposed dolostone between Paradox Formation evaporate and Cutler Formation arkosic fluvial sediments on the southwest flank of the Castle Valley salt wall and similar carbonates at the welded northwest termination of the wall adjacent to the Moenkopi Formation were studied by Shock (2012). Shock (2012) interpreted that the dolostone clasts present within fluvial channels in Cutler and Moenkopi deposits are not from depositional carbonates associated with Lower Cutler beds. The dolostone formed, rather, as carbonate caprock while in a horizontal attitude above the salt wall followed by rotation to a flanking position by halokinetic drape folding within halokinetic sequences. Erosion by Cutler and Moenkopi fluvial systems incorporated the dolostone as clasts. Carbonate caprock, previously unrecognized in the Paradox Basin, likely formed along the top of the Castle Valley salt wall through anaerobic sulfur reduction of anhydrite caprock associated with hydrocarbons (Shock, 2012).

1.4.3 Paleoclimate

Gypsic paleosols, detrital and eolian gypsum and halite casts within the Tenderfoot, Ali Baba and Sewemup members in Castle Valley indicate regional hyperaridity during Early Triassic deposition of the Moenkopi Formation (Lawton and Buck, 2006). Calcic aridisols and root traces in the Pariott Member indicate a shift to arid and semiarid climate conditions between Early and Middle Triassic time (Prochnow et al., 2006).

1.4.4 Tenderfoot Member

Although the basal unit in Castle Valley is conventionally assigned to the Tenderfoot Member, Lawton and Buck (2006) mapped the lowermost Moenkopi unit in Castle Valley as heterolithic siltstone and sandstone and assigned it to the Hoskinnini Member. The Hoskinnini Member is well exposed in the Canyonlands National Park region and is considered to be older or partially equivalent to the basal

Tenderfoot Member (Shoemaker and Newman, 1959; Stewart, 1959). Stewart (1959) reassigned the Hoskinnini tongue from the underlying Cutler Formation to the basal Moenkopi on the basis of close stratigraphic relationship and from study of areas where rocks assigned to the Tenderfoot Member are physically continuous with the Hoskinnini. Banham and Mountney (2013) use the conventional Tenderfoot name for the basal unit adjacent to the Castle Valley and Fisher Valley salt walls. This study uses the Tenderfoot name and does not recognize Hoskinnini in the study area.

A lateral change in clast size reduction in the Tenderfoot from the type locality at Tenderfoot Mesa, Colorado to the study area corresponds to a lateral facies change and clast size reduction in the Cutler Formation (see, Mack and Rasmussen, 1984). At Tenderfoot Mesa, the Tenderfoot unit contains pebbles and cobbles composed of gneiss, schist and granite reworked from alluvial fan deposits of the underlying Cutler Formation (Shoemaker and Newman, 1959). The range of grain sizes decreases in Castle Valley outcrops to coarse-grained sand and granules where braided stream deposits of the Cutler were reworked by channels of the Tenderfoot Member. In the study area the member is characterized by laterally continuous, horizontally interbedded siltstones and sandstones with sheet-like architecture and subordinate massively bedded sandstones (Banham and Mountney, 2013). Banham and Mountney (2013) interpret Tenderfoot sediment as being deposited by repeated flooding and desiccation in a restricted tidal flat or embayment with a restricted opening. Despite the heterolithic character of the Tenderfoot member, Lawton and Buck (2006) argue that, in this local region, evidence for tidal deposition is lacking and the strata represent a continental origin with deposition in a continental flood basin or inland sabkha based on distance to time-equivalent shoreline (Blakey, 1989). A distinctive 0.7-2.5-m thick white gypsum bed in the lowermost part of the member contains faint tabular cross-beds as high as 30 cm, interpreted as an eolian sand sheet by Lawton and Buck (2006). Banham and Mountney (2013) interpret the gypsum bed as a precipitate from a brine pool, but recognize that in the Parriott

minibasin the gypsum may have been partially reworked and deposited by wind based on Lawton and Buck's (2006) interpretation.

1.4.5 Ali Baba Member

Lawton and Buck (2006) do not use the name 'Ali Baba' in their study. Sediments that they term thick-bedded sandstone association and conglomerate and rippled sandstone association are equivalent to the descriptions of Ali Baba in Shoemaker and Newman (1959). The Ali Baba Member unconformably overlies the Tenderfoot with ~ 6° of discordance adjacent to Castle Valley salt wall and records a change from unconfined flow in Tenderfoot to a more confined transport that deposited sheet-like heterolithic units and a thick-bedded sandstone with a series of amalgamated channel elements, preferentially adjacent to the salt wall in the rim syncline (Lawton and Buck, 2006; Banham and Mountney, 2013). Lawton and Buck (2006) mapped one sandstone body on the northeast flank of the salt wall, three on the downthrown southeast side of the weld and one on the northwest side of the weld. Lawton and Buck (2006) documented rounded quartz, subangular dolostone, angular to subangular intraclastic sandstone and shale and subangular white gypsum clasts as much as 12 cm in diameter within associations equivalent to the Ali Baba Member in Castle Valley outcrops. These deposits record ephemeral and intermittent fluvial systems in a wadi environment (e.g., Glennie, 1970) that encroached an inland sabkha (Lawton and Buck, 2006). Banham and Mountney (2013) suggest that this may reflect change from arid to more humid conditions.

1.4.6 Sewemup Member

Based on prominence of sheet-like elements, Banham and Mountney (2013) propose that during Tenderfoot and Ali Baba deposition there were higher rates of subsidence/salt-wall rise with relatively low rates of accommodation fill than during the overlying Sewemup Member deposition. Based on a 'unique' presence of gypsum-clast-bearing horizons in the Sewemup, they infer geomorphic instability and surface breach by the Castle Valley salt wall in Sewemup time. Contrastingly Lawton and Buck

(2006) infer that the change from abundant coarse-grained diapiric detritus in the Ali Baba to extensive gypsic paleosol development from episodic geomorphic stability in the Sewemup are the result of decreased topography along the salt wall and/or reduced rates of salt-withdrawal subsidence and/or climate-induced decrease in erosion and sediment supply. Gypsic paleosols are most extensive in the Sewemup Member and represent the oldest recorded gypsic paleosols on Earth (Lawton and Buck, 2006).

The differing models are the result of Banham and Mountney's (2013) study lacking recognition of gypsum- and dolostone-bearing clasts within Ali Baba strata and documenting pebble- and cobble-grade gypsum clasts within Sewemup strata, which Lawton and Buck (2006) do not describe or discuss. However, Lawton and Buck (2006) do document detrital gypsum throughout Moenkopi strata in their measured sections.

Lawton and Buck (2006) do not use the name 'Sewemup'; they describe a mudstone and gypsum association that is stratigraphically and lithologically equivalent to the Sewemup of Shoemaker and Newman (1959). This member is dominated in the Castle Valley vicinity by thick reddish-brown mudstone with repetitive cycles of gypsic paleosols 0.5-1.5-m thick, often capped by 0.1-2-m tabular beds of gypsum interpreted as eolian sand sheets (Lawton and Buck, 2006).

1.4.7 Pariott Member

The Pariott Member records a shift to channelized fluvial transport and deposition with an increase in multi-storey channel elements, mostly deposited in rim synclines along both margins of the Castle Valley salt wall (Banham and Mountney, 2013). The Pariott Member was not addressed by Lawton and Buck (2006), other than to suggest that it represents meandering river and lacustrine delta deposits, and was not assigned a lithologic association by them.

1.5 Data and Methods

Facies observations and depositional interpretations presented in this study are based on field mapping (Plate 1) and analysis of outcrops and hand samples of Moenkopi Formation strata along the northeastern flank and northwestern end of Castle Valley. Six stratigraphic sections were measured and logged (Fig. 1.8; Plate 2) to record lithofacies and determine facies associations: Castleton Tower (1), Pariott Mesa (2), Red Hills (3, 4, 5) and northwest Porcupine Rim (6) -. Logged section locations were based on accessibility, quality of exposure and position relative to the Castle Valley salt wall. The sections were measured using a standard 1.5-meter Jacob's staff, a measuring tape and Brunton compass (2005 magnetic declination of 11 degrees, 36 minutes east). Paleocurrent data (recorded in Appendix A) were derived from current ripples, parting lineations on bedding surfaces and trough cross-stratification in channel deposits of the Ali Baba Member; current ripples in the Sewemup Member; and trough cross-stratification in the Pariott Member. Paleocurrent data were measured with a Brunton compass directly (on outcrop surfaces) and where acquired indirectly (using line of sight). Paleocurrent data from Banham and Mountney (2013) are also incorporated in this study. Units were mapped in the field on parts of two USGS 7.5-minute (1:24,000) topographic maps with the aid of aerial photos. Field mapping was later recorded onto a single digital version of part of the southwestern Fisher Towers quadrangle and part of the southeastern Big Bend quadrangle using Adobe Illustrator Creative Suite.

Chapter 2

LITHOFACIES AND FACIES ASSOCIATIONS OF THE MOENKOPI FORMATION AT THE CASTLE VALLEY SALT WALL

Nine unfossiliferous facies associations (Table 2.1), determined from groups of lithofacies, classified using Miall (1978) facies codes (Fig. 2.1) were defined within the Moenkopi Formation on the flanks of the Castle Valley salt wall. Facies associations are based on lithology, sedimentary structures, pedogenic features, geometry and nature of bedding contacts with underlying and overlying units. The identified facies associations are: 1) channel-form sandstone and organized conglomerate (FA1), 2) thinly interbedded siltstone and fine-grained sandstone (FA2), 3) tabular-to-lenticular siltstone and sandstone sheets (FA3), 4) structureless to weakly-bedded sandstone (FA4), 5) disorganized conglomerate (FA5), 6) well-sorted, well-rounded siliciclastic sandstone (FA6), 7) gypsic sandstone (FA7), 8) gypsic paleosol (FA8) and 9) calcic paleosol (FA9).

Table 2.1: Lithofacies associations.

Lithofacies Association	Color Code	Description	Miall (1978) Facies Codes	Members Present In	Interpretation	Associated With
FA1		Channel-form sandstone and organized conglomerate	St, Sp,Sh,Sr,Gt	Ali Baba Pariott	Axial fluvial	FA2, FA6
FA2		Thinly interbedded siltstone and fine-grained sandstone	Sh, Sr, Fh, Fl	Ali Baba Pariott	Fluvial overbank	FA1, FA8, FA9
FA3		Tabular-lenticular siltstone and sandstone sheets	Sh, Sr, Sd, Fh, Fl	Tenderfoot Sewemup	Unconfined channels and sheet floods	FA5, FA6, FA7
FA4		Structureless to weakly-bedded sandstone	Sx	Tenderfoot	Distal wadi fan	FA7
FA5		Disorganized conglomerate	Gmm, Sr	Tenderfoot Ali Baba Sewemup	Debris flow from exposed diapir	FA3
FA6		Well-sorted, well-rounded sandstone	Sp, Sh	Ali Baba Sewemup Tenderfoot	Eolian sand sheets	FA1, FA3
FA7		Gypsic sandstone	E	Tenderfoot Sewemup	Eolian sand	FA3, FA4, FA8
FA8	N/A	Gypsic paleosol	Pe	Tenderfoot Ali Baba Sewemup	Paleosol, stages I-III gypsic (diapir exposure)	FA2, FA3, FA7
FA9	N/A	Calcite paleosol	Pc	Pariott	Paleosol (semi-arid environment)	FA2

Facies code	Characteristic	Interpretation
Gmm	Matrix-supported conglomerates. 5-50 cm thick. Subrounded granules, angular pebbles and small cobbles in matrix of fine to medium sand. Structureless with rare weak reverse grading. Quartz granules, gypsum, sandstone and dolostone (caprock?), pebbles and cobbles up to 12 cm.	Debris flows
Gt	Coarse sandstone-matrix supported, trough cross-stratified conglomerates. Angular to subrounded, pebble to cobble, normal grading with some imbriication. Sandstone, dolostone, calcite replaced gypsum and mudstone rip-ups	3-D gravel dunes, channel-fill (Miall, 1996)
St	Trough cross-stratified sandstone. Fine to coarse-grained, occassionally pebbly (angular to subangular)at base of scours. Single Quartz, gneissic and granitic grains with pebble lags also containing mudstone rip-ups and multi-storey with high width to depth ratio.	Dune migration, lower flow regime
Sp	Planar cross-stratified sandstone. Fine to medium-grained. Occurs as multi-storey fining upward beds and well-sorted sand sheets. Some outcrops exhibit wind ripple cross-lamination perpendicular to foresets	2D dunes, lower flow regime and eolian
Sh	Horizontally laminated sandstone. Fine to medium-grained. Moderate to well sorting, cm-scale beds fine upward	Upper pane-bed flow, upper flow regime
Sx	Poorly laminated to massive sand. Fine to coarse-grained with minor component of rounded granules. Where discernable, bedding is horizontal or lenticular with weak normal to reverse grading.	Rapid deposition from heavily sediment-laden flows (Maizels, 1993)
Sr	Ripple cross-laminated sandstone. 1-100 cm thick. Fine to medium sand. Current, climbing, oscillation, and interference ripple types are all present.	2D or 3D ripples, upper flow regime current and wave ripples (Miall, 1996; Harms et al., 1982)
Sd	Deformed sandstone beds. Associated with fine to coarse sandstones. deformation includes load casts, slump folds and dewatering structures	Post-depositional soft-sediment deformation by differential loading
Fl	Interlaminated mudstone, siltstone and sandstone. Cm-scale beds. Sand generally fine-grained with some scours filled with medium sand. Small-scale ripples exhibited.	Unconfined suspension deposits, small-scale channel fill
Fh	Horizontally laminated to massive siltstone. Mm-scale bedding. Abundant mica.	Deposition from suspension, lower flow regime
Pc	Pedogenic carbonates. Stage II and III calcic paleosols developed in mudstone of lithofacies Fh (restricted to Pariott Member)	Mature soil development
Pe	Pedogenic evaporites. Stage I-III gypsic paleosols developed in silt of lithofacies Fh, Fl and Sr.	Mature soil development
E	Evaporites (gypsum). Continuous beds a few cm to 1.5 m thick and in lenses up to 0.5 m in height and 1 m in width. Some sheet-like beds with intermixed fine sand grains and weak cross stratification	Eolian deposited sand sheets and abandoned channel fill.

Figure 2.1: Lithofacies codes, descriptions and interpretation from Miall (1978, 1996).

2.1 Facies Association 1: Channel-Form Sandstone and Organized Conglomerate

The channel-form sandstone and organized conglomerate facies association (FA1) is present in the Ali Baba and Pariott members and is not present in the Tenderfoot or Sewemup members. FA1 is commonly associated with the interbedded, thinly interbedded siltstone and fine-grained sandstone (FA2) and well-sorted, well-rounded siliciclastic sandstone (FA6) associations.

2.1.1 Description

FA1 is characterized primarily by 0.5 -1 m thick channel-form beds of poorly to well-sorted fine, medium-, and coarse-grained sandstones with lesser amounts of granule to pebble and cobble conglomerates and exhibits sandy bedforms. FA1 contains trough (St), planar (Sp), and horizontally (Sh) stratified sandstone, exhibits ripple cross-lamination, including climbing ripples (Sr) (Fig. 2.2) and in some areas contains trough cross-stratified conglomerate (Gt). FA1 is reddish-brown dark or pale gray-purple in the Ali Baba Member and in the Pariott Member it is light to reddish-brown to purplish-brown. Channel-fill sandstones occur most commonly as single-storey sandstone bodies and less commonly as amalgamated multi-story units. Single-story channels have vertical thicknesses between 0.5m to 3.0m (Banham and Mountney, 2013) and high width-to-depth ratios (≥10), sharp erosive bases and contain internal erosion surfaces. Erosional surfaces are commonly overlain by gravel lags composed of extraformational, subrounded to angular granule to pebble clasts of quartz, gneiss and schist and intraformational sandstone and mudstone. In some exposures, clasts of subangular dolostone, sandstone and mudstone are present (Lawton & Buck, 2006). Gravel lags containing intraformational rip-up clasts of FA2 are common at the base of channels that overlie FA2. Trough cross-stratified conglomerate (Gt) (Fig. 2.3) is restricted to the Red Hills near the weld (e.g., Lawton and Buck, 2006) and is composed of mudstone rip-up, dolostone and limestone clasts.

2.1.2 Interpretation

The channel-form sandstone and organized conglomerate association represents braided ephemeral stream (wadi) deposits (e.g., Glennie, 1970) that flowed northwest, parallel to salt the wall (Fig. 2.4). High width-to-depth channels indicate streams flowed sporadically and discharge and grain size were not sufficient to permit incision of deep channels, but upper and lower flow regimes were sustained for long enough time to form structured deposits (Fielding, 2006). Upward transition from dune migration (St and Sp) to current-ripple laminated sandstone (Sr) records decrease in flow energy

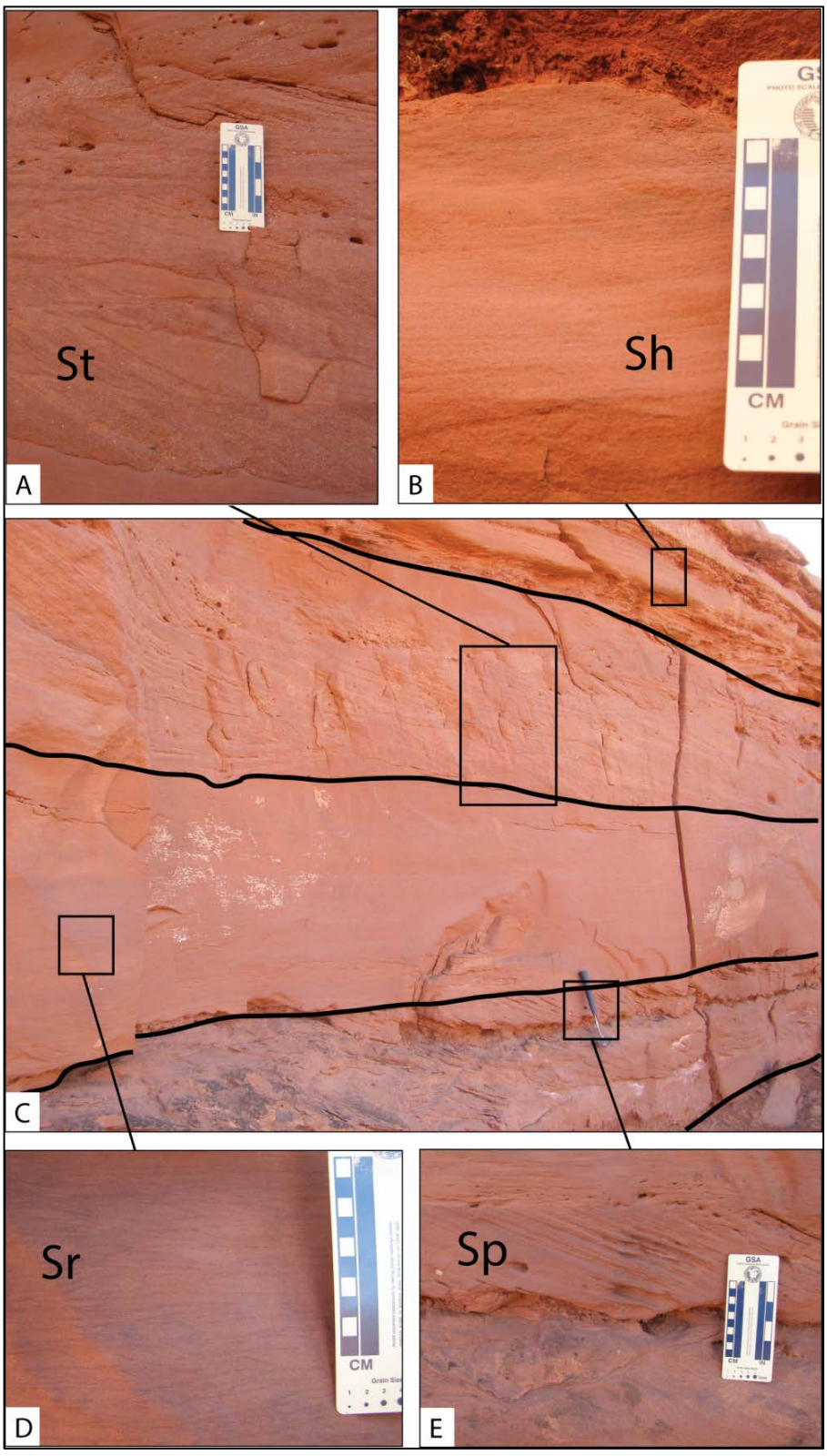

Figure 2.2: Outcrop photographs of FA1 in the Ali Baba Member within measured section 2 (Fig. 1.8). (A) St, trough cross-stratified sandstone. (B) Sh, horizontally laminated sandstone. (C) Outcrop showing relationships of Sp, Sr, St and Sh. Rock hammer in center of photo is 25 cm long. (D) Sr, ripple cross-laminated sandstone. (E) Sp, planar cross-stratified sandstone.

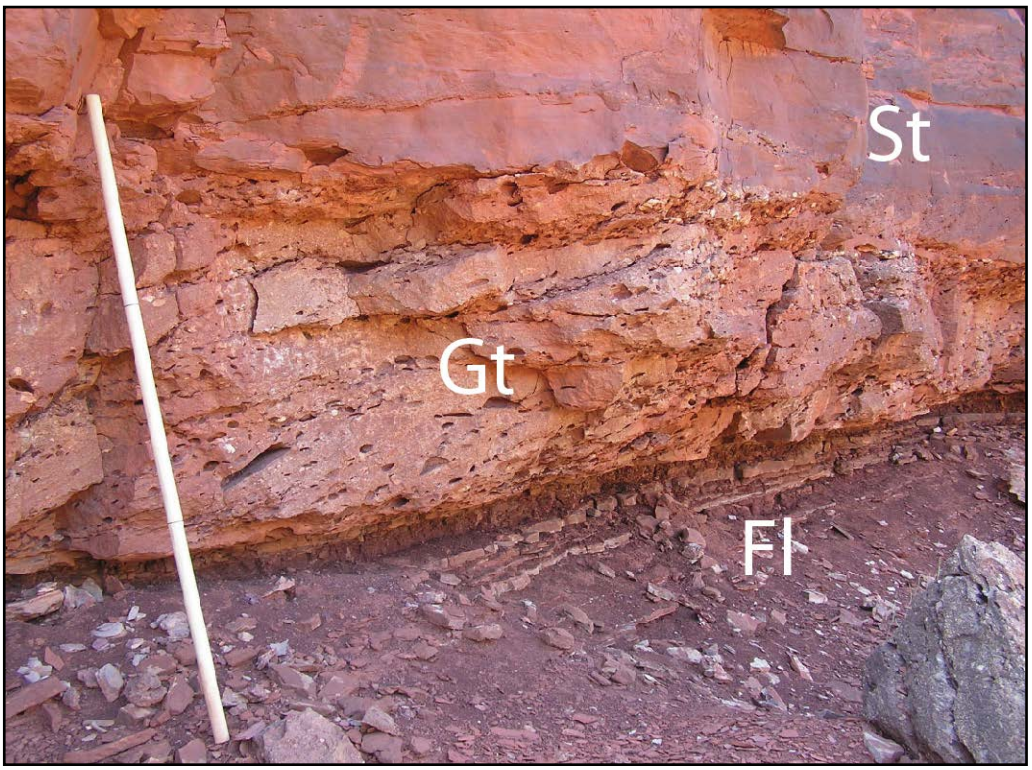

Figure 2.3: FA1 in Red Hills along measured section 5 (Fig. 1.8) with lithofacies Gt and St. Clasts of Gt are composed of mudstone rip-ups from underlying facies Fl within the thinly interbedded siltstone and fine sandstone association (FA2) and dolostone and calcite likely eroded from Paradox Formation that was exposed in the adjacent diapir.

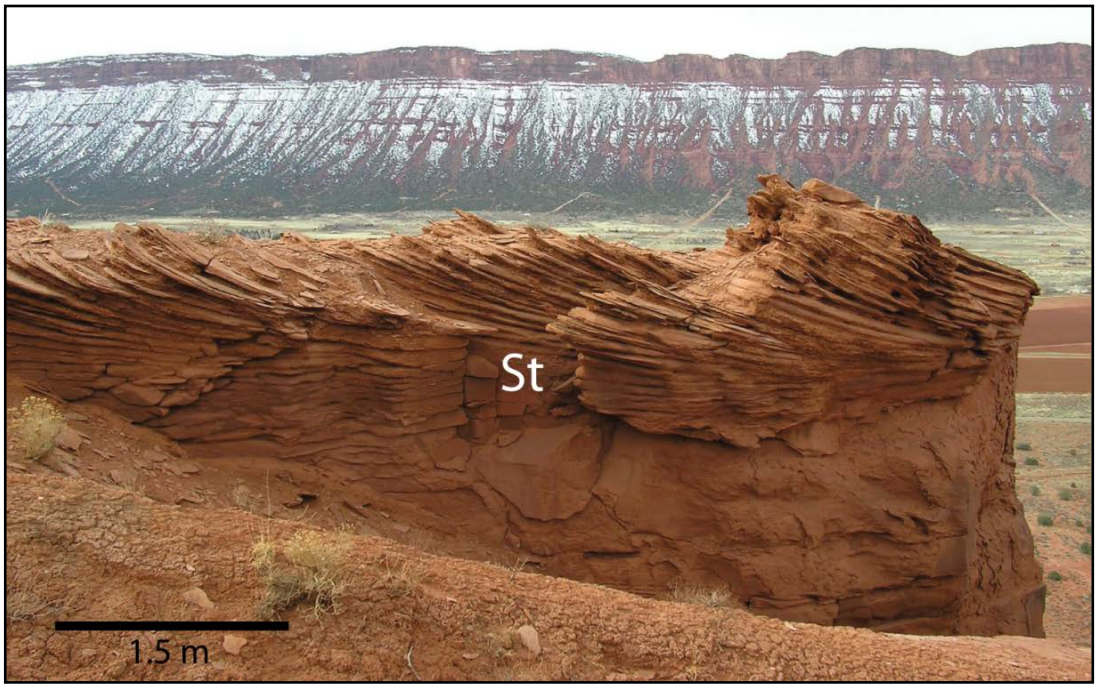

Figure 2.4: Trough crossbeds (St) in FA1 within the Ali Baba Member that indicate northwestward paleocurrent (left to right), parallel to Castle Valley trend. View is to southwest between Pariott Mesa and Castleton Tower (measured section 2, Fig. 1.8).

during waning flood stages. Horizontally laminated fine-grained sandstone (Sh) (Fig. 2.5) represents unconfined sheet flood deposits and crevasse splay deposits.

Figure 2.5: Horizontally laminated, thick bed of medium-grained sandstone (Sh) in Ali Baba Member along measured section 1 (Fig. 1.8). These beds indicates upper flow regime. Jacob staff is 1.5 m.

Crevasse splays and avulsions are uncommon in arid fluvial systems due to the absence of levees. A lack of vegetation results in overbank flows that are unimpeded and any levees that may have formed are prone to erosion. Due to infrequent precipitation, flood events tend to be large in magnitude with flow velocities on the floodplain similar to those within the channel, resulting in unconfined flow where deposition on the floodplain is not immediate (North et. al. 2007).

2.2 Facies Association 2: Thinly Interbedded Siltstone and Fine-Grained Sandstone

The thinly interbedded siltstone and fine-grained sandstone facies association (FA2) is present in the Ali Baba and Pariott members, is commonly interbedded with FA1 and commonly exhibits a scoured contact (Fig. 2.6). FA2 deposits are also overprinted in areas with the gypsic paleosol (FA8) and calcic paleosol (FA9) facies associations.

2.2.1 Description

This facies association is characterized predominantly by interbedded, laterally continuous cm-scale siltstone and fine-grained sandstone. Lithofacies that comprise FA2 include horizontally laminated

sandstone (Sh), ripple cross-laminated sandstone (Sr), horizontally laminated to massive siltstone (Fh) and interlaminated mudstone, siltstone and sandstone (Fl). Beds of fine-grained sandstone commonly underlie scour surfaces overlain by channel-form sandstone bodies of FA1. Sedimentary features in sandstone include halite casts (Fig. 2.7), load casts, desiccation cracks, soft-sediment deformation (dewatering) and rip-up clasts composed of siltstone and gypsum nodules within stage I-III gypsic paleosols (e.g., Buck and Van Hoesen, 2002; Lawton and Buck, 2006).

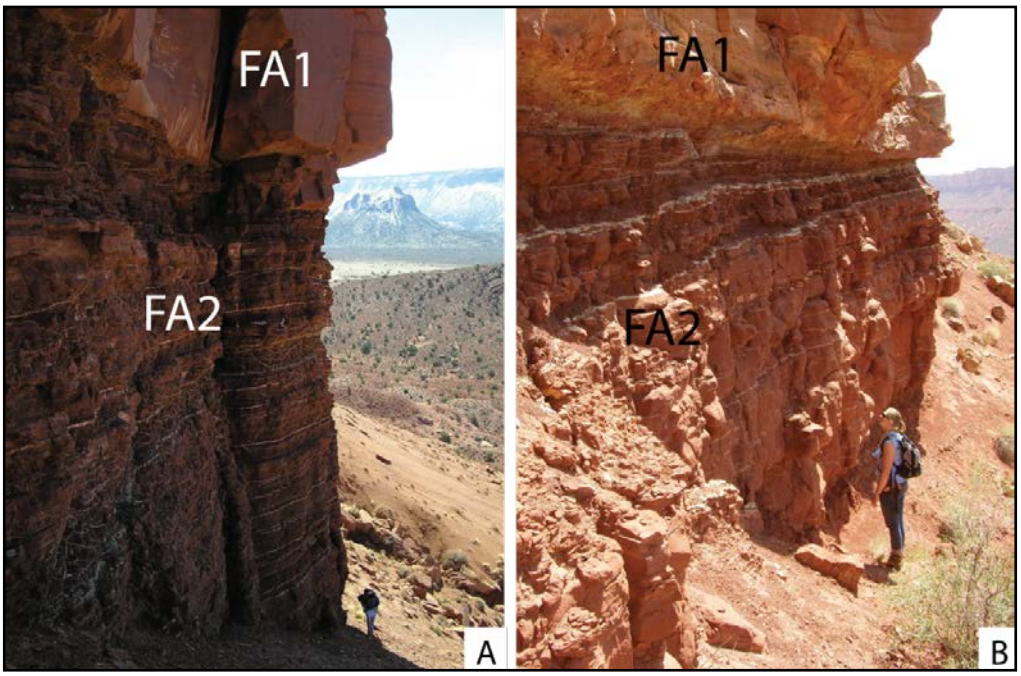

Figure 2.6: Erosional contact of FA2 and overlying channel-form sandstone bodies of FA1. (A) Ali Baba Member below Castleton Tower along measured section 1 (Fig. 1.8). Round Mountain in distance. (B) Pariott Member below in Red Hills along measured section 5 (Fig. 1.8). Person is 1.8 m.

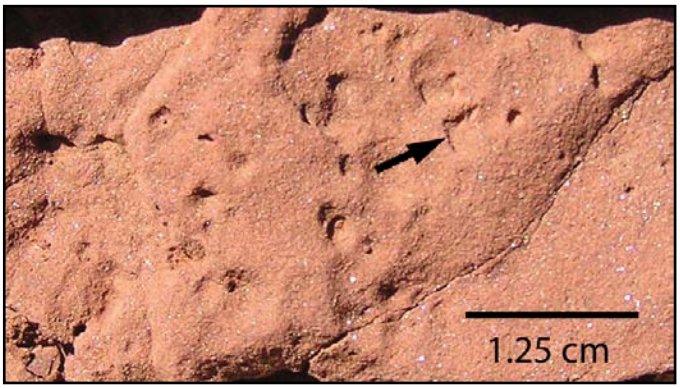

Figure 2.7: Salt casts displaying cubic form in medium-grained sandstone of FA2 within Ali Baba Member. Measured section 2 (Fig. 1.8).

2.2.2 Interpretation

The laminated (Fl) bed fabric, thin cm-thick beds and relationship to overlying channel bodies likely indicate deposition from suspension during overbank floods (Miall, 1996). Alternating wet and dry events resulted in desiccation features developed at the tops of these sediments. Climbing ripples in sandstone beds as thick as 50cm record episodic flooding that deposited large amounts of sediment during a short time (Allen, 1970; Ashley et. al, 1982). During times of standing water, sediment was reworked by wind currents to form wave ripples. Mature soil development (FA8) indicates long periods of time between sedimentation events. Abundant ripple cross-laminations have been noted in overbank deposits of modern ephemeral streams, sometimes extending un-interrupted for many kilometers (McKee et. al., 1967; Karcz, 1970; Stear, 1985).

Convolute laminations are structures commonly found in floodplain deposits, in both ephemeral and perennial river systems. At Bijou Creek, McKee et al. (1967) interpreted these to have formed during the late stages of flow when current velocities were waning and sediment was the consistency of quicksand.

2.3 Facies Association 3: Tabular-To-Lenticular Siltstone and Sandstone Sheets

The tabular-to-lenticular siltstone and sandstone sheets facies association (FA3) is present in the upper portion of the Tenderfoot Member and entire Sewemup Member. Along the edges of FA3 is interbedded throughout the Tenderfoot and Sewemup members with disorganized conglomerates (FA5) and in the Sewemup with well-sorted, well-rounded siliciclastic sandstone (FA6). FA5 is interpreted as debris flow deposits. In the Sewemup Member, FA3 interbeds with lenticular bodies of eolian gypsic sandstones (FA7).

2.3.1 Description

This facies association is characterized by laterally continuous sheets of interbedded siltstone and fine- to medium-grained sandstone bodies composed of thin, tabular to lenticular, centimeter- and

decimeter-scale beds of horizontally laminated (Sh), ripple cross-laminated (Sr) and deformed (Sd) sandstone beds, horizontally laminated siltstones (Fh) and interlaminated mudstone, siltstone and sandstone (Fl) (Fig. 2.8). Sedimentary features include climbing ripples, interference ripples, load casts, soft-sediment deformation structures, halite casts, desiccation cracks and reworked gypsic paleosol nodules (Fig. 2.9). Lack of internal erosional surfaces and moderate erosional basal contacts are present.

Figure 2.8: Laterally continuous sheets of interbedded siltstone and fine- to medium-grained sandstone of FA3 within Sewemup Member on northwest side of the Red Hills. View is to north.

2.3.2 Interpretation

The lithofacies distribution of thin sheet geometry and couplets of sands that grade vertically to pedogenically altered siltstone beds of FA3 indicates deposition in poorly confined channels by flash and sheet floods into an inland sabkha (e.g., Glennie, 1970). Interference ripples indicate episodes of standing water following flood events, where wind-generated waves formed transverse to the direction of waning current flows. Gypsic soil development records ephemeral deposition by flood events in an

Figure 2.9: Select sedimentary features of FA3. (A) Load casts below Castleton Tower along measured section 1 (Fig.1.8). (B) Interference ripples within Sewemup Member northwest of measured section 5. (C) Convoluted lamination within Sewemup Member, along measured section 1. Hammer in B and C is 25 cm

arid to hyper arid environment. This facies association is interpreted as Rill Type sheetflow deposits (e.g., Jutson, 1919). The term sheetflow is preferred in this case over sheet flood due to the non-erosive nature of the deposits (Jutson, 1919; Hogg, 1982). Only minor channels roughly a meter wide and deep formed in FA3 during flooding events, later filling with eolian material, including gypsum sand during dry times. Conditions favorable for sheetflow deposits to occur are outlined by Hogg (1982) and include heavy rainfall in a short period of time, a lack of channelization in the drainage area, low permeability of the underlying sediments and a lack of vegetation on the floodplain.

2.4 Facies Association 4: Structureless to Weakly-Bedded Sandstone

The structureless to weakly-bedded sandstone facies association (FA4) records the onset of the Tenderfoot Member deposition adjacent to Castle Valley salt wall and exhibits an erosive base above Permian Cutler Formation sandstone and conglomerate (Fig. 2.10) with angular discordance ~6-12° throughout study area. FA4 is present only in the lower part of the Tenderfoot Member and is interbedded with a distinct gypsic sandstone facies association (FA7) (Fig. 2.11).

2.4.1 Description

FA4 is characterized by indistinctly bedded fine-, medium- and coarse- grained, poorly sorted silty sandstone and granules (Sx) (Fig. 2.12). Granules and coarse grains of sub-rounded to rounded frosted-quartz are supported within a matrix of mica-rich, arkosic, silty sand. Bedding is internally structureless and tends to be nearly massive in some outcrops with some floating granules of quartz and feldspar. Where bedding is discernable, small-scale scours as much as 10 cm deep are exhibited. Normal and slight reverse grading were observed. Soft-sediment deformation is also present in some outcrops.

2.4.2 Interpretation

This association is interpreted as distal parts of an alluvial fan system within salt-controlled wadis. Upward coarsening intervals, poor sorting, massive bedding, slight reverse grading and some floating granules indicate hyperconcentrated flow in mid-distal fan environment (Marren, 2002). The small scale of sedimentary structures, poorly developed bedding and lack of large clasts indicates a distal source and low water discharge (Glennie, 1972). Frosted grains and granules, as well as stratigraphic proximity of this facies association to the White Rim Sandstone, indicate that reworked Permian Cutler Formation sediments were a significant source for this association.

These sediments are interpreted as being reworked from a nearby source due to the poorly developed lamination and lack of sedimentary structures. A sediment-laden slurry was likely transported only a short distance, preventing better sorting and sedimentary structure development

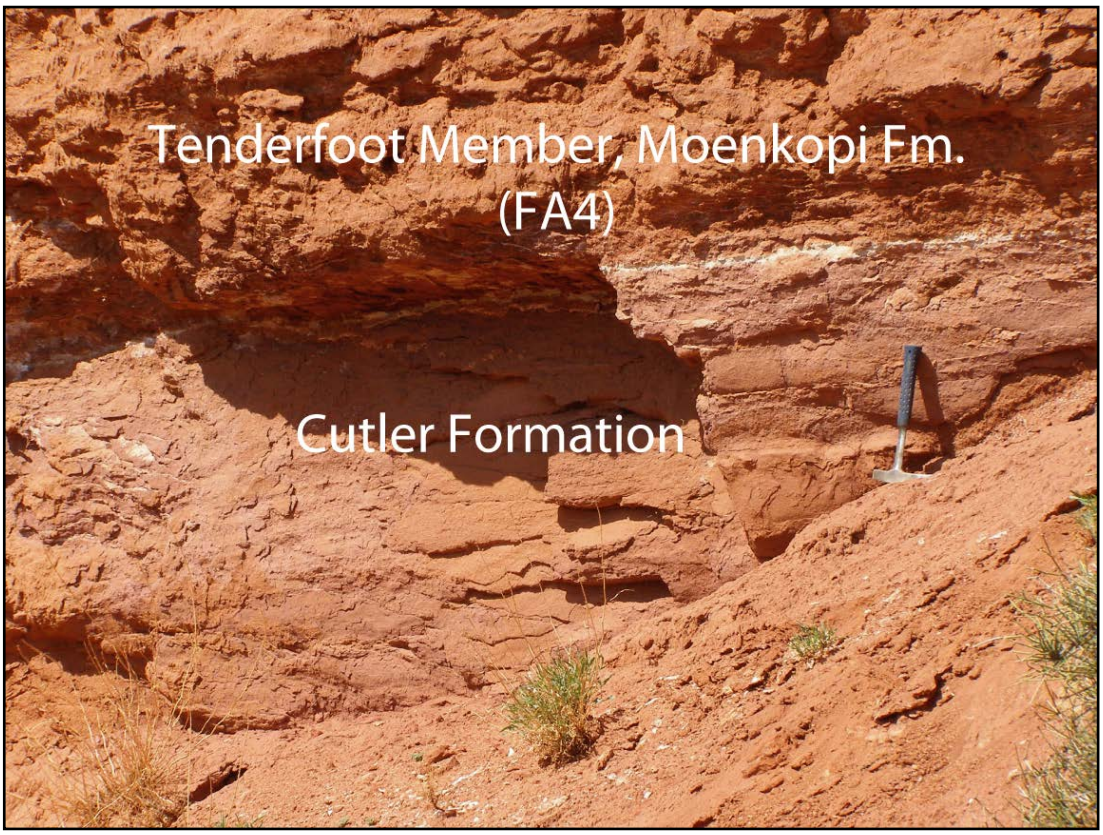

Figure 2.10: Photo showing erosional contact between underlying Permian Cutler Formation and overlying FA4 within the Tenderfoot Member of the Triassic Moenkopi Formation. Base of measured section 2 (Fig 1.8). Hammer is 25 cm.

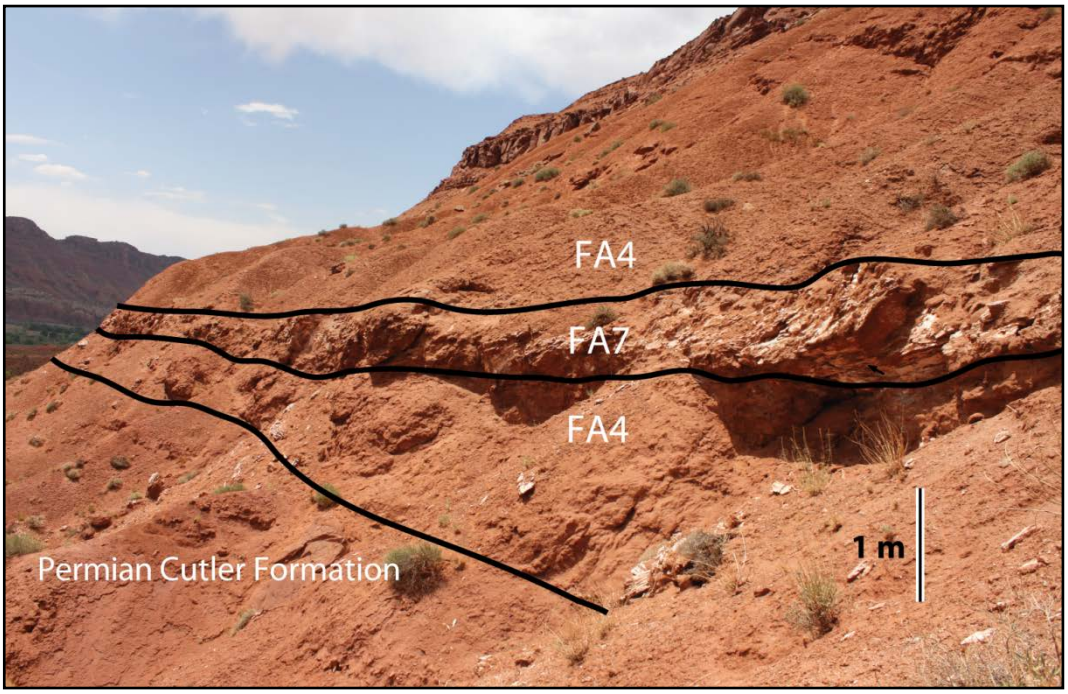

Figure 2.11: FA4 with interbedded FA7 near base of measured section 2 (Fig. 1.8).

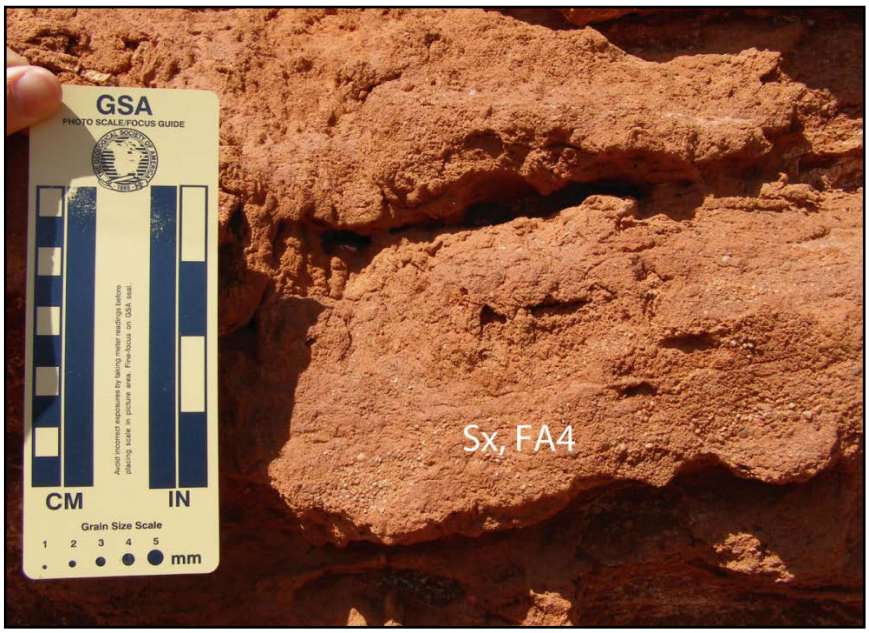

Figure 2.12: Poorly laminated to massive sand (lithofacies Sx) in FA4 with faint reverse grading near base of measured section 2 (Fig. 1.8).

(Glennie, 1972). Frosted quartz gains are interpreted as being sourced from underlying White Rim sandstone in the southwestern part of the field area and are most abundant where FA4 is in direct contact.

2.5 Facies Association 5: Disorganized Conglomerate

The disorganized conglomerate facies association (FA5) is present in the upper part of the Tenderfoot Member (interbedded with FA3), the Ali Baba Member (interbedded with FA2) and Sewemup Member (interbedded with FA3). FA5 lateral distribution is confined to close proximity (<750m) to the Castle Valley salt wall.

2.5.1 Description

FA5 is characterized by angular to subrounded clasts of gypsum, dolostone and sandstone up to 12 cm in size, in a poorly sorted matrix of fine- to coarse-grained sandstone (Gmm), with uncommon ripple cross laminated sandstones (Sr) at the tops of beds (Fig. 2.13). Beds are thin, ranging in thickness from a few cm to 50 cm, most commonly on the small end of the scale. Beds have erosive bases and overlie scour surfaces developed on underlying units.

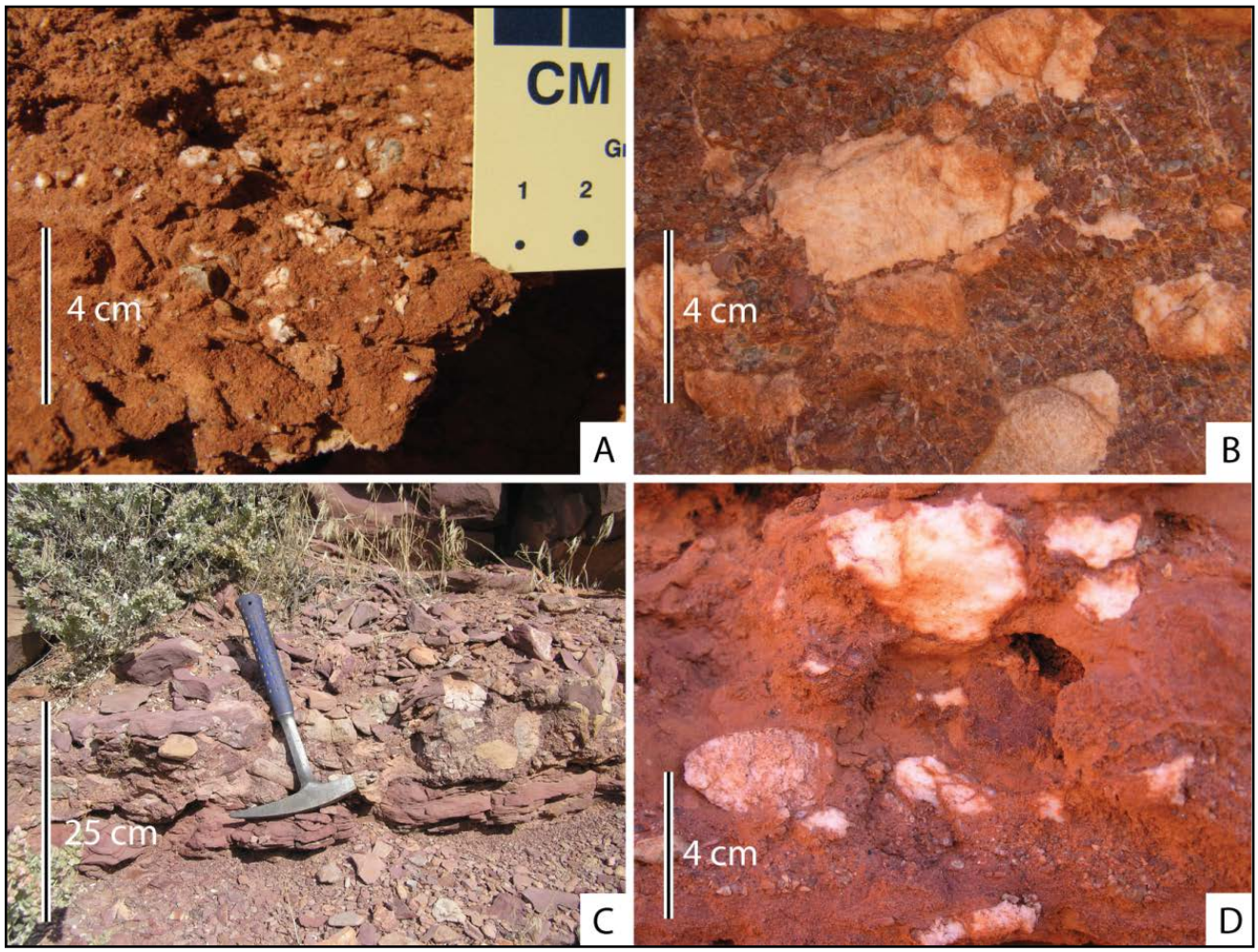

Figure 2.13: Disorganized conglomerate facies association (FA5). (A) Granule conglomerate in sand matrix containing mm-sized gypsum clasts within FA4 of the Tenderfoot Member. Along measured section 2 (Fig. 1.8) (B) Pebble conglomerate in sand-granule matrix containing pebble to small cobble sized gypsum clasts within FA2 of the Ali Baba Member. In road cut at northeast end of Castle Valley. (C) Cobble conglomerate in granule and small pebble matrix composed of dolostone clasts, interbedded with FA1 of the Ali Baba Member. Near base of measured section 4 (Fig. 1.8). (D) Upward coarsening sand to pebble conglomerate in sand and silt matrix containing pebble-sized gypsum clasts within FA2 in the Ali Baba Member. Along measured section 1 (Fig.1.8).

2.5.2 Interpretation

This association is interpreted as diapir-derived, alluvial-fan deposits that were most likely single failure events with episodes of small, organized fan development that extended from tens of meters up to 1000m from the salt wall. During dry times the exposed diapir was subject to weathering. During sporadic, heavy rainfall events the weathered material of the diapir, including gypsum, dolostone and more soluble evaporites such as halite and sylvite, was transported down slope in debris flows. A high sediment-to-water ratio likely produced a slurry and deposited material as an unsorted mudflow

conglomerate (i.e., Glennie, 1972). These flows are well preserved within the fluvial overbank association and sheet flood and inland sabkha association because there was insufficient stream activity to rework them entirely.

2.6 Facies Association 6: Well-Sorted, Well-Rounded Sandstone

The well-sorted, well-rounded sandstone facies association (FA 6) is most commonly associated with channel-form sandstone and organized conglomerate (FA1) within the Ali Baba Member and is interbedded with tabular-lenticular siltstone and sandstone sheets (FA3) within the Sewemup Member and subordinately interbedded with weakly-bedded to homogeneous sandstone (FA4) in the Tenderfoot Member.

2.6.1 Description

This association is characterized by well sorted and well-rounded fine- to medium- grained sandstone (Fig. 2.14). Beds with planar cross laminations (Sp) are up to 1 m thick and occur as laterally discontinuous bodies above channel-form sandstone (FA1) and as laterally continuous and discontinuous sand sheets within the tabular-to-lenticular siltstone and sandstone sheets facies association (FA3). Some planar cross laminated beds display ripple laminations with crests perpendicular to foreset dips. Horizontally laminated beds (Sh) are interbedded with FA3 and are up to approximately 20 cm in thickness.

2.6.2 Interpretation

This association is interpreted as eolian deposits. Thin, horizontally laminated beds (Sh) represent eolian deposited sheet sands (Glennie, 1970; Fryberger et al., 1979, Fryberger et al., 1983) and cross-stratified sandstone in association with channel-fill sand represents reworked fluvial deposits within wadi channels between flood events during dry periods (Glennie, 1970; Horne, 1975). The fluvial wadi sediments were likely the main source for the interbedded eolian sediment with subsequent flooding also reworking some of the eolian sediment (Glennie, 1972). Some planar cross-stratified

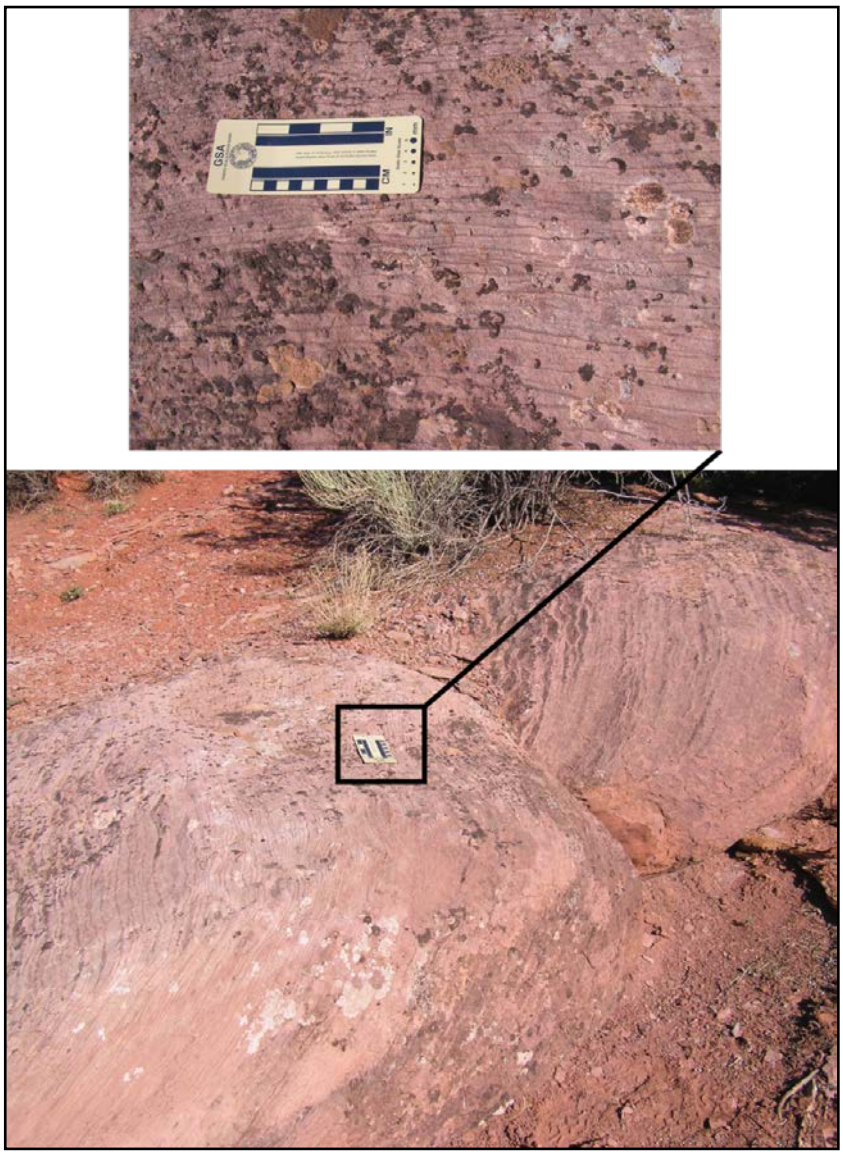

Figure 2.14: Exposure of facies Sp within FA6 of Ali Baba Member in the Red Hills along measured section 5 (Fig.1.8), interpreted as eolian dune. Ripple lamination transverse to slipfaces shown in top photo. View is to east, paleocurrent to north, northwest.

sandstone (Sp) contains ripple-cross laminations perpendicular to foresets (Fig. 2.14). These ripples are interpreted as forming after each primary slipface deposit from shifts in wind direction transverse to slipfaces and with lower velocity than wind that produced the slipface deposits (i.e., Sharp, 1978).

2.7 Facies Association 7: Gypsic Sandstone

The gypsic sandstone facies association (FA7) is present in the Tenderfoot and Sewemup members. The evaporitic material in this association has been interpreted in this study as eolian, rather

than as primary evaporite deposits of a tidal flat sabkha. Because the gypsic sandstone facies association (FA7) is distinguished from FA6 based on grain type, where FA6 is composed solely of lithic grains whereas FA7 is composed dominantly of evaporite grains with subordinate lithic grains, they are described individually.

2.7.1 Description

This association consists of beds of gypsum as much as 2.2 m in thickness. The gypsum ranges from very clean to mixed with ~ 10-45 % siliciclastic grains. In the Tenderfoot Member, a distinct gypsum bed between 1.0-1.5 m thick is present near the base of the member and is laterally continuous throughout the study area and interbedded with FA4 (Fig. 2.15). In the Sewemup Member, gypsum beds up to 0.8 m thick are interbedded with FA3 and are present as lenticular beds up to 5 m wide and as laterally continuous sheets (Fig. 2.16). Sedimentary structures are difficult to discern, likely due to a digenetic recrystallization, but some faint planar cross-laminations are still visible where a significant percentage of siliciclastic grains are present.

2.7.2 Interpretation

This association is interpreted as deposits of eolian gypsum based on planar cross-laminations. The locally exposed salt walls in the area were likely reworked by wind, contributing most of the gypsum detritus to FA7. Gypsum and halite beds deposited in sabkhas and playas that were likely situated to the west, were likely reworked by wind after infrequent periods of rainfall or runoff followed by desiccation (e.g., Talmage & Wootton, 1937; Bowen et al., 2008). These low areas were likely filled with water saturated with gypsum from groundwater and erosion of salt walls.

The gypsum bed near the base of the Tenderfoot Member represent a period where wind was the dominant mode of erosion and deposition in this region, allowing for gypsum sand to blanket the flanks of the Castle Valley salt wall and adjacent mini-basins. The lenticular beds and sheets of gypsum sand in the Sewemup Member were deposited following cycles of sheetflows and inland sabkha of FA3

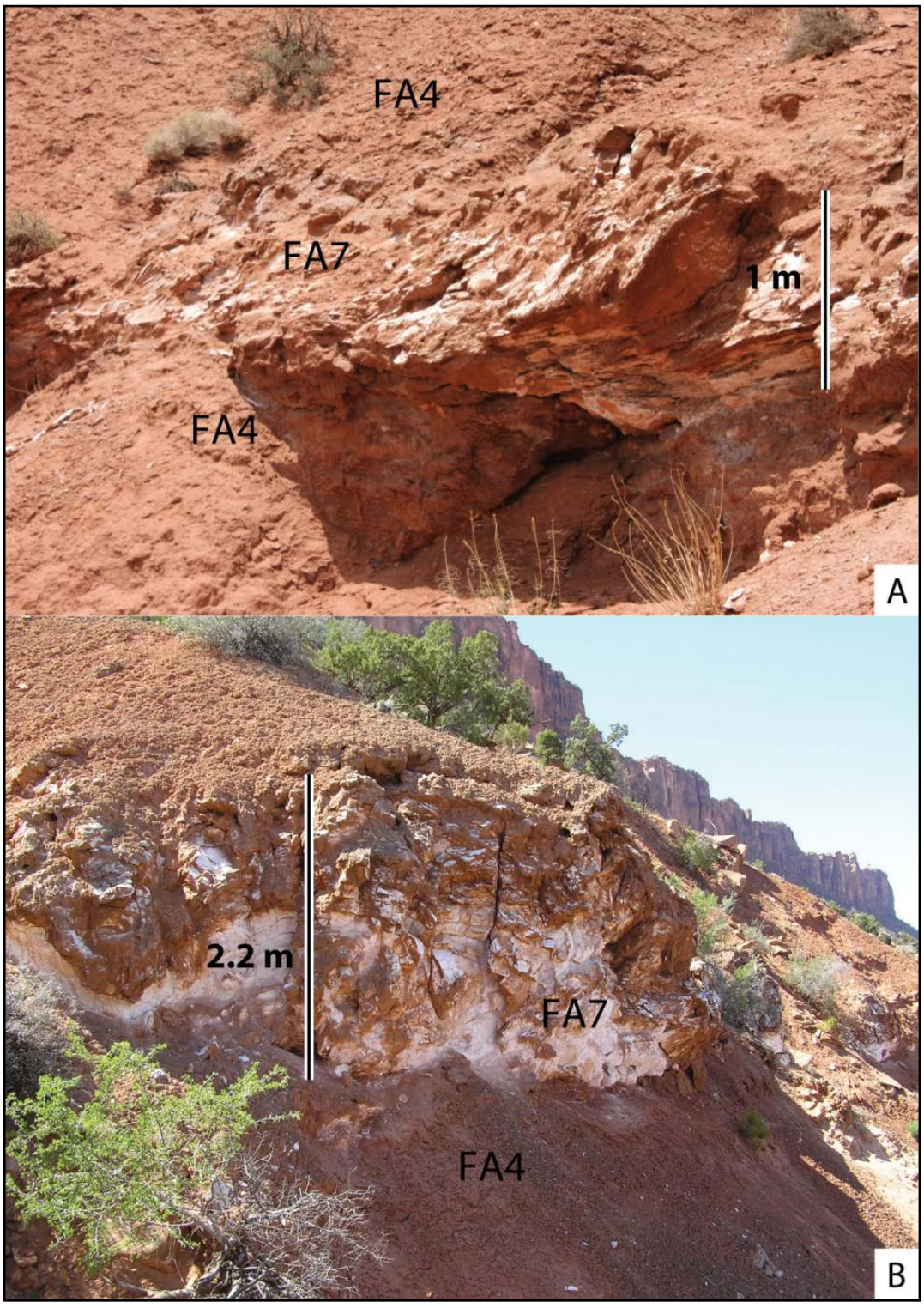

Figure 2.15: Gypsic sandstone facies (FA7) within FA4 of the Tenderfoot Member. (A) Gypsum bed near base of measured section 2, below Pariott Mesa (Fig. 1.8). (B) Gypsum bed on below the Porcupine Rim on southwest side of Castle Valley.

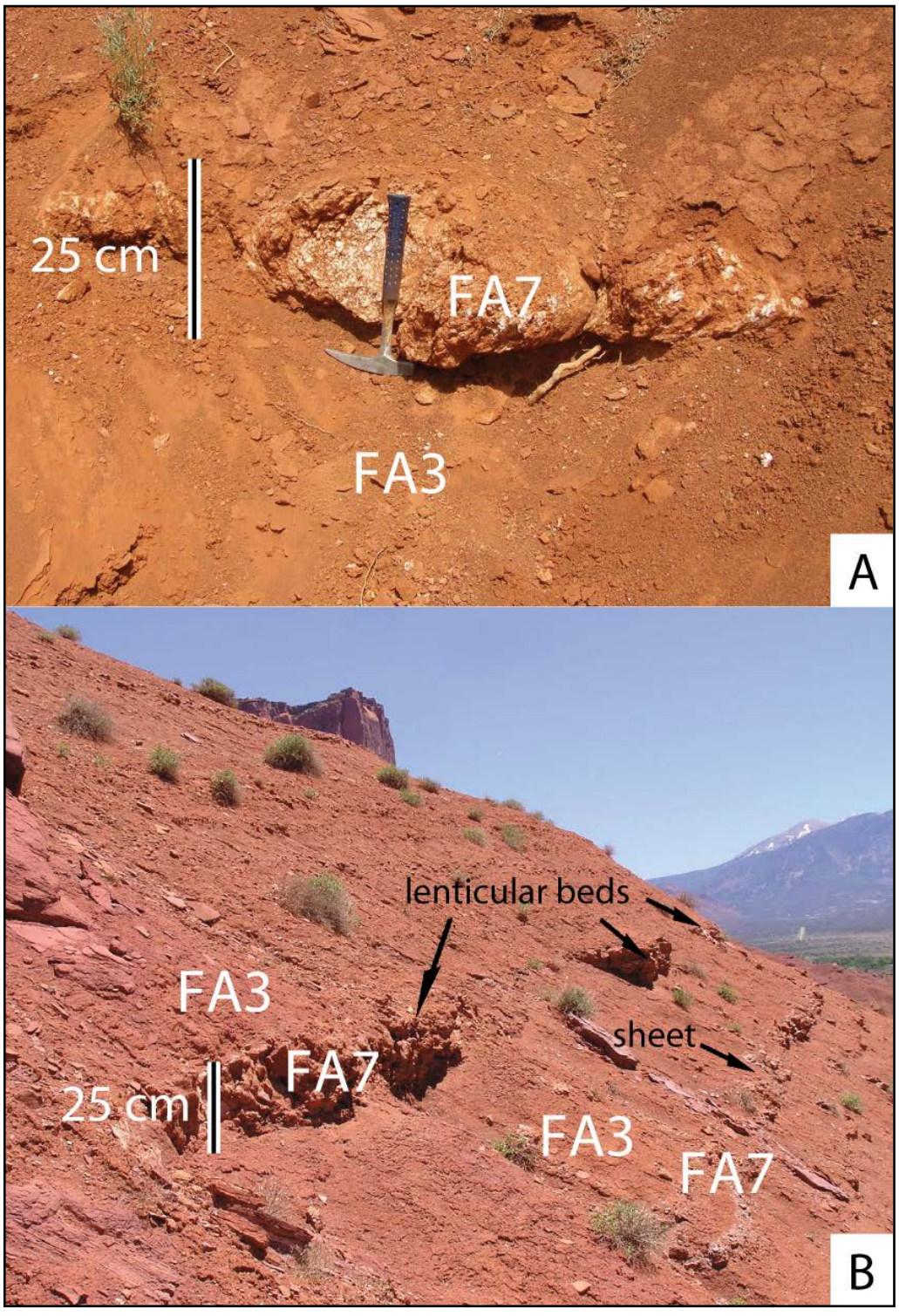

Figure 2.16: Gypsic sandstone facies (FA7) within FA3 of the Sewemup Member. (A) Lenticular gypsum bed near measured section 5 (Fig. 1.8). (B) Lenticular beds and sheet of gypsum along measured section 3 (Fig. 1.8). Lenticular beds are likely filled abandoned channels that flowed away from salt wall (right to left in photo).

deposition and during gypsic paleosol (FA8) development. Episodic rainfall dissected sediments flanking of the Castle Valley salt wall where gypsum sand was deposited within abandoned, lenticular channels that flowed away from the salt wall.

2.8 Facies Association 8: Gypsic Paleosols

The finer-grained facies associations throughout the Moenkopi Formation in the study area show evidence of pedogenesis. Because of their significance and distribution, these features are discussed separately as the gypsic paleosols facies association (FA8) and calcic paleosols facies association (FA9). The most prominent gypsic paleosols are within FA2 of the Ali Baba Member (Fig. 2.17) and in FA3 of the Tenderfoot and Sewemup members. Gypsic paleosols in the lower three members of the Moenkopi are the oldest recorded gypsic paleosols in the world (Lawton and Buck, 2006).

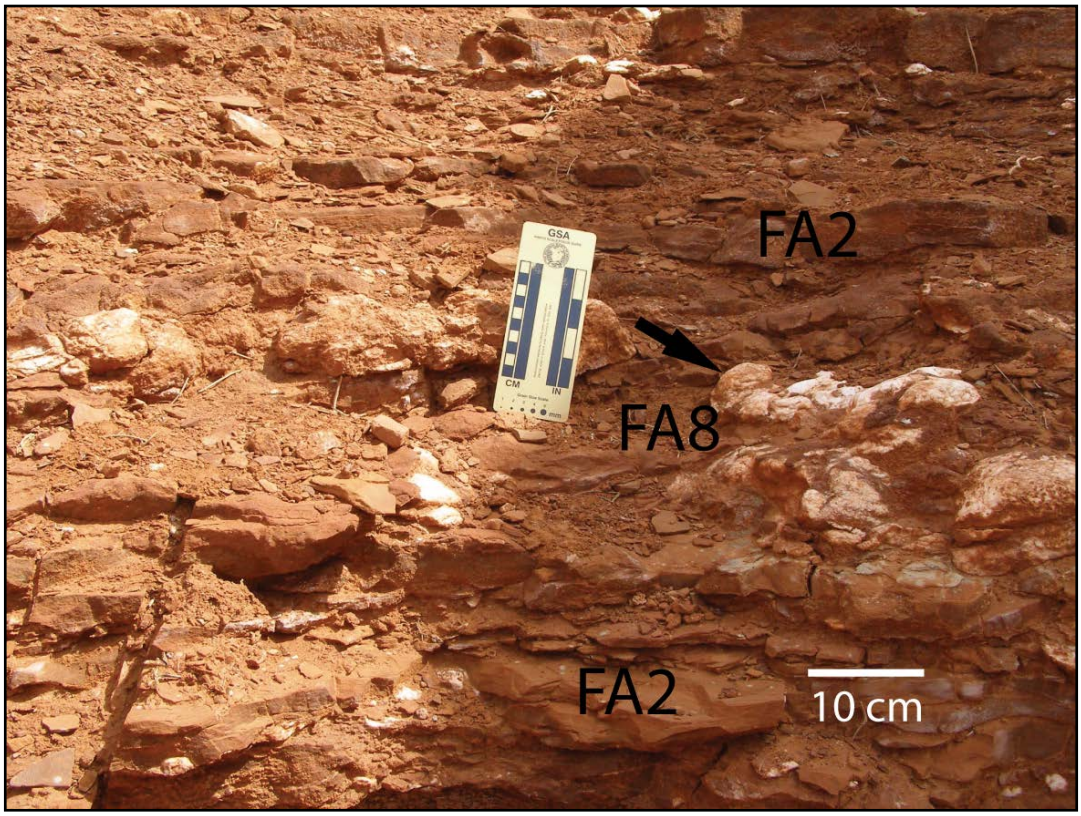

Figure 2.17: Stage III gypsic paleosol (FA8) within siltstone and sandstone of FA2 within the Ali Baba Member along measured section 1 (Fig. 1.8).

2.8.1 Description

This association is characterized by nodules of gypsum ranging in size from mm-scale 'snowballs' (Buck and Van Hoesen, 2002) to 20 cm developed in siltstone and mudstone matrix of the Tenderfoot, Ali Baba (Fig. 2.17) and Sewemup members. The Pariott Member lacks gypsum nodules.

2.8.2 Interpretation

This association is interpreted as stage I through incipient stage III gypsic paleosols developed in siltstone and fine-grained sandstone of FA2 and FA3 (Lawton and Buck, 2006). Gypsic paleosols are an indication that the Castle Valley diapir was periodically exposed during hyper-arid environmental conditions. Gypsum was transported to the adjacent mini-basin by wind as eolian detritus or dissolved in flood waters.

2.9 Facies Association 9: Calcic Paleosols

The Calcic Paleosols facies association (FA9) is only present within the uppermost member, the Pariott Member and is best exposed in the Red Hills.

2.9.1 Description

This facies association is characterized by cm-scale nodules of calcite in siltstone and mudstone matrix (Fig. 2.18) and lacks gypsum nodules. Other pedogenic features present within the Pariott Member include mottled, variegated shales with blocky structure, root traces and faint, mm-scale burrows.

2.9.2 Interpretation

This association is interpreted as stage 2 calcic paleosols developed in siltstone and fine-grained sandstone of FA2 and FA1. Calcic paleosols of the Pariott Member developed during a semi-arid paleoclimatic conditions (Prochnow et al., 2005).

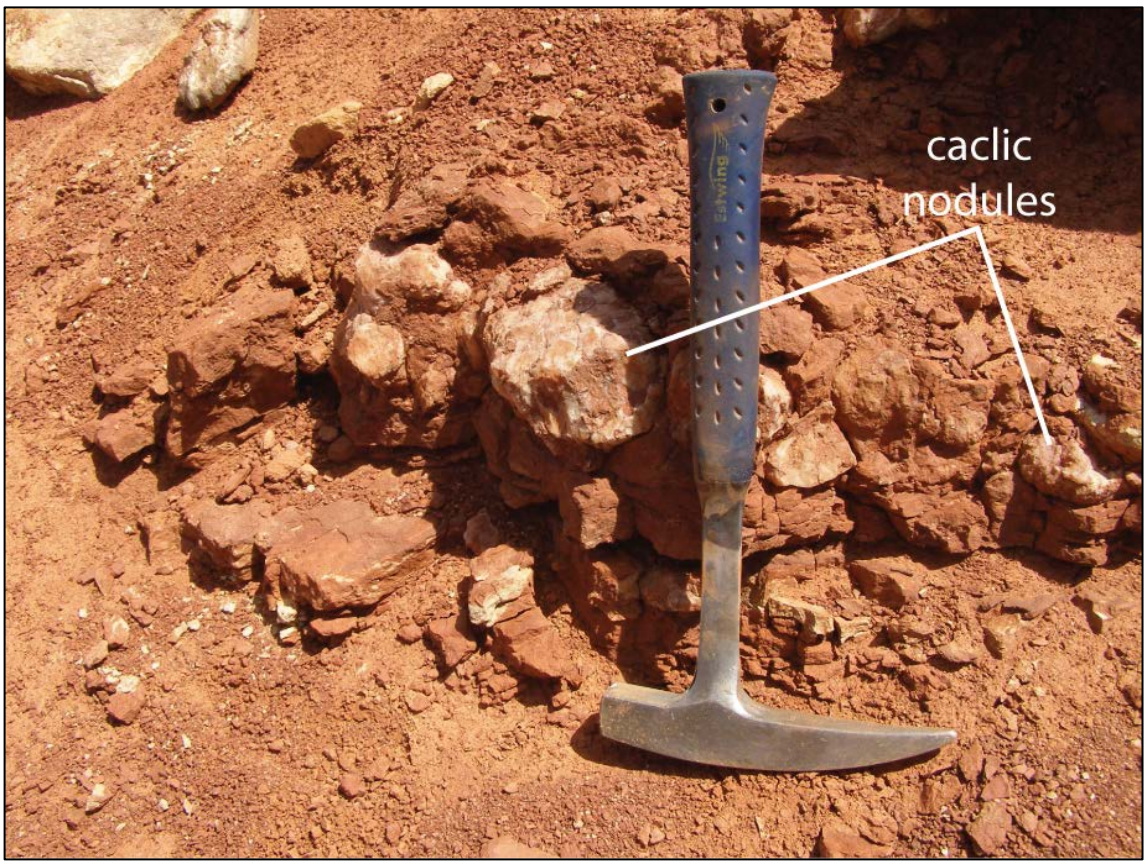

Figure 2.18: Calcic nodules within FA2 of Pariott Member. Near measured section 5 (Fig. 1.8) in Red Hills. Hammer is 25 cm.

Chapter 3

STRATIGRAPHIC DISTRIBUTION OF FACIES ASSOCIATIONS

Nine facies associations in this study record fluvial and eolian deposition and pedogenesis in four Moenkopi Formation members on the margins of the Castle Valley. This section describes Moenkopi member thickness variations and how the facies associations are stratigraphically arranged in the Moenkopi Formation (Fig. 3.1, Plates 1 and 2). Based on these, interpretations of salt-wall highs, exposure of salt and areas of subsidence are presented as four stages of development.

3.1 Tenderfoot Member

The Tenderfoot Member is subdivided into two correlatable units: a lower unit of FA4 with an interbedded FA7 and an upper unit of FA3. From section 5, the Tenderfoot Member thickens to the west-southwest from 29m (FA4=25m, FA3=4m) to 48m (FA4=33m, FA3=15m) at section 6. It also thickens away from the weld to the east at section 2 to 65m (FA4=20m, FA3=45m). From the thickest exposure at section 2, it thins to the east at section 1 to 24m (FA4=17m, FA3=7m). The thickness of the member at sections 3 and 4, where it is not exposed, is inferred to be thicker than the 45m at section 2 based on thickness variations in overlying strata. The eolian gypsic sand sheet (FA7) ranges between 1.0m to 1.5m across the study area. It is present on the margins of the salt wall but is absent on the west-southwest side of the weld at the northwestern end of the valley.

A shift from distal wadi fan deposits (FA4) with an interbedded eolian gypsic sandstone (FA7) in the lower part to unconfined channel and sheet flood (FA3) deposits in the upper. The Tenderfoot is laterally continuous in the Parriott minibasin and is exposed throughout the walls bounding Castle Valley. It dips below the surface within the Red Hills, ~1km east of the weld near the base of measured section 3 (Fig. 1.8). Tenderfoot strata overlie the Permian Cutler Formation on an angular unconformity (6°-12°) along the margins of Castle Valley, within ~200m-250m of the salt wall. It is best exposed and most accessible in the study area on the northeast margin of Castle Valley (Figs. 1.8 and 3.2) where all

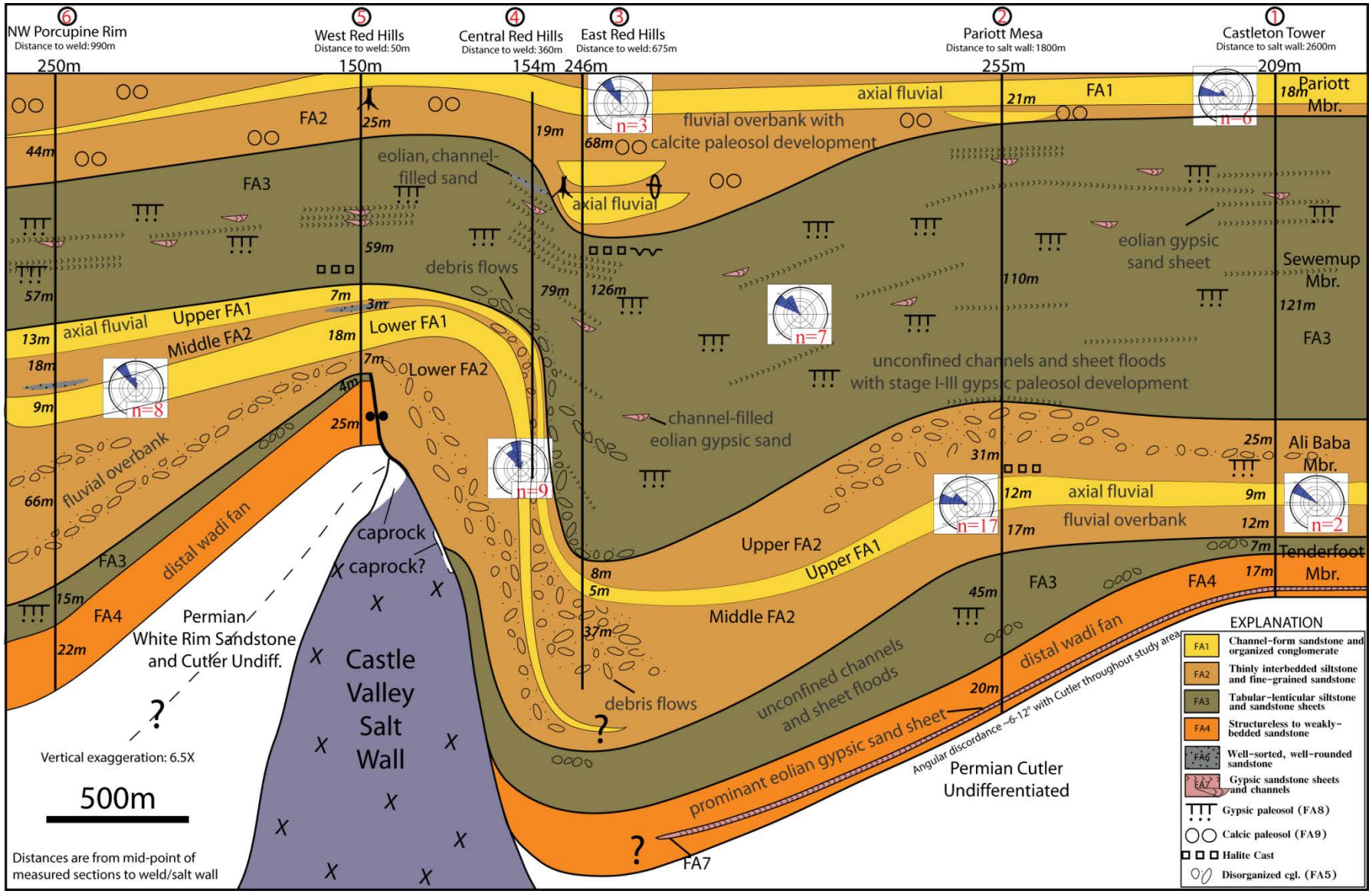

Figure 3.1: Schematic cross-section of Moenkopi-member stratigraphy and distribution of depositional facies associations, flattened on the top of the Pariott Member. Distances between measured sections are to axis of the Castle Valley salt wall.

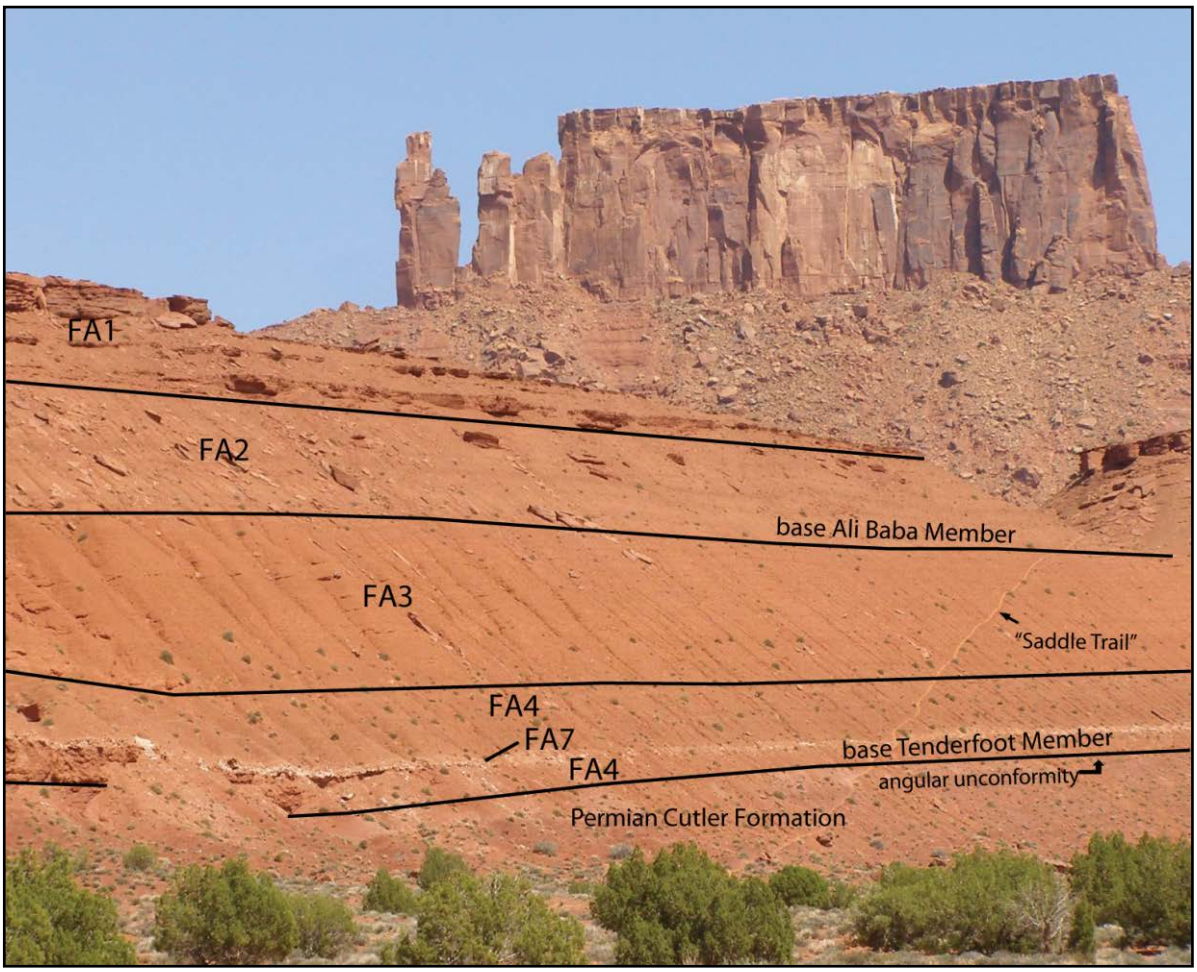

Figure 3.2: Facies associations and subtle contacts through "Saddle Trail" between Pariott Mesa (left of photo) and Castleton Tower (right of photo). The Tenderfoot Member is best exposed here with distal wadi fan deposits of FA4, a prominent eolian gypsic sandstone (FA7) within the FA4 and deposits of unconfined channels and sheet floods of FA3. The Ali Baba Member overlies the Tenderfoot Member here with fluvial overbank deposits of FA2 and axial fluvial deposits of FA1.

three facies associations (FA4, FA3 and FA7) that comprise the member (Fig. 3.3) are well-exposed. Minor occurrences of weakly developed gypsic paleosols are also present here (FA8). These strata are offset at the weld, between measured sections 4 and 5.

An approximately 17- to 20-m bed of distal fluvial wadi-fan (FA4) sediments directly overlies the contact with the Cutler Formation (Figs. 3.3) along the northeast margin of the valley (recorded in measured sections 1 and 2). Sediment within this unit is interpreted to be derived by reworking Cutler sediment based on the abundance of mica, frosted grains and the small grain size of similar composition as Cutler Formation (Shoemaker and Newman, 1959). A prominent 1.5 m to 2.2 m eolian gypsum bed is

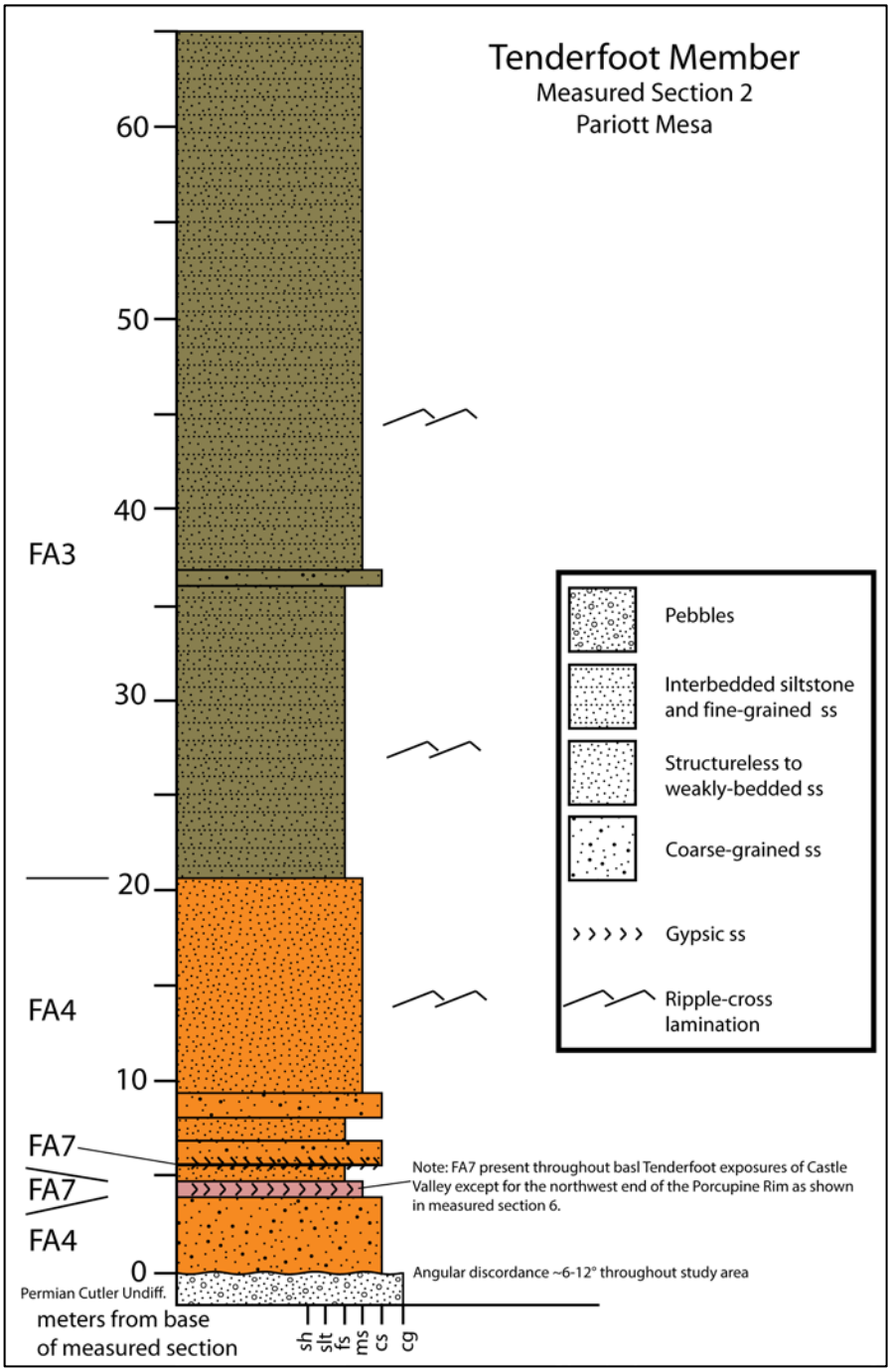

Figure 3.3: Tenderfoot Member stratigraphic section from Pariott Mesa showing representative distribution of facies associations within the member. See Plate 2 for lateral variation.

present within the distal wadi-fan deposits of FA4, ~1.5-m from the base of the member and is well-exposed on the northeast and southwest (based on facies mapping, not in measured section) margins of Castle Valley. On the west side of the weld, FA4 is 25-m thick, ~50m from the weld (measured section 5), and is 23-m thick at measured section 6 below the Porcupine Rim. Here it thickens to ~30m toward

the west, 600m from the weld before it dips subsurface (Fig. 3.4) and lacks the distinctive gypsic sand of FA7 present east of the weld (Plate 2). On the southwest margin of Castle Valley, the gypsum bed is ~2.2m thick and thins to zero to the northwest in the vicinity of the diapir/weld and measured sections 5 and 6, where it appears to have been eroded or not deposited.

The upper part of the Tenderfoot Member is characterized by distal wadi-fan deposits (FA4) that grade upward into unconfined channel and sheet flood deposits (FA3) (Figs. 3.2 and 3.3) containing weakly developed gypsic paleosols (FA8) and occasional interbeds of thin (<0.20cm) debris-flow deposits (FA5). FA3 thickens from ~7m at section 1, ~1km from salt wall, to 45m thick at section 2 below Pariott Mesa (~600m from salt wall margin) at measured section 2. On the west side of the weld, FA3 is much thinner at measured section 5 (~4m) and it thickens from ~4m to 15m at measured section 6 (Porcupine Rim). It thickens from ~4m at section 5 to ~55m within ~800m before it dips subsurface.

3.2 Ali Baba Member

The Ali Baba is subdivided into five correlatable units; a lower FA2, a lower FA1, a middle FA2, an upper FA1 and an upper FA2 (Fig. 3.1). From section 5 the Ali Baba Member thickens from 35m to 106m at section 6 and thickens to the east to 60m at section 2. Between sections 5 and 2, at sections 3 and 4, the base of the Ali Baba is not exposed and is estimated to be at least 75m thick.

The Ali Baba Member is composed of predominantly of fluvial overbank (FA2) siltstones with abundant debris-flow conglomerates (FA5) alternating with axial-fluvial channels (FA1). The member is divided into five sub-units; in ascending order they are a lower FA2, a lower FA1, a middle FA2, an upper FA1 and an upper FA2 (Fig. 3.1). The lower contact of the Ali Baba Member with the Tenderfoot Member, described regionally as a surface of erosion by Stewart et al. (1972) and locally as an angular unconformity by Shoemaker (1959), is overlain by fluvial channel-form sandstones. However, in Castle Valley the contact is less distinct and is regionally recognized by a color change from reddish-brown (Tenderfoot Member) to chocolate-brown (Ali Baba Member) sandstone (Fig. 3.5) that corresponds to a

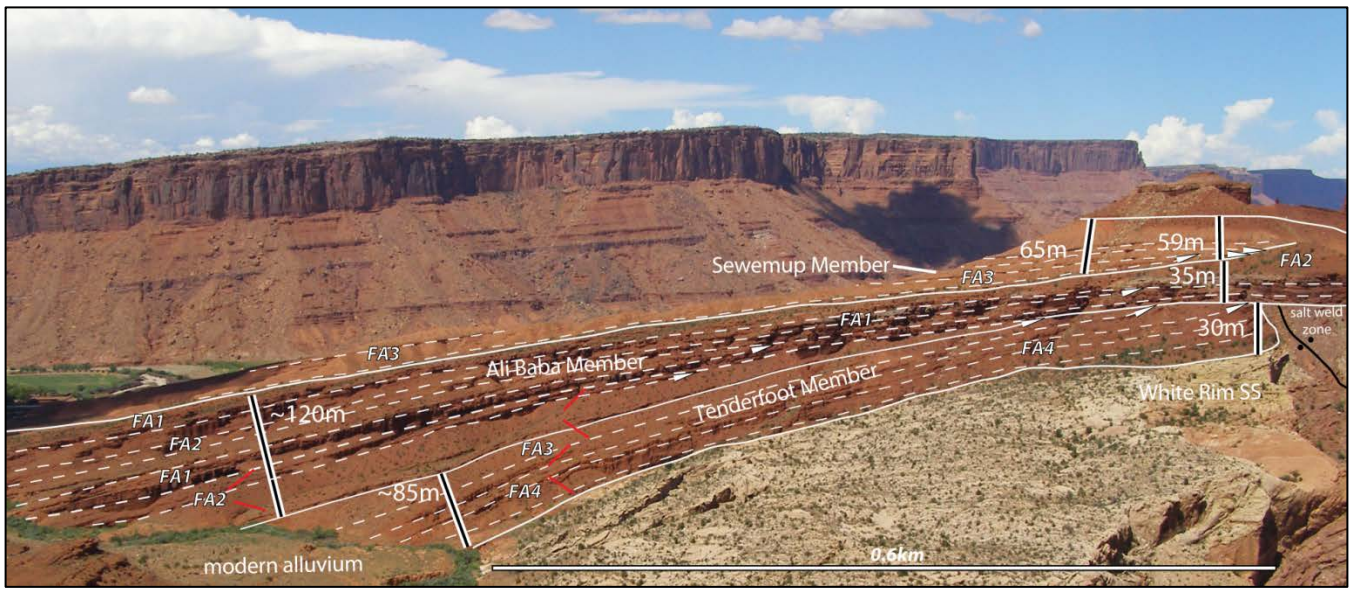

Figure 3.4: Thickening of the Tenderfoot, Ali Baba and Sewemup members to the west, away from the weld (approximately located at right) showing facies associations. Solid lines are boundaries between members. Dashed lines along bedding surfaces show angular relationships within and between members. Arrows locate selected stratal terminations.

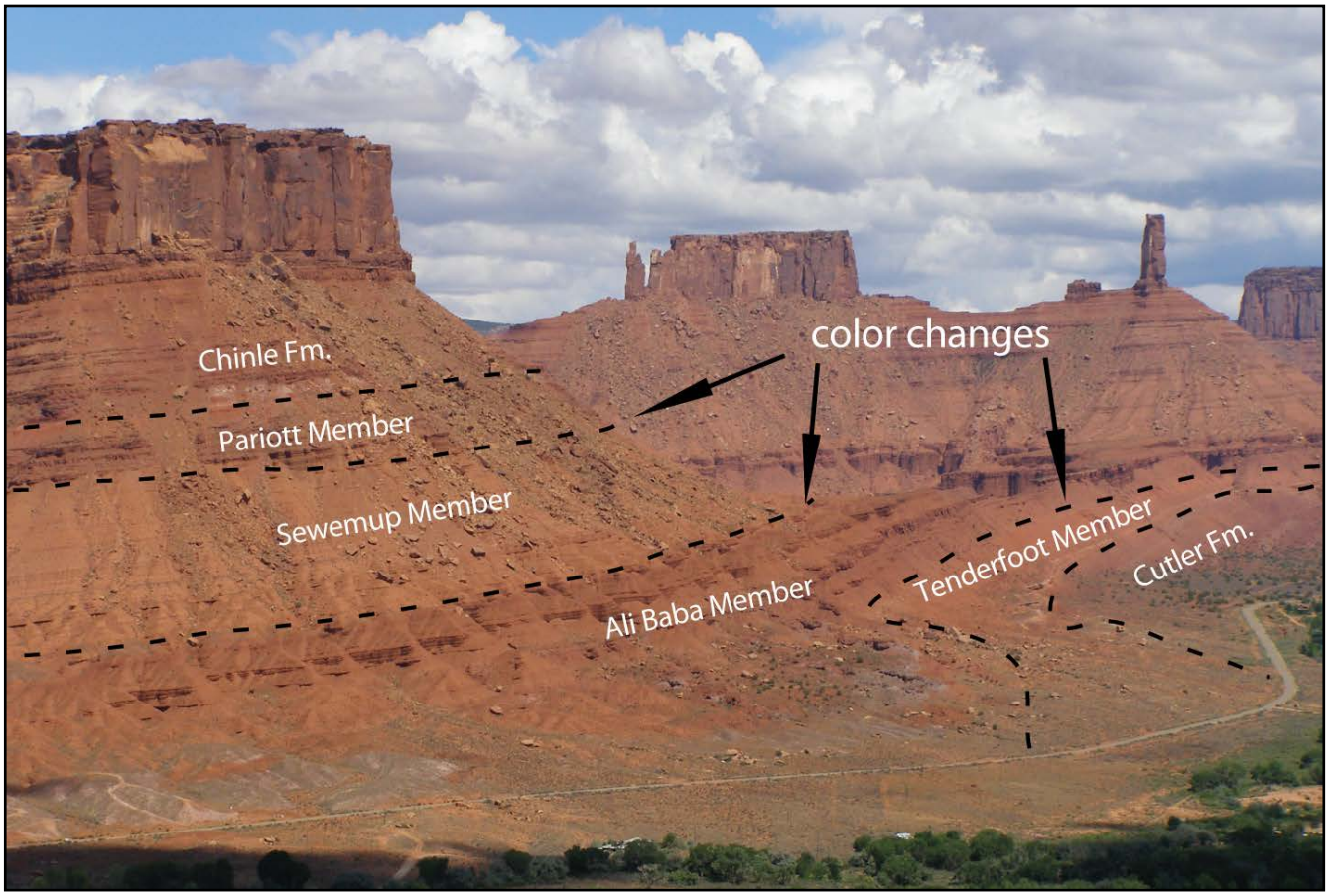

Figure 3.5: Subtle color changes between the Tenderfoot and Ali Baba Members and between the Sewemup and Pariott members help distinguish the members.

change in facies association from tabular-to-lenticular siltstone and sandstone sheets (FA3) to thinly interbedded siltstone and fine-grained sandstone (FA2) that contain thin, disorganized conglomerate beds containing gypsum and dolostone clasts (FA5) (Fig. 3.6, Plate 2). In Castle Valley the contact is gradational and apparently conformable along the margins of the valley, as is the case in Moab Valley (Stewart, 1959).

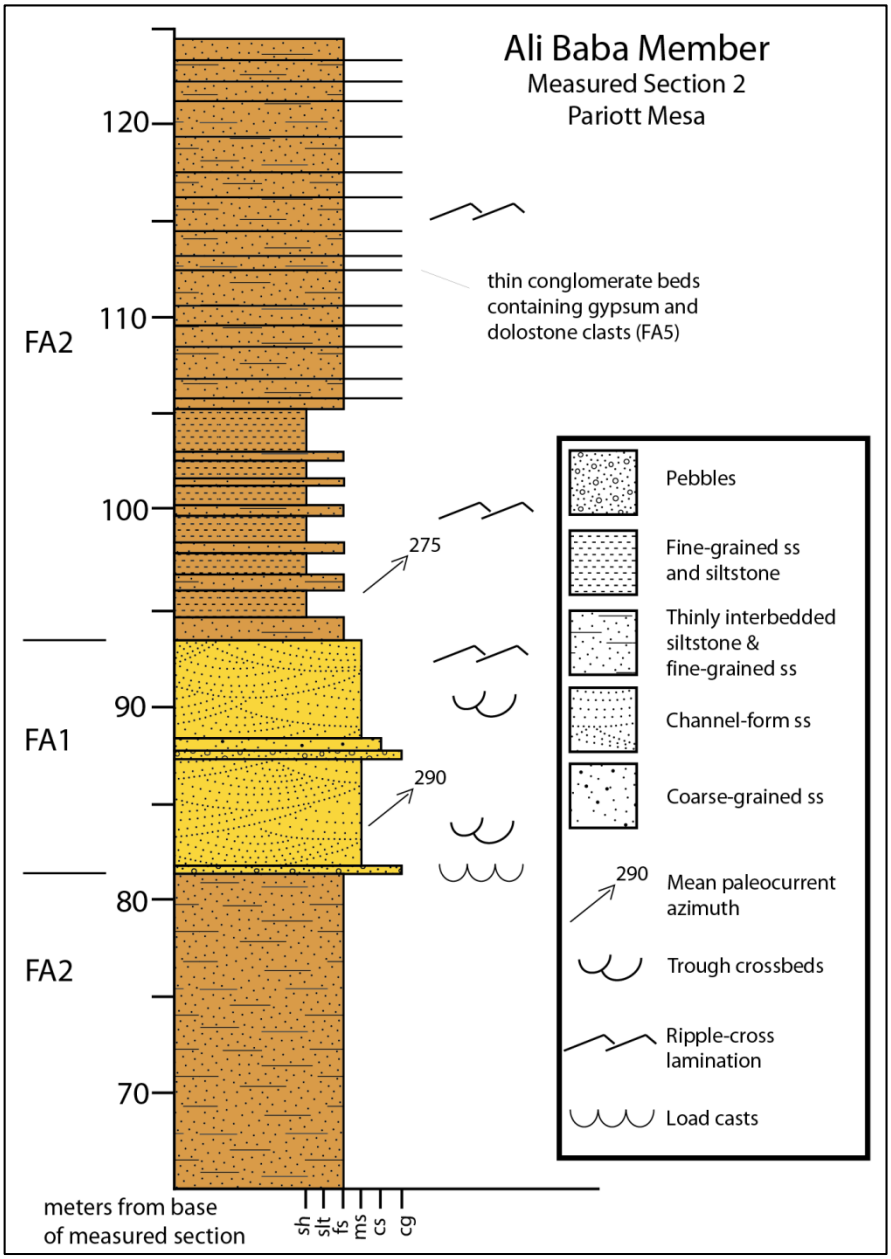

Figure 3.6: Ali Baba Member stratigraphic section from Pariott Mesa showing representative distribution of facies associations within the member. See Plate 2 for lateral variation.

The Ali Baba Member is largely characterized by fluvial overbank association (FA2) (lower, middle and upper units) that contains abundant debris flows (FA5) and minor, weakly-developed stage I-III gypsic paleosol development (FA8) (e.g., Buck and Van Hoesen). It is interbedded with subordinate, but prominent lower and upper axial fluvial (FA1) deposits, which are channelized into underlying deposits and commonly contain intraclasts composed of soil nodules (organized conglomerate component of FA1). Sandstone bodies of FA1 are channel-form, occurring commonly as single stories and less commonly multi-stories adjacent to the Castle Valley salt wall. Composite thicknesses range from 50 cm to 10 m. Channels have a high width-to-depth ratio and are often trough cross-bedded with abundant rip-up clasts at their bases and grade upward into climbing ripple cross-laminations. At sections 1 and 2, one axial fluvial association (FA1) is present as a middle unit. At measured sections 4, 5 and 6, and in exposures in a deeply incised gully near the location of the Grand River 1-State well (Fig. 3.7), the member is characterized by a two axial fluvial (FA1) units within FA2. From section 1, under Castleton Tower, to section 2 under Pariott Mesa, ~2km to the west, these strata exhibit overall thickening from 46m to ~60m. The stratigraphic exposure is incomplete further to the west near the weld at measured sections 3 and 4, but based on thickening of overlying strata, the presence of a second, lower axial fluvial unit (FA1) in measured section 4 and growth strata geometries within these strata over the weld (Figs. 1.8 and 3.8, Plate 1), the thickening likely continues under measured sections 3 and 4, just east of the weld to at least an estimated 75m. The inferred thickness is due to unexposed strata at measured sections 3 and 4 and based on assumption that subsidence and thickness was similar to that on the west side of the weld during this interval. Ali Baba strata thin over the weld to ~35m thick (Fig. 3.8), ~50m away from the weld at measured section 5.The strata thicken dramatically to 106m ~1km to the south at measured section 6 and to ~120m thick 1km to the west (Fig. 3.4).

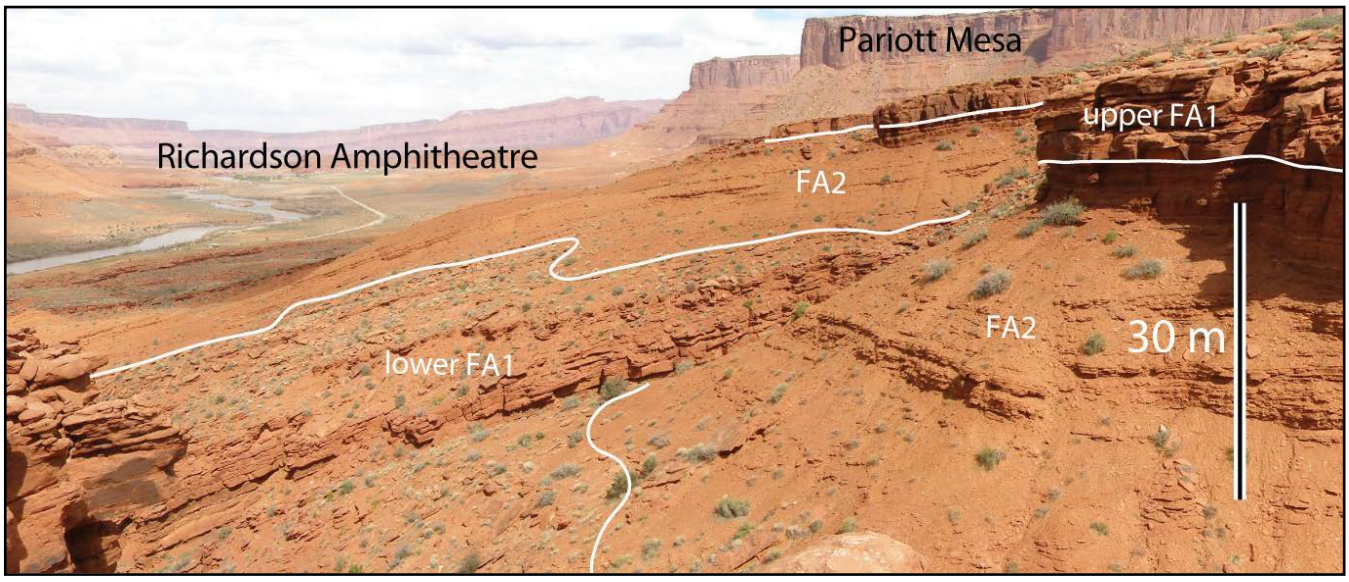

Figure 3.7: Thick cycles of FA1 and FA2 on the north side of the Red Hills.

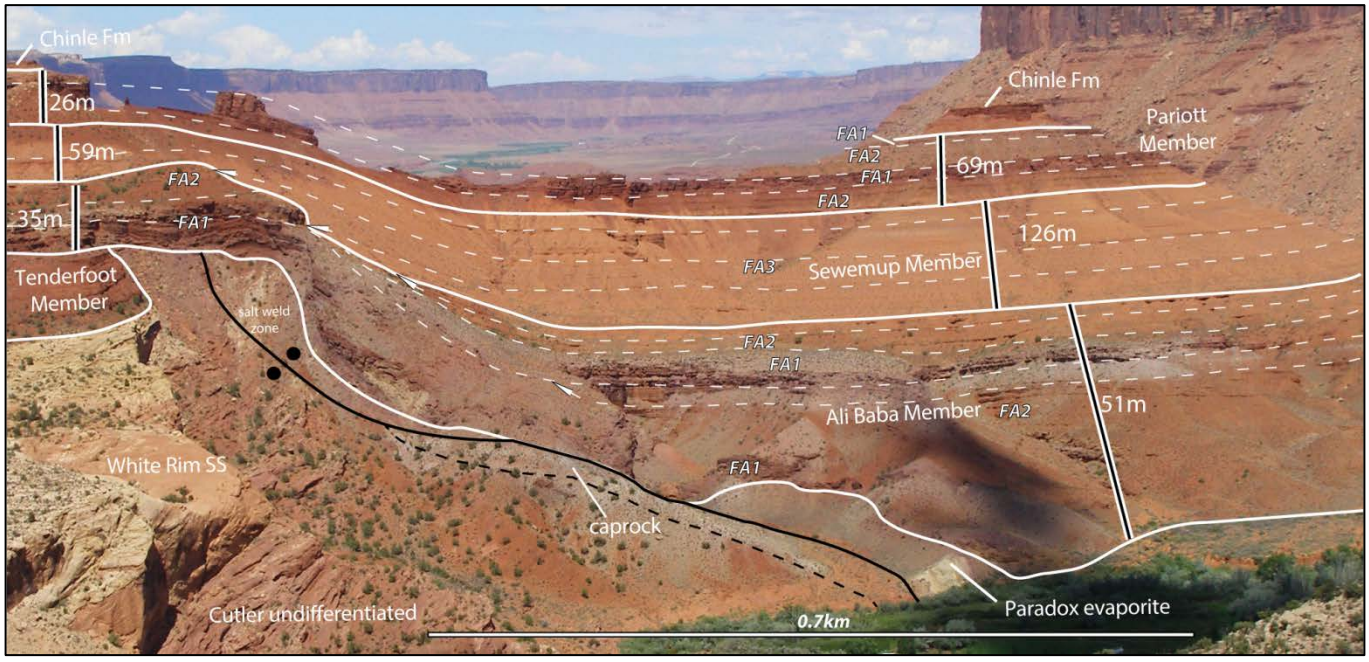

Figure 3.8: Thickening of the Tenderfoot, Ali Baba, Sewemup and Pariott members to the east, away from the weld (approximately located at left). Solid lines are boundaries between members. Dashed lines along bedding surfaces show parallel and angular relationships within and between members. Arrows locate selected stratal terminations.

The lower fluvial overbank (FA2) unit is not present at measured sections 1 and 2 on the northeast margin of Castle Valley but may be present in the subsurface at measured section 3 in the Red Hills. The thickness of the lower FA2 cannot be determined east of the weld but projection from mapping and measured thicknesses from sections 3 and 4 show that there is likely thinning within 700m

of the weld, from >50m (based on thickness at measured section 6) to ~7m over the weld at measured section 5. The lower FA2 laps up against the Paradox Formation on the east side of the weld, where FA2 thins over the weld. From the weld, the lower FA2 thickens dramatically to the west-southwest to ~66m, exhibiting unconformable surfaces within the member and with the underlying Tenderfoot Member (Fig. 3.4). Debris flows with diapir-derived material are present over and adjacent to the weld near measured section 5 and at measured section 6.

The lower axial fluvial (FA1) unit is not present at measured sections 1 and 2 and is likely present in the Red Hills subsurface at measured section 3. At measured section 4, the lower FA1 is ~12m thick, exhibits single- and multi-storied bodies and northerly paleocurrent indicators that are parallel to sub-parallel to the axis of the weld (Fig. 1.6, Plate 2) and thickens to the west over the weld to 18m at measured section 5 where it exhibits increase in multi-storey bodies. From here, the lower FA1 thins to ~9m to the south, ~1km from the weld at measured section 6, where it exhibits northwesterly paleocurrent indicators, subparallel to the axis of the weld. To the northwest of the weld, ~1km away, it maintains thickness or thickens slightly as much as ~15m and exhibits northwesterly paleocurrent indicators, transverse to the axis of the weld (Fig. 1.6).

The middle fluvial overbank (FA2) unit from measured sections 4, 5 and 6 is present as the basal facies association in measured sections 1 and 2, as well as the incomplete measured section 3 in the Red Hills. This unit thickens from ~12m at Castleton Tower to ~37m in the Red Hills at measured section 3, which lacks exposure of the lower part of the facies association and, thus is likely thicker. From measured section 3, the middle FA2 thins significantly to the west to 26m at measured section 4 and then to 3m over the weld at measured section 5 (Fig. 3.8). South of the weld it thickens from 3m to 18m at measured section 6, ~1km away and thickens to the west to ~10m, ~ 800m away (Fig. 3.4). Debris flows (FA5) with diapir-derived material are absent within the middle FA2 west of the weld at measured sections 6 and 5 and they are absent further east at measured sections 1 and 2. However, they are thick

150m-700m east of the weld in measured sections 3 and 4. These FA5 deposits are more abundant in the Ali Baba than in any other Moenkopi member in the study.

The upper axial fluvial (FA1) unit is present throughout the study area and thickens away from the weld to the west and east. From section 5 at the weld, it thickens from ~7m to the east to ~12m at section 2 (~600m from salt wall margin). From the weld it thickens slightly to the west to ~12m at measured section 6. Channel bodies are primarily single-storied with a moderate increase in multi-storied bodies on the northeast flank of the salt wall at measured sections 1 and 2, where it also exhibits westerly and northwesterly paleocurrent indicators (Fig. 1.6), sub-parallel to the axis of the salt wall.

The upper fluvial overbank (FA2) unit is not present west of the weld at measured sections 6 and 5. East of the weld, the upper FA2 thickens from ~2.5m at measured section 4 to 31m at measured section 2, under Pariott Mesa. It thins slightly to 24m at measured section 1. Debris flow (FA5) deposits are abundant in the upper part of measured section 2 (~600m from salt wall margin), with only a couple of debris-flow deposits present at measured section 1 (~1km from salt wall margin).

3.3 Sewemup Member

The Sewemup Member (Fig. 3.9) is not subdivided as it is composed primarily of FA3 with interbedded FA7 and FA5 and gypsic paleosol (FA8) development. Sewemup strata in section 5, adjacent to the weld, are 59m thick. To the south at section 6, the strata are essentially the same thickness at 57m. To the north and east, strata is largely eroded and dips subsurface and thickens to ~>150m 2.2km away, in cliffs north of the Colorado River (Fig. 1.6). From the weld the strata thicken to the east to126m at section 3, 800m away (Fig. 3.8). Thickness further to the east at measured sections 1 (~600m from salt wall margin) and 2 (~1km from salt wall margin) are 110m and 121m, respectively.

The basal contact of the Sewemup Member with the Ali Baba Member is gradational and conformable within the field area. The contact is marked by a color change from dark brown beds of the Ali Baba below to light brown beds of the Sewemup Member (Shoemaker and Newman, 1959) and is

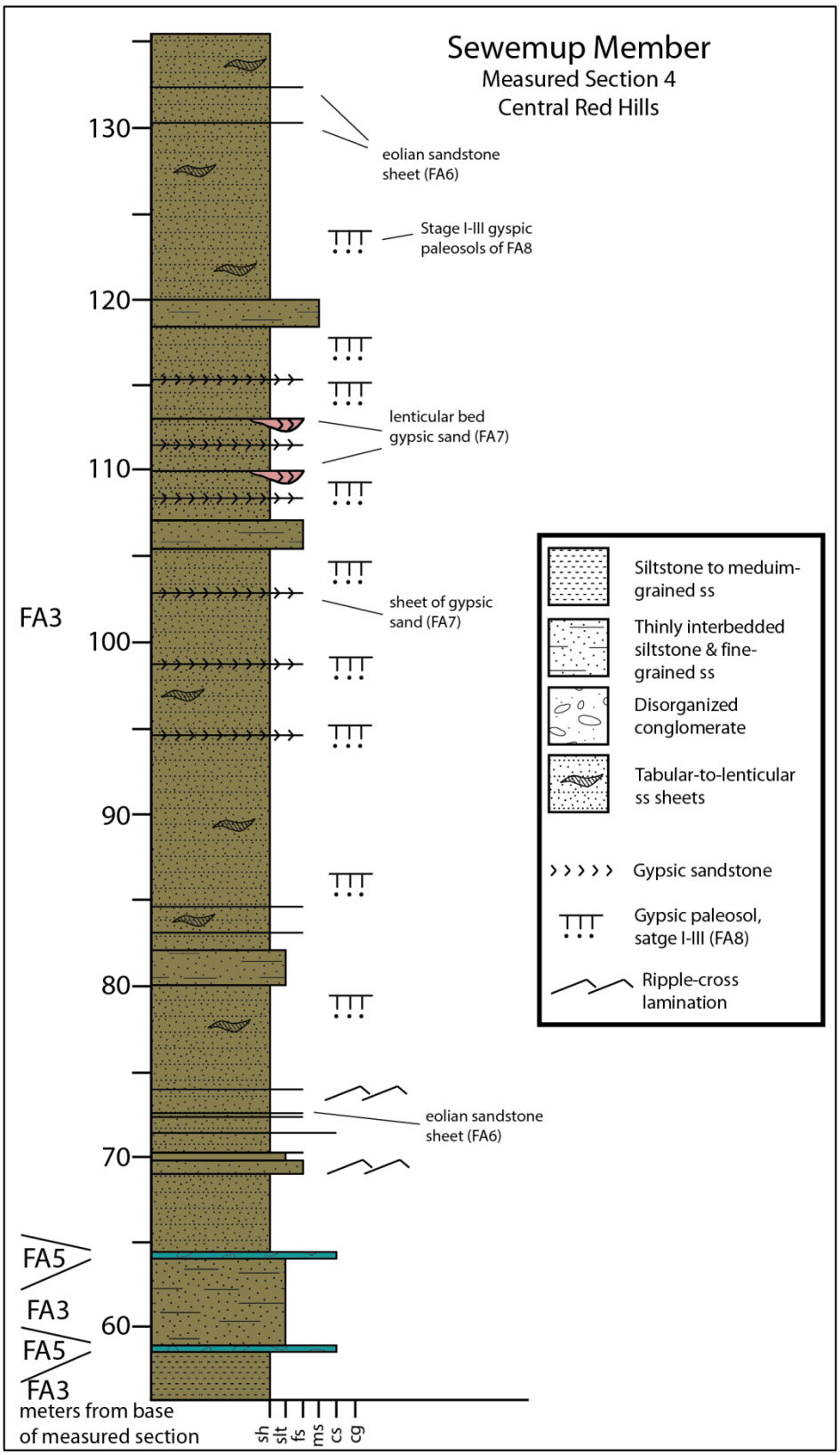

Figure 3.9: Sewemup Member stratigraphic section from the central part of the Red Hills showing representative facies associations within the member. See Plate 2 for lateral variation.

composed predominantly of tabular-lenticular siltstone and sandstone (FA3) as laterally continuous beds ranging from a few cm to 3-m thick (Fig. 3.9) that were deposited in unconfined channels and sheet floods. The Sewemup Member, overall, is more thinly bedded than other Moenkopi members in the study area. Sandstones are ripple-cross laminated and contain desiccation cracks and cubic halite casts. Stage I-III gypsic paleosols as much as 2-m thick are developed in siltstones and mudstones throughout Sewemup strata. Gypsum is also present as laterally continuous sheets as much as 30-cm thick and as laterally discontinuous lenses as much as 0.5 m in height and 1 m wide. These are interpreted as eolian gypsum sand sheets and channels filled with eolian gypsum, respectively. Channels filled with eolian gypsic sand appear to run perpendicular to the salt wall. Both gypsic paleosols and gypsic sand sheets are more abundant and more closely spaced near the top of the member. And debris-flow deposits (FA5) are not commonly present. FA5 are present in the Red Hills, east of the weld at measured sections 3 and 4 and are restricted to a few beds in the lower part of the Sewemup Member (Plate 2). These deposits contain smaller clast sizes (up to 3 cm) than in the underlying Ali Baba Member.

3.4 Pariott Member

The Pariott Member (Fig. 3.10) is composed of FA2 with interbedded FA1 (Fig. 3.11). Correlation of FA1 is difficult due to limited exposures. At measured section 5 the Pariott is 25-m thick and thickens to 44m, 1-km away to the southwest at measured section 6. Thickness changes immediately to the west or north of the weld cannot be determined as the Pariott Member is mostly eroded away in the Red Hills area. To the east of the weld, the Pariott thickens from 26m above the weld to 69m within 800m at measured section 3. The Pariott thins to ~20m further east at Pariott Mesa (~ 600m from salt wall margin) and Castleton Tower (~1km from salt wall margin). Axial fluvial (FA1) beds are more abundant in the eastern Red Hills at measured section 3 (Fig. 3.11), where the Pariott Member is thickest, and along the northeast flank of the salt wall at measured sections 1 and 2, where Pariott Member strata are thinnest (Fig. 3.1). Multi-storied bodies are more prevalent in sections 1, 2 and 3.

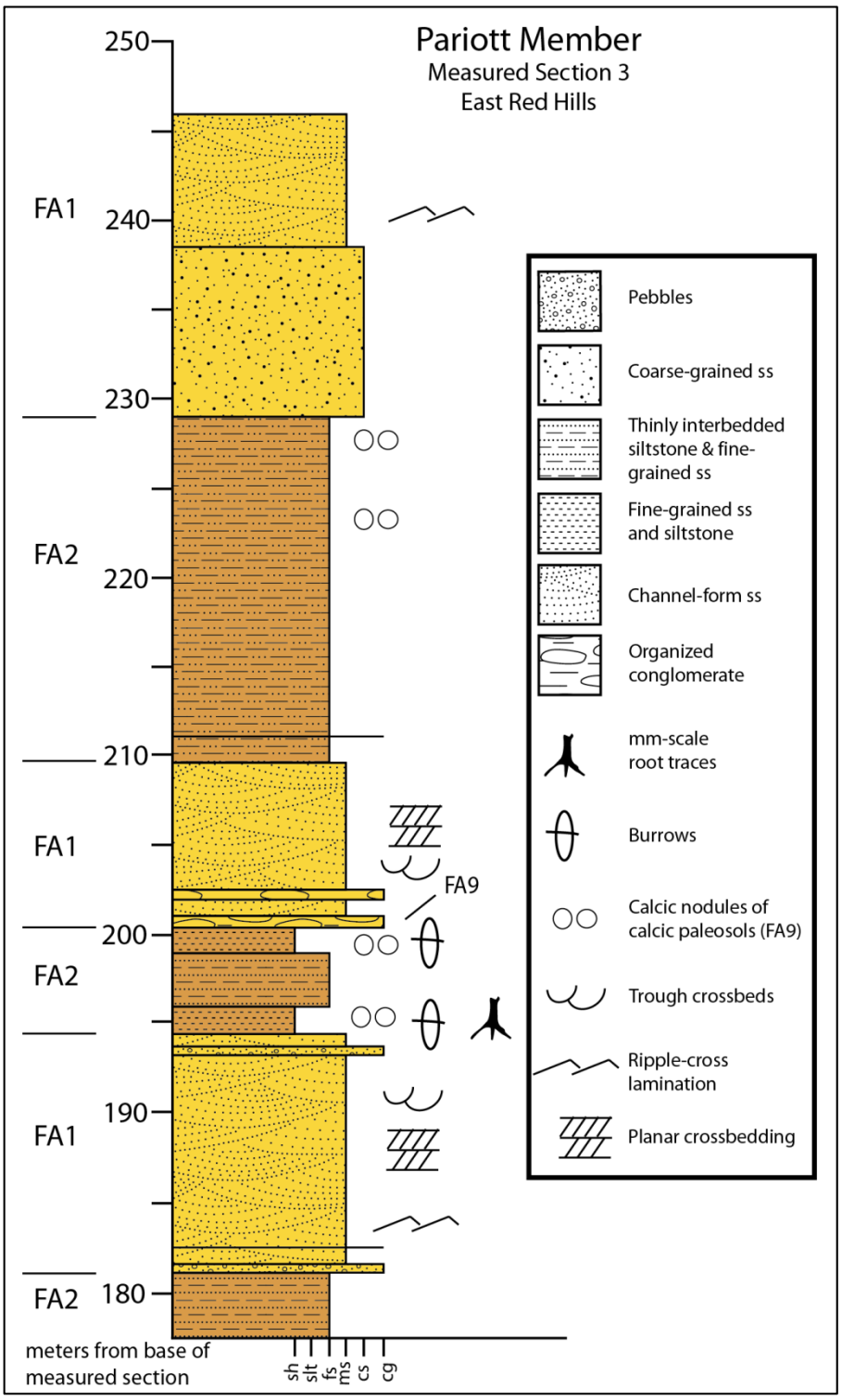

Figure 3.10: Pariott Member stratigraphic section from the east part of the Red Hills showing representative distribution of facies associations within the member at measured section 3. See Plate 2 for lateral variation.

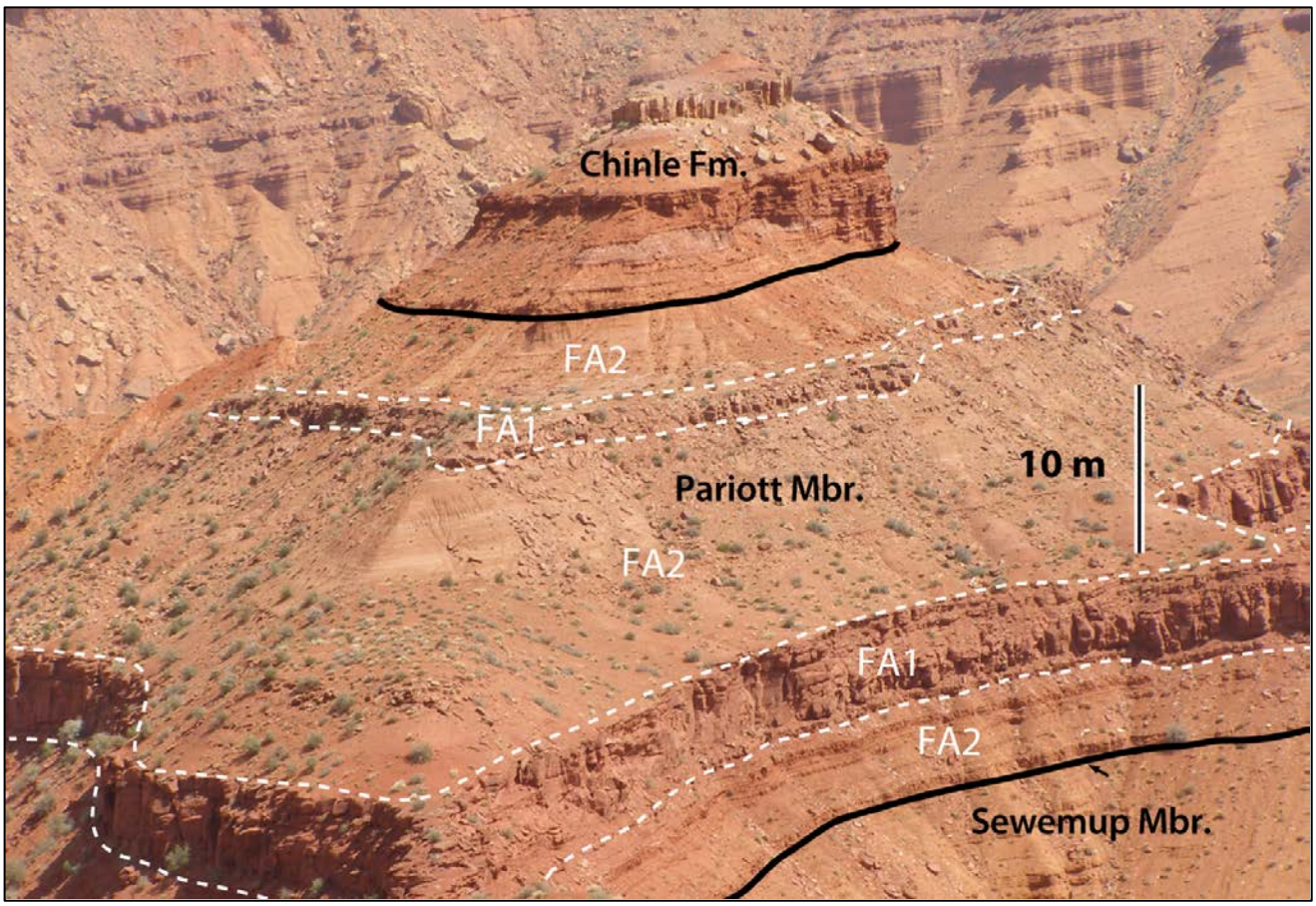

Figure 3.11: Multiple channel-form units (FA1) separated by thinly interbedded siltstone and fine sandstone (FA2) within the Pariott Member in the eastern Red Hills at measured section 3 (Fig. 1.8). FA2 also contains calcic nodules resulting from pedogenesis (FA9).

The Pariott Member disconformably overlies the Sewemup Member on a sharp contact marked by a color change from yellowish-brown to brick-red siltstone and sandstone (Fig. 3.12) and an abrupt reduction in the number of gypsum beds present (Fig. 3.5). The Pariott Member is strikingly different than the underlying members of the Moenkopi Formation. It contains a higher abundance of quartz clasts in conglomerates, detrital gypsum is absent and paleosols are calcic, in contrast with the gypsic paleosols within the underlying Moenkopi members. Gypsic beds, clasts and veins are not present within the member while they are abundant in the lower three Moenkopi members. Debris-flow deposits are absent in the Pariott Member whereas they are present in the underlying members. Mica content is much less in sandstone and fine-grained overbank sediments of the Pariott than in the lower three members.

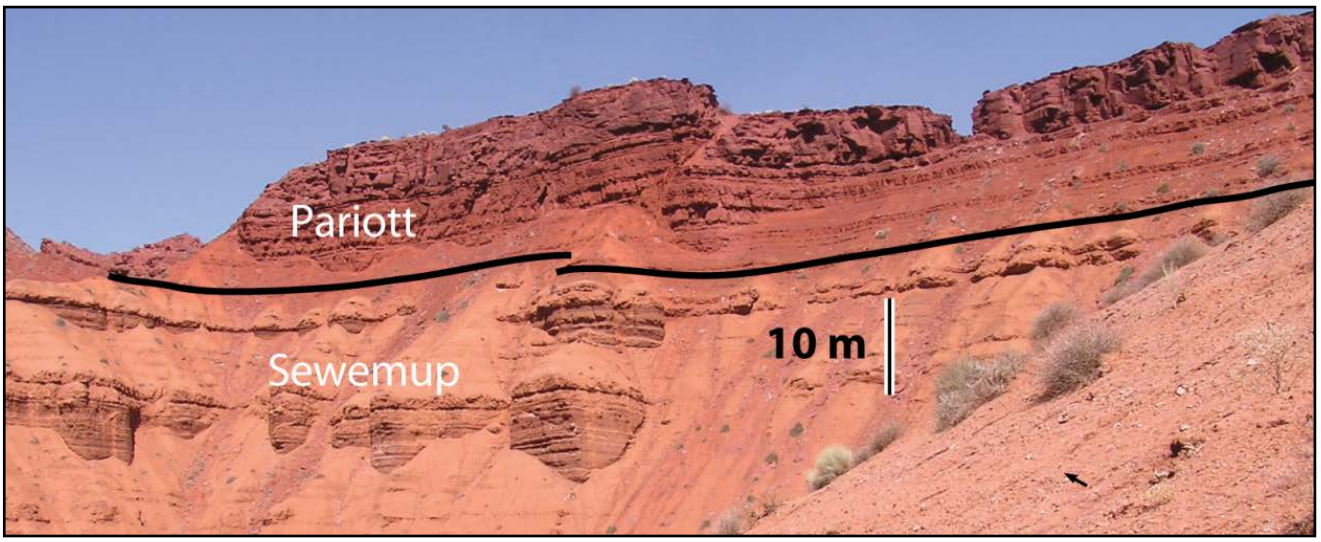

Figure 3.12: Base of Pariott Member in the Red Hills, near measured section 4 (Fig. 1.8), is characterized by a color change to a darker reddish-brown associated with a fine- to medium-grained friable sandstone ~50 cm thick.

The Pariott Member is also the only member of the Moenkopi Formation in the study area with root traces and burrows. The root traces and burrows are on the mm-scale.

The Pariott is composed of axial fluvial (FA1) and associated overbank deposits (FA2). The siltstones and shales of FA2 are variegated with red, orange and purple colors and contain a calcic paleosol (FA9) overprint. Axial fluvial deposits are characterized by both single- and multi-storeys that are difficult to correlate between measured sections in the lower part of the member. The base of the Pariott Member is also difficult to discern. Below Castleton Tower and in the western Red Hills, the basal unit is fine- to medium-grained friable sandstone about 50 cm thick (Figs. 3.10 and 3.11). Below Porcupine Rim at measured section 6 and below Parriott Mesa at measured section 2, this sandstone is absent. The base of the member in these locations is a unit of siltstone, mudstone and fine-grained sandstone interpreted as fluvial overbank deposits (FA2). This is overlain and scoured by fluvial sandstone (FA1) that exhibits variable thickness. In the eastern Red Hills there are multiple sets of channels (FA1) separated by overbank facies (FA2) (Fig. 3.12).

3.5 Stages of Deposition and Salt-Sediment Interaction

Based on these distinctive thickness variations and facies association distributions, four distinct stages of salt-sediment interaction that correspond to each member are defined (Figure 3.13).

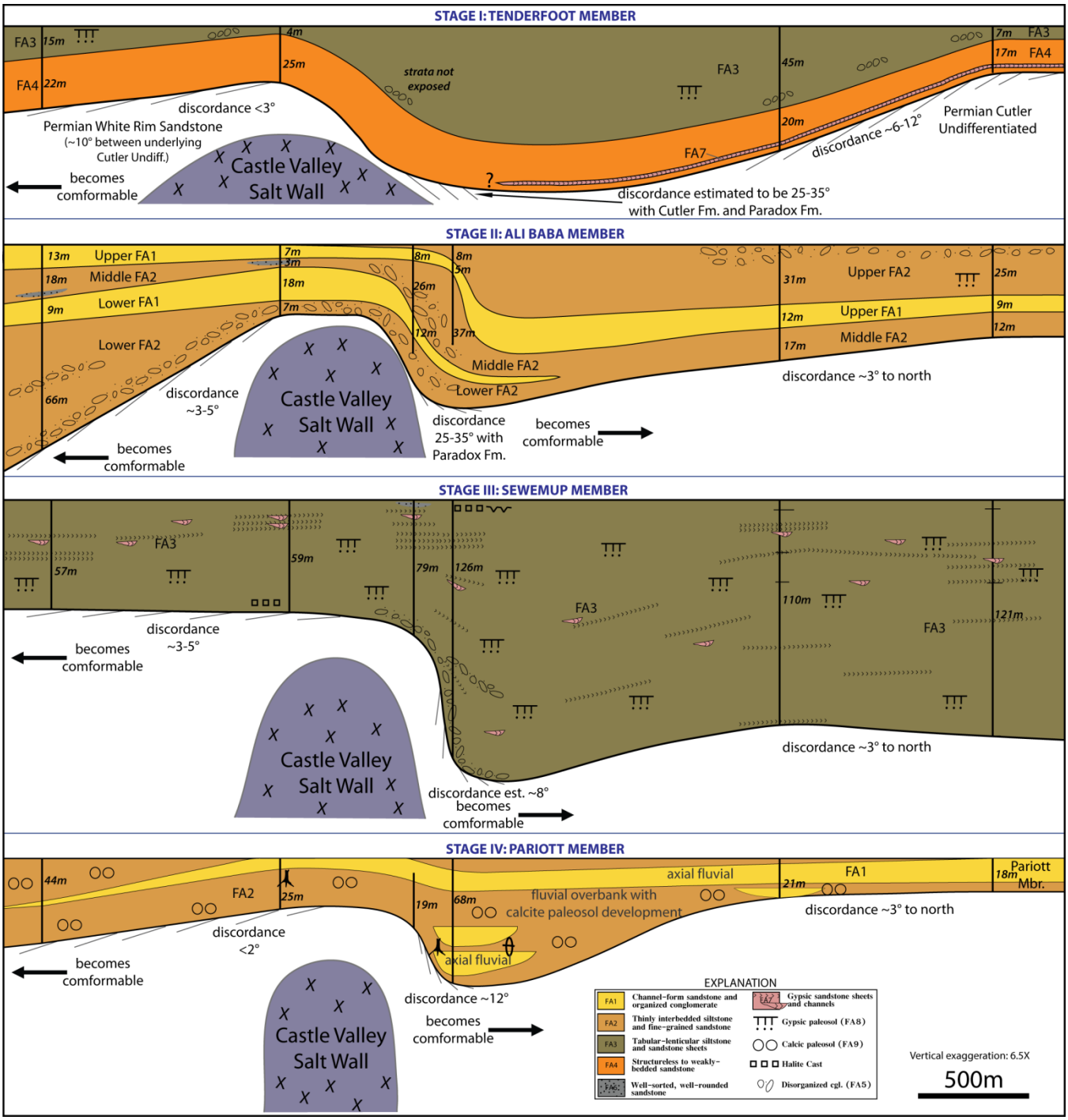

Figure 3.13: Stages of deposition of members of the Moenkopi Formation and salt-sediment interaction.

3.5.1 Stage I: Tenderfoot Member

The thickness and distribution of FA4 suggests that the lower part (FA4) of the Tenderfoot Member was deposited fairly evenly across the study area with slightly increased subsidence rate at the location of the weld relative to the salt wall to the east and west-southwest. The lower sub-unit of FA4 was not offset during deposition of Tenderfoot strata. The thickness distribution of the FA4, in combination with the lithologic homogeneity indicates the salt wall had minimal influence on deposition and distribution of facies with very slight subsidence at the location of the weld. The presence of the eolian gypsic sand sheet (FA7) on the margins of the salt wall, in combination with a lack of salt wall-derived debris flow material in the FA4 also indicate relatively low topographic relief over salt wall and stable tectonics along the flanks of the salt wall. The absence of FA7 on the west-southwest side of the weld may suggest control by prevailing wind direction.

The thicker upper part (FA3) of the member at measured section 2, as well as inferred thicker strata at sections 3 and 4 (>45m), with relation to section 1 (7m) and to section 5 (4m) adjacent to the weld records salt withdrawal to the east of the weld from the Red Hills area to Pariott Mesa (Fig. 3.13). The thicker upper part of FA3 at section 6 (16m), with relation to section 5, records subsidence away from the weld to the west. The withdrawal to the east and west of the welded area indicates a relatively subtle rise rate of the wall at the present location of the weld.

The appearance of infrequent thin (<20cm) debris-flow deposits in the upper part of the Tenderfoot Member indicate rise in topographic relief of the salt wall with influence on deposition and distribution. The lack of diapir-derived material, which would have been preserved during the prevailing arid climate, suggests that, despite the rise in topographic relief, the salt wall was not exposed during deposition of the upper Tenderfoot Member.

The thickness and distribution of FA3 suggests that the upper part of the member was not offset during deposition but growth strata developed west and east of the weld area during deposition. It is

during the deposition of the upper part of the Tenderfoot that the welding of the salt wall began with the east side subsiding more rapidly than the west, creating slightly higher angular discordance between beds of the lower part (FA4) and upper part (FA3) on the east side (<5°) than the west side (2°). Halokinetic drape folding extends to ~1000m to the west of the weld and is within ~200m to the east of the weld (Fig 3.1).

3.5.2 Stage II: Ali Baba Member

The thickness changes of the Ali Baba Member constitute growth strata, which lapped onto paleotopography at the weld area and documents diapiric rise. Thickening of 96m west-southwest away from the weld at section 6 indicates significant subsidence within ~1000m while similar estimated thickening to the east of section 5 at sections 3, 4 and 2 indicate significant subsidence during the same interval (Fig. 3.13).

The Ali Baba Member represents a shift from distal wadi fan deposition (FA4) containing a prominent eolian gypsic sand (FA7) and unconfined channels and sheet flood (FA3) deposits in the underlying Tenderfoot Member to a package of alternating fluvial overbank (FA2) and single- and multi-storied axial fluvial channels (FA1) (Fig. 3.1). This shift indicates increased sediment influx, possibly due to slight climate change with increase in precipitation locally in source catchments (Banham and Mountney, 2013, i.e., Foster 2009). Channel migration was controlled by the salt wall, whereby channels (FA1) were directed to areas of subsidence and overbank (FA2) flood material lapped onto the flanks of salt wall topographic highs. Abundant debris-flow deposits (FA5) containing diapir-derived clasts that are interbedded with overbank (FA2) deposits (Fig. 3.1) represent times of diapiric rise and exposure of the salt wall where debris flows shed material from the topographic high. The presence of the lower fluvial overbank (FA2) and lower axial channel (FA1) sub-units west of the weld at measured sections 6 and 5 and north of the weld near the Grand River 1-State, and their absence to the east of the weld at Castleton Tower and Pariott Mesa, characterize stage II.

Depositional thickening of lower FA2 strata from measured section 5 (7m) to measured section 6 (66m), in combination with increase in angularity (from ~1° to ~3°) of intraformational unconformable surfaces within the lower FA2 and with the underlying Tenderfoot FA3 (Fig. 3.4) indicates significant increased subsidence to the west-southwest of the weld. During the same interval, on the east side of the weld, strata thicken to greater than 65m (base not exposed) within ~ 700m east of the weld. Deposition of lower FA2 against the Paradox Formation on the east side of the weld, where FA2 drapes and thins over the weld, records exposure of the salt wall post-Tenderfoot deposition, indicating the Tenderfoot strata was offset either prior to Ali Baba deposition or early during deposition of the lower FA2 of Ali Baba. Exposure of the salt wall is also recorded by the presence of FA5 deposits in the lower FA2, only on the flanks of the weld, at least ~1000m to the west-southwest and likely ~150-200m to the east of the weld where the lower FA2 is not exposed.

FA2 material was the result of flood events related to axial channels (FA1) associated with the Ali Baba. The presence of the lower FA2 where exposed in the study area indicates subsidence in the adjacent Pariott minibasin was greater than subsidence flanking the salt wall, directing channels away from the salt wall and allowing for only deposition of overbank material from episodic flood events to lap onto the flanks of the salt wall. The lack of lower FA2 at Castleton tower suggests that this area had higher topographic relief than at measured sections to the west during this stage, shifting both axial channel and overbank environments toward Pariott minibasin. This also indicates depositional rate was less than subsidence rate.

The appearance of the lower axial fluvial (FA1) sub-unit records a shift to greater subsidence adjacent to the salt wall, driving axial channels toward the northeastern flank of the salt wall. The presence of multi-storied channel bodies at measured section 5 and thinning of the lower FA1 away from the weld, ~100m to the east (0m pinchout) and ~1000m to the west (9m) indicate the area over and immediately adjacent to the weld was subsiding during lower FA1 deposition. Absence of FA1 on the

northeast flank of the salt wall at measured sections 1 and 2 indicate axial channels shifted away from that part of the salt wall. Absence of the lower FA1 here also indicates depositional rate was less than subsidence rate. Northerly paleoflow on the east side of the weld was parallel to the weld, indicating that despite the area around the weld being a topographic low during lower FA1 deposition, salt wall topography was significant enough to control channel-flow direction. North of the weld, flow was to the northwest (Fig. 1.6), indicating channel flow at that location was outboard of the plunging Castle Valley salt wall and was no longer controlled by it.

The middle FA2 records a return to greater subsidence in the Pariott minibasin than on the flanks of the salt wall. Axial channels (FA1) migrated away from the salt wall and only allowing episodic floods to deposit overbank (FA2) material on the flanks of the topographic high. The presence of the middle FA2 on the northeast flank of the salt wall at measured sections 1 and 2 indicates that depositional rate outpaced subsidence in the minibasin. Debris-flows (FA5), containing larger clasts up to 12cm of diapir-derived material in the middle FA2 than other debris-flow deposits, were restricted to the eastern flank of the weld and extended east between approximately ~150m-700m (Fig. 3.1). The debris-flows record continued salt wall exposure and erosional stripping over the diapir. Thickening ~675km to the east of the weld to measured section 3, where it is likely as much as 60m thick or greater (52m measured, lower part not exposed), followed by thinning to the east, ~1km away, to 16m thick indicates greater subsidence in the Red Hills area between the weld and measured section 2 with most of the subsidence occurring within ~700m east of the weld.

Westward thickening of middle FA2 from measured section 5 (3m) to measured section 6 (18m) ~1km away records subsidence west-southwest of the weld. Relatively thinner middle FA2 in combination with the lack of debris flow material west of the weld toward the Porcupine Rim at measured section 6, and along the northeast flank of the salt wall at measured sections 1 and 2, suggest minimal to no exposure of the salt wall and associated lower rates of salt diapiric rise in those areas.

The upper FA1 unit is present throughout the study area and records a return to greater subsidence rate on the margins of the salt wall than in the Pariott minibasin, when rivers shifted toward the salt wall. The distribution of facies and the relatively consistent thickness indicates that accommodation space was similar across the area. In combination with no overlying upper FA2, it also suggests that the subsidence rate west of the weld began to wane. Paleocurrent data on the northeast flank of the salt wall indicate a westerly flow (Fig. 1.6), parallel to sub-parallel to the axis of the salt wall and indicate flow was controlled by salt wall topography. The relatively consistent thickness across the study area, over the weld and east and west of the weld, in combination with paleocurrent flow data, suggest that the salt withdrawal in the Red Hills area was waning significantly during upper FA1 deposition.

The uppermost sub-unit of the Ali Baba Member, the upper FA2 is not present west of the weld or over the weld at measured sections 5 and 6. The upper FA2 thins to 0m onto the east flank of the weld within growth strata. To the east it thickens to 31m at measured section 2, ~1.5km away, where it contains abundant debris-flow (FA5) deposits containing diapir-derived clasts that shed from ~600m southwest from an exposed salt wall. The distribution of this sub-unit indicates the area over the salt weld was a topographic high, where fluvial deposition either did not outpace diapiric rise or deposits were subsequently eroded. A few debris-flow deposits in the overlying Sewemup, that are only in the lower 15m and extend to the east of the weld ~700m, may indicate that upper FA2 was thinly deposited over the weld and was subsequently eroded with some clasts preserved in overlying unconfined channels and sheet floods

3.5.3 Stage III: Sewemup Member

The thickness changes of the Sewemup Member constitutes growth strata, which lapped onto paleotopography at the weld area and documents the final stages of diapiric salt rise (Fig. 3.13). This in turn indicates that the local supply of salt to the diapir was greatly reduced. In the Red Hills area around

measured section 3, the Sewemup strata are 126m thick. It thins to 59m over the weld, ~675m away, and maintains thickness to measured section 6 at 57m, indicating no subsidence within ~1000m west-southwest of the weld. To the east of section 3, the strata thins to 110m, showing that the area around section 3 in the Red Hills experienced the most subsidence in the study area. The strata slightly thickens to 121m approximately 800m further east of section 2, indicating slightly more subsidence east of section 2.

The Sewemup Member facies associations record a second interval composed predominantly of unconfined channels and sheet floods (FA3) in the study area as well as a shift from channelized and overbank fluvial (FA1 and FA2) transport to a thick package of unconfined channel and sheet flood (FA3) deposits with a strong gypsic paleosol (FA8) overprint and abundant gypsic sand sheets and channel-filled gypsic sandstone (FA7). These facies assemblages, in combination with halite casts and desiccation cracks indicate repetition of flooding cycles followed by drying periods and eolian deposition of gypsic sand, in channels and sheets, during a hyper-arid environment.

The minor occurrence of debris-flow material, high gypsum content in the form of gypsic paleosols, gypsic sand sheets and channel filled lenses indicate exposure of the salt wall during this time. The lack of debris-flow deposits and abundance of gypsic soil development throughout the strata suggests that the topographic relief and diapiric rise was low due to lack of local salt supply to the diapir. Subsidence rates were correspondingly very low, allowing episodic sheet floods and unconfined channel material to lap onto the salt wall. The topographic relief was significant enough to control depositional current, evidenced by northwest paleocurrent data (Fig. 1.6).

3.5.4 Stage IV: Pariott Member

Thickness changes and distribution of axial fluvial (FA1) sediments indicate that axial channels were shifted toward the salt wall during times of greater subsidence adjacent to the salt wall and axial flow was concentrated away from the salt wall when subsidence was greater in the minibasin. Subtle

subsidence to the west of the weld is indicated by slight thickening (19m) from measured sections 5 to 6 (Fig. 3.13). Significant subsidence ~600m east of the weld around measured section 3 is indicated by thickened (43m) strata and concentration of multi-storey channels of FA1 in the lower part of the member.

Pariott strata records the second stage composed predominantly of axial channel (FA1) and fluvial overbank (FA2) deposits in the study area and marks a change to axial fluvial (FA1) and overbank (FA2) deposits characterized by calcic paleosol development (FA9). The facies change, in addition to depositional and post-depositional features that differ from each of the underlying members- i.e., higher quartz clast content, lack of detrital gypsum and debris-flow deposits, lower mica content and presence of calcic paleosols and mm-scale root traces and burrows- indicate deposition during a much wetter, semi-arid climate and a new source rock type.

The location of a multi-storied upper FA1 along the northeast margin of the salt wall that extends from measured section 1 across the weld and to measured section 6 under the Porcupine Rim indicates greater subsidence rates along the flanks of the salt wall than in the minibasin late in Pariott time. Paleocurrent data show that the salt wall maintained control on channel flow with westerly flow on the northeast flank and northwesterly flow on the east flank of the weld, both roughly parallel to the axis of the salt wall.

Chapter 4

HALOKINETIC SEQUENCES

4.1 Halokinetic Sequences

Halokinetic sequences (HS) are packages of thinned and drape-folded growth strata, locally bound at tops and bases by angular unconformities, that occur exclusively adjacent to passively rising salt bodies (Giles and Lawton, 2002; Giles and Rowan, 2012). Halokinetic sequences are discordant only within a few kilometers of a diapir and form as a response to temporal variations in topographic relief over a diapir (Giles and Lawton, 2002). In contrast, traditional depositional sequences extend regionally across sedimentary basins and form in response to regional changes in accommodation and sediment accumulation rates. Halokinetic sequences can be geometrically organized into two end-member types; hook and wedge halokinetic sequences (Fig. 4.1, Giles and Rowan, 2012). Hook halokinetic sequences (hook HS) contain narrow (50-200m) zones of deformation with >70° of angular discordance and are typically associated with mass-wasting deposits and abrupt facies changes (Giles and Rowan, 2012). Minor cusps at the intersection of unconformities and the diapir are characteristic of hook HS. Wedge halokinetic sequences (wedge HS) tend to occur as broad (300-1000m) zones of deformation with low-angle (typically 5-10°) truncation and broader, gradual facies changes (Giles and Rowan, 2012).

4.2 Composite Halokinetic Sequences

Stratigraphically stacked halokinetic sequences bounded by angular unconformities of greater extent than individual HS are referred to as composite halokinetic sequences (CHS). CHS have been recognized in field exposures and subsurface seismic data sets as having two end-member stratal geometries termed tabular or tapered (Fig. 4.2, Giles and Rowan, 2012). Vertically stacked hook HS form larger-scale stratal packages with a tabular form, comprising tabular composite halokinetic sequences (tabular CHS) that exhibit parallel to sub-parallel upper and lower bounding surfaces. Stratal

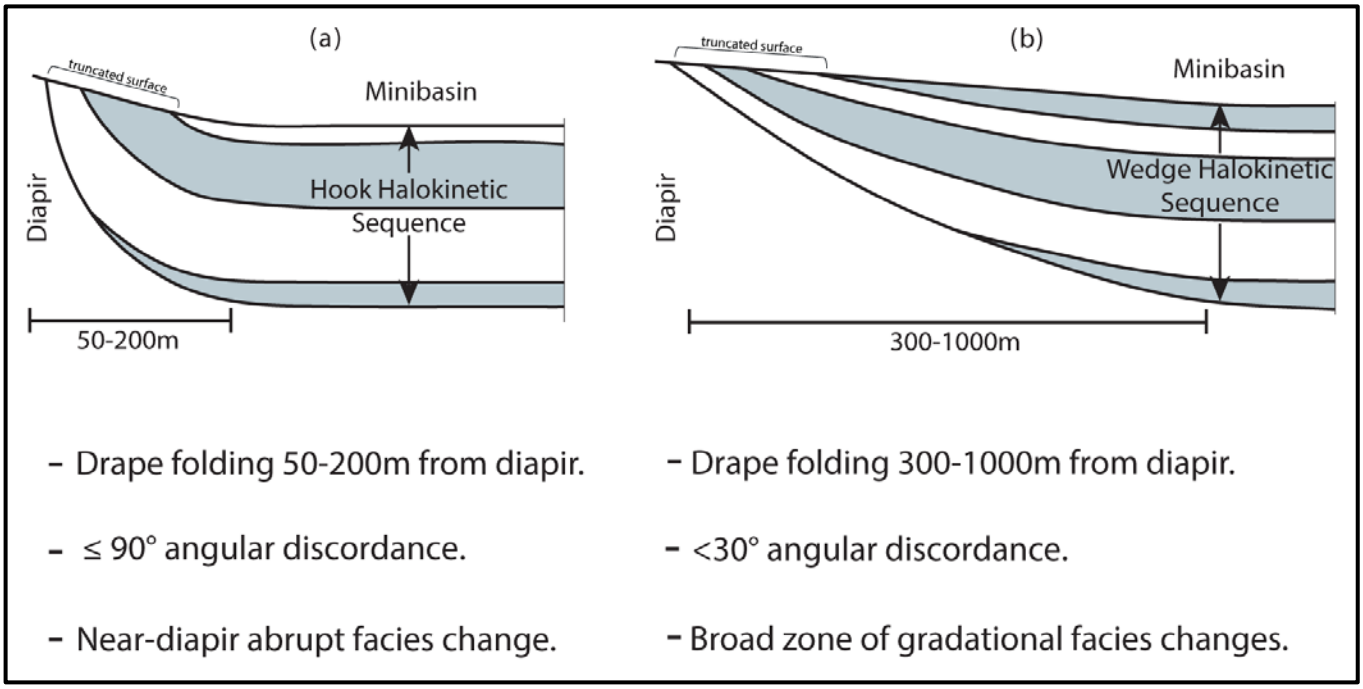

Figure 4.1: Two end-member types of halokinetic sequences: (a) hook halokinetic sequence; and (b) wedge halokinetic sequence (modified from Giles and Rowan, 2012).

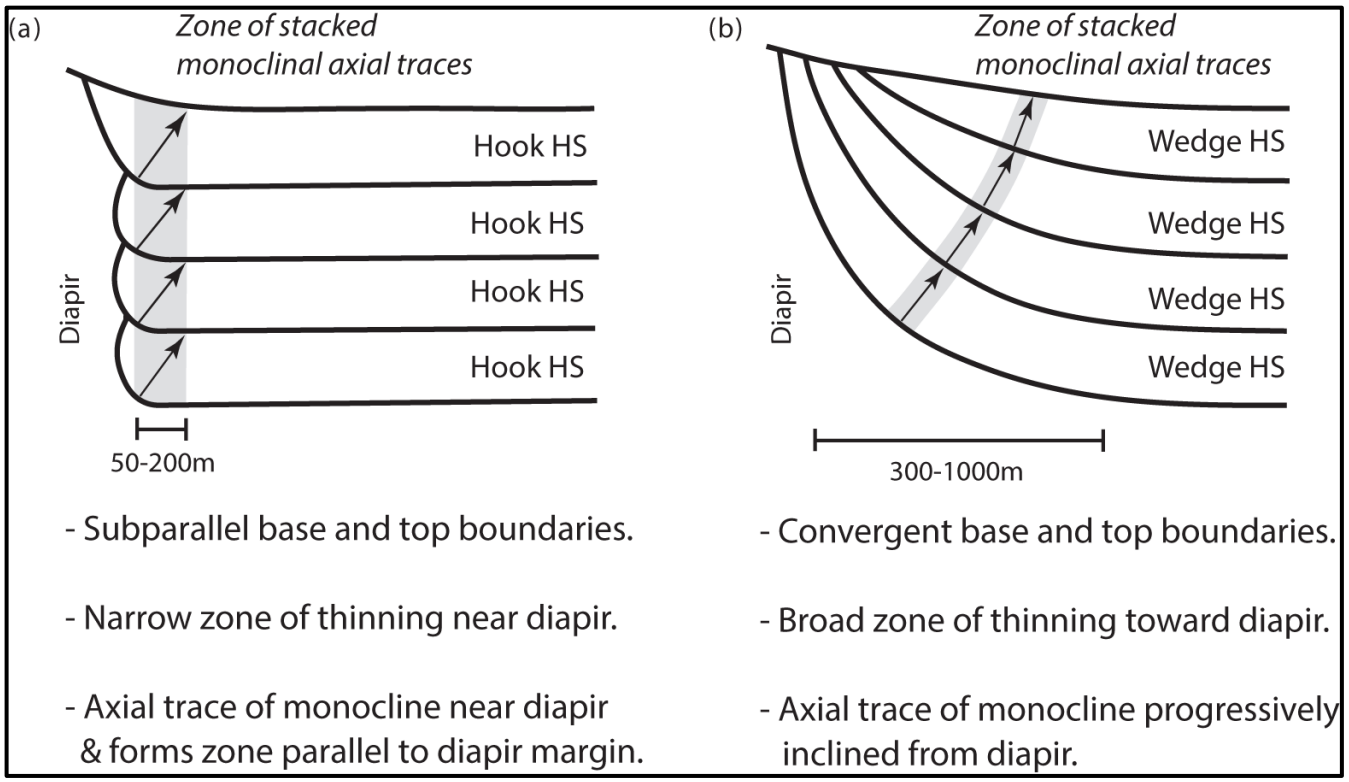

Figure 4.2: Halokinetic sequences (HS) comprising end-member types of composite halokinetic sequences (CHS): (a) tabular CHS are composed of stacked hook HS (b) and tapered CHS are composed of stacked wedge HS (from Giles and Rowan, 2012).

thinning and drape-folding of each hook HS generally extends less than 200 m from the diapir and the axial traces between each hook HS are slightly offset (Giles and Rowan, 2012). In contrast, vertically stacked wedge HS form larger-scale packages with a tapered profile referred to as tapered composite halokinetic sequences (tapered CHS) (Giles and Rowan, 2012). Similarly to individual wedge HS, tapered CHS have upper and lower bounding surfaces that gradually converge toward the diapir with the basal boundary folded between 300-1000 m from the diapir so that thinning occurs over that distance. The axial traces between each wedge HS are offset so that they trend in a curved inclined trace away from the margin of the diapir.

4.3 Halokinetic Sequences in the Study Area

Moenkopi members on the northwest end of Castle Valley are classified in this study as individual halokinetic sequences. Wedge HS are recognized on the northeast flank and in the western Red Hills and hook HS are recognized in the eastern Red Hills. The wedge HS comprise tapered CHS and the hook HS comprise a tabular CHS.

4.3.1 Northeast Flank Moenkopi Stratal Architecture

The partially exposed upper beds of the underlying Cutler Undifferentiated are the closest strata to the salt wall (Figs. 1.8 and 4.3, see Plate 1 for detailed map) and, below valley fill (Qau), are likely in contact with the Paradox Formation evaporite that comprises the salt wall. Cutler strata along cross-section B-B' (Fig. 4.3) are projected to have similar strike and dips away from the wall and presumed to have steeper dips against the wall (Fig. 4.3).

The Tenderfoot Member is eroded further back from the salt wall along the valley wall than the underlying Cutler (Fig. 1.8); ~200m at measured section 2 and ~650m at Castleton Tower. Along the northeast walls of Castle Valley near Castleton Tower, Tenderfoot strata overlie the Cutler with an angular unconformity of approximately 6°-12°, forming a CHS boundary (Fig. 4.3), and become roughly parallel to the Cutler within 1000m of the salt wall in Ida Gulch.

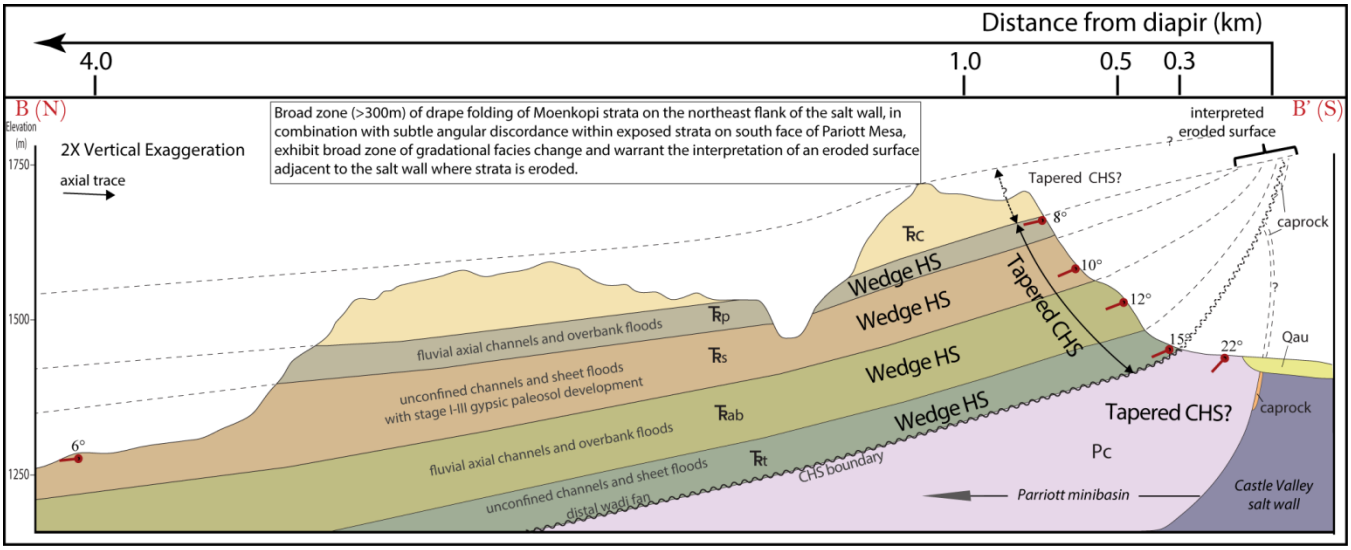

Figure 4.3: Northeast flank wedge halokinetic sequence (HS) on the northeast margin of Castle Valley. Where eroded, geometries of HS interpreted (dotted lines) as being truncated by Chinle Formation. Tadpoles indicate dip-direction of beds with dip angle.

Discordance between the Ali Baba Member beds and underlying Tenderfoot appear to be in the few degrees (3° at measured section 2) within 300m of salt wall at measured section 2, while discordance at measured section 1 under Castleton Tower, ~700m from the salt wall, is <2°. The contact between the Ali Baba Member and Tenderfoot become conformable ~2.5km away from the salt wall in exposures along the walls of Ida Gulch, where discordance is not discernable.

The Sewemup Member is unconformably overlies the Ali Baba with <2° of discernable discordance at outcrops ~550m from the salt wall at measured section 2 and ~800m from the salt wall at measured section 1. The contact between the members becomes conformable ~2.25km from the salt wall within exposures of Pariott Mesa and north of Castleton Tower.

The Pariott Member unconformably overlies the Sewemup with ≤2° of discernable angular discordance in outcrops on the southern face of Parriott Mesa (~550m from the salt wall) and below Castleton Tower (~950m from the salt wall). However, mapping shows that the Pariott Member beds are parallel to underlying strata, indicating shallowing of beds to ~6° within 1km from the salt wall along Pariott Mesa and ~2.5km from the salt wall north of Castleton Tower.

4.3.2 Interpreted Halokinetic Sequence on the Northeast Flank of the Castle Valley Salt Wall

Erosion of strata on the northeast margin of Castle Valley has removed direct evidence of stratal relationships between Parriott minibasin fill and the Castle Valley salt wall. Remaining strata, however, provide evidence of the stratal relationships and the four members in this study display drape folding between 300m-1000m of the salt wall boundary, <30° angular discordance and a broad zone of gradational facies changes. These characteristics define the stratal architecture of a composite tapered halokinetic sequence (CHS) on the northeast margin of the Castle Valley salt wall (Fig. 4.3). The basal boundary is with the underlying Cutler Undifferentiated, which has a much higher angular discordance than the individual wedge HS within the Moenkopi CHS. This, in combination with Hook HS within Cutler strata on the opposite, southwest side of the valley (Buller, 2009; Shock, 2012), indicate that the Cutler undifferentiated is not part of the northeast flank tapered CHS. The overlying Chinle Formation members were not measured in this study. Mapping and reconnaissance show that Chinle beds display wedge HS geometries and likely comprise a tapered CHS, separate from the Moenkopi. It is also possible that the Chinle represents a continuation of the Moenkopi CHS.

4.3.3 Halokinetic sequences at the Northwest Termination of the Castle Valley Salt Wall

The Castle Valley salt wall bends to the north and terminates at a weld in the Red Hills. The Moenkopi members in the Red Hills are deposited continuously over the Red Hills weld with thinning from the west and east. Folding of these beds along a monoclinal axis (Fig. 1.8) produced a shared drape folding hinge parallel to the weld axis, here called a halokinetic anticlinal hinge. The stratal architecture flanking the east side of the weld is more complex than the west flank of the salt wall (Fig. 4.4) as Moenkopi strata exposed on the west and east sides of the weld display different stratal architecture from one side to the other (Fig. 4.4).

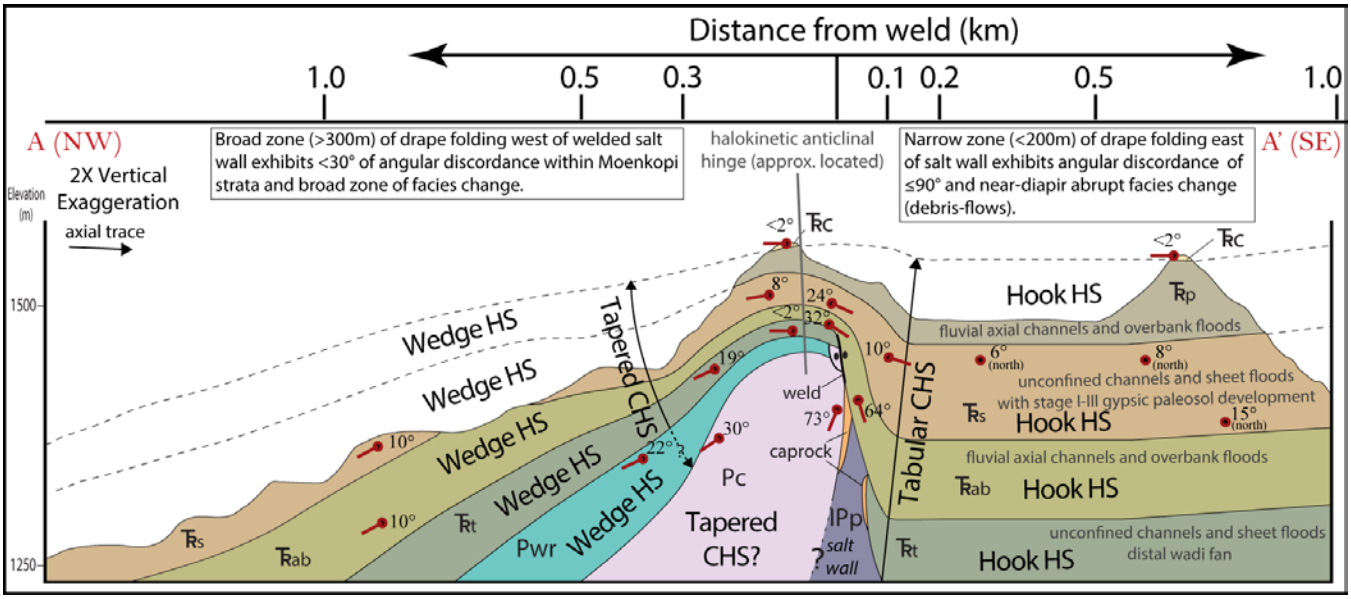

Figure 4.4: Western Red Hills wedge halokinetic sequence (HS) and eastern Red Hills hook HS at the northwest termination of the Castle Valley salt wall. Geometries of HS projected where eroded (dotted lines). Tadpoles indicate dip-direction of beds with dip angle.

4.3.4 Moenkopi Stratal Architecture on the West Side of the Red Hills Welded Salt Wall

Strata of the Permian Cutler Undifferentiated bound the west edge of the Red Hills weld and salt wall (Paradox Formation and caprock). Here, west-southwest dips >70° (348° northward strike) were measured against vertical carbonate caprock and the dip decreases to 30° west within 200m of the diapir wall (Figs. 1.8 and 4.4). Exposures do not extend further to the northwest or northeast, as these units plunge into the subsurface within 250m west of the salt wall. The Permian White Rim Sandstone (i.e. Parr, 2012) overlies the Cutler Undifferentiated with a ~10° angular discordance, forming a CHS boundary, and is also exposed adjacent to the west side of the weld and plunges northwest into the subsurface within 600m of the diapir.

The overlying Tenderfoot Member has ~700m of limited exposure on the west side of the weld (Fig. 1.8, Plate 1) and dips below the surface 1.5km to the northwest. In this area it overlies the Permian White Rim Sandstone (~700m exposure) with ≤3° angular discordance, forming a wedge HS boundary. The Tenderfoot strata also contain subtle internal stratal discordance (<1°) (Fig. 3.4).

Ali Baba Member beds 90m west of the weld, and tens of meters west of the halokinetic anticlinal hinge, exhibit a northeast strike of 27° and northwest dip ≤2°, with no discernable discordance with the underlying Tenderfoot. Approximately 300m to the west of the weld the Ali Baba strata exhibit ~3°-5° discordance with the underlying Tenderfoot, forming a wedge HS boundary. The contact becomes conformable ~1.5km further northwest of the weld, where the Tenderfoot dips into the subsurface. Strikes and dips of Ali Baba strata ~1000m to the north-northwest, near the Grand River 1-State well location, exhibits a northeast strike 65° and northwest dip of 11°. Discordance, then, likely ends between 300-1000m from the weld. The stratal architecture is also associated with thickening of strata away from the weld (Figs. 3.1 and 4.4).

Sewemup Member beds within tens of meters of the weld and halokinetic anticlinal hinge show no discernable discordance with the underlying Ali Baba. Approximately 300m to the west of the weld Sewemup strata exhibit ~3°-5° discordance with the underlying, Ali Baba forming a wedge HS boundary. ~1000m west of the weld the contact exhibits a ≤1° discordance with the underlying Ali Baba. Discordance between the Sewemup and underlying Ali Baba, then, terminates between 250m-1000m of the weld. Much of the upper Sewemup strata to the west of the weld have been erosionally removed.

The Pariott Member has been entirely erosionally removed in the Red Hills area and is limited to two peaks and a narrow ridge between them (Fig. 1.8). It is not exposed west of the Red Hills for ~1800m, until cliff exposures north of the Colorado River. To the southwest, ~1100m from the axis of the salt wall, the Pariott exposures in the walls below the Porcupine Rim are limited and structural measurements were not acquired. Mapping and reconnaissance of strata along the walls of the Porcupine Rim reveal thickening to the northwest and broad internal angular discordance (estimated ≤2°). Strata of the Pariott Member extend approximately 175m west of the weld, where it exhibits no discernable

discordance with the underlying Sewemup. Chinle stratal architecture cannot be determined in the Red Hills due to lack of exposure.

4.3.5 Interpreted Halokinetic Sequence on the West Side of the Red Hills Welded Salt Wall

Erosion of much of the strata west of the Red Hills weld limits documentation of stratal architecture, but remaining strata is adequate enough to define halokinetic sequence architecture. The unique preservation and exposure of strata adjacent to and over the welded salt wall provides an exclusive look into halokinetic stratal architecture. The Moenkopi strata on the west side of the Red Hills weld display drape folding between 300m-1000m of the weld, <30° of angular discordance and a broad zone of gradational facies changes. A monoclinal axial trace can also be identified in cross-section A-A' (Fig. 4.4). These characteristics define the Moenkopi members as individual wedge HS comprising a tapered CHS (Fig. 4.4). Additionally, the Permian White Rim Sandstone exhibits wedge HS geometries and is likely part of the tapered CHS. The basal boundary of the CHS is with the underlying Cutler Undifferentiated, which has a much higher angular discordance than the individual wedge HS within the Moenkopi CHS. This indicates that the Cutler is not part of the northeast flank tapered CHS.

4.3.6 Moenkopi Stratal Architecture on the East Side of the Red Hills Welded Salt Wall

Stratal architecture on the east side of the Red Hills weld and salt wall is more complex than on the west side. On the east side, vertical beds of Pennsylvanian Paradox Formation and carbonate caprock (remnants of the salt wall) are locally exposed on the down-thrown east side of the fault along with Permian Cutler Undifferentiated (Fig. 1.8). Permian strata are not exposed on the east side of the weld or salt wall. The Tenderfoot Member and some of the lower part of the Ali Baba Member are also not exposed within ~1000m east of the weld, as they plunge beneath the valley floor (Fig. 1.5). The majority of the upper part of the Ali Baba Member is exposed on the east side of the weld as it is in contact with the Paradox Formation and the weld.

The beds of Ali Baba 50m east of the halokinetic anticlinal hinge, and roughly over the weld, strike roughly parallel (23°) to the axis of the weld and dip steeply to the southeast 32° (Fig. 1.8). These beds lie directly over the fault and Cutler beds in a narrow zone (150m), where angular discordance is high, estimated between 50°-90°, forming a CHS boundary. Beds of the Ali Baba on the downthrown side of the fault steepen to 64° (north-northeast strike of 16°, east dip), within 50m of the Paradox Formation and exhibit internal angular discordance of several degrees (Fig. 3.8). Angular discordance to the north is estimated to be between 5°-10°, ~150m away from the salt wall boundary. Debris-flow deposits containing carbonate caprock clasts increase in abundance in this area with large (12cm) clasts. The angular discordance Between Ali Baba and the Paradox Formation, based on the vertical nature of the Cutler on the west side of the Paradox (Paradox beds were not accurately measurable), is between 36°-25°. Away from the weld, ~850m to the east, the Ali Baba thickens dramatically (Fig. 3.1) and the strike of the beds parallel the bend of the salt wall axis to a northwest strike of 291°and the bed dips shallow to ~20°-25° north-northeast. Internal angular discordance is not clearly discerned in these beds as the view in south facing exposures appear to be horizontal and parallel, as displayed in cross-section A-A' (Fig. 4.4). In this cross-sectional view, beds shallow to near 'horizontal' within 200m of the weld. Overall, the Ali Baba on the east side of the weld thins dramatically over the weld, displaying growth strata.

The Sewemup Member also thins dramatically onto the weld where it has an 8° of angular discordance with the underlying Ali Baba, forming a hook HS boundary, and exhibits the same pattern of steep dips over the weld (10° strike, 24° east dip) and shallows ~150m from the weld to 10° (11° strike) and to nearly 'horizontal' <200m from the weld, where beds appear to be parallel to the underlying Ali Baba.

The overlying Pariott Member also thins dramatically over the weld where beds east of the halokinetic anticlinal hinge strike 12° and dip east 12° and have angular discordance with the Sewemup

of 12°, forming a hook HS boundary. The contact becomes conformable 150m away from salt wall. Lack of outcrop away from the Red Hills peaks do not allow for further stratal architecture analysis.

4.3.7 Interpreted Halokinetic Sequence on the East Side of the Red Hills Welded Salt Wall

Geometries of the Cutler Undifferentiated, the Tenderfoot Member and lower part of the Ali Baba Member cannot be determined on the east-southeast side of the weld due to lack of exposure. Drape folding throughout the exposed strata on the east side of the weld occurs within 200m of the weld and exposed salt wall (Paradox Formation), strata exhibit angular discordance of ≤90° and near-diapir abrupt facies change (debris-flows containing diapir-derived clasts) are present. These characteristics define the Moenkopi strata on the east side of the weld as a series of hook HS (Fig. 4.4). These stack into a tabular CHS.

Although there is limited exposure of strata to the north of the Red Hills, it appears that strata >200m from the weld (north-northwest orientation) dip away from the salt wall that bends to a west-northwest orientation and likely have, in that orientation, stratal geometries that fit a wedge HS model. This is consistent with the wedge HS defined on the northeast flank of the salt wall as it appears to be a continuous trend. This would mean that, in the Red Hills area, there is a transition from wedge HS/tapered CHS geometries on the western side of the weld to hook HS/tabular CHS on the eastern side of the weld.

The halokinetic sequence stratigraphy indicates that the Castle Valley salt anticline was asymmetrically growing during Moenkopi time due to asymmetric salt withdrawal at the northern end of the Castle Valley salt wall, climaxing in salt weld formation.

Chapter 5

DISCUSSION

The observed strata, thickness variations, stratal geometries and orientation of the salt wall and weld at the northwest end of Castle Valley record a complex history of salt tectonics and salt-sediment interaction involving various relative rates of sediment accumulation and diapiric rise (Table. 5.1). The contemporaneous formation of a wedge HS west of the welded salt wall, a hook HS on the east side and a wedge HS on the east side along the northeast flank of the wall indicates sediment accumulation outpaced diapiric rise throughout Moenkopi time on both the west-southwest and northeast sides of the Castle Valley salt wall, except for a localized area within ~1000m east of the weld in the Red Hills where diapiric rise outpaced sediment accumulation, accelerating salt withdrawal in this area. This area, termed the Red Hills 'low', is located adjacent to a sharp bend in the wall boundary from a northwest trend to a north trend and is also characterized by abundant debris-flow deposits containing diapir-derived material, indicating diapir exposure and further supporting the interpretation that diapiric rise outpaced sediment accumulation in this area.

Table 5.1: Halokinetic sequence types documented at the northwest end of the Castle Valley salt wall, Castle Valley, Utah and interpreted rates of salt rise and sediment accumulation at three defined halokinetic sequences for Moenkopi and White Rim stratigraphic units.

Stratigraphic Unit	Sed Accumulation Rate	Climate	Relative Salt-Rise Rate			Halokinetic Sequence Type		
			West of Weld	East of Weld	Northeast Flank	West of Weld	East of Weld	Northeast Flank
Pariott Mbr	fast	semi-arid	slow	moderate	slow			
Sewemup Mbr	slow	hyperarid	slow	fast	slow			
Ali Baba Mbr	moderate	arid	slow	fast	slow	Tapered CHS	Tabular CHS	Tapered CHS
Tenderfoot Mbr	slow	arid	fast	fast	slow			
White Rim SS	slow	arid	slow	N/A	N/A			

Although there is a pronounced abrupt facies change proximal to the east side of the weld (i.e., abundant debris-flow deposits) and only subtly abrupt changes in places on the west side of the weld and on the northeast side of the salt wall, broadly distributed sediments from two intervals of axial channels and overbank floods, followed by episodic sheet floods characterized by soil generation suggest that

depositional environment type and inherent sedimentation rate associated with them (Table 5.1) did not significantly influence subsidence within the Red Hills ‘sag’. In other words, facies-type did not significantly influence salt withdrawal and resulting topographic low. Rapid deflation occurred independent of preferential sediment facies loading. Additionally, climate change from the drier, arid-hyperarid times of Tenderfoot through Sewemup deposition to the semi-arid time of Pariott deposition did not disrupt diapiric rise rate versus sediment accumulation rate in the ‘sag’ either.

Regardless of different diapiric rise versus sediment accumulation rates associated with the northwest end of the Castle Valley salt wall, the topographic high generated over the salt wall controlled the location and distribution of axial fluvial channel and overbank flood deposits. The location of axial channel deposits from the Ali Baba and Pariott members along the walls of Castle Valley represent times when channels shifted toward the salt wall and flowed parallel to it because subsidence on the flanks of the salt wall was greater than subsidence away from the wall in Parriott minibasin. Paleocurrent data in these deposits show that the channels flowed west along the flank of the wall until it reached the bend in the wall, where flow followed the bend to the north. Interbedded overbank flood deposits in the same position represent times when subsidence away from the salt wall was greater and drew channels away from the wall, allowing flood material to lap onto the topographic high.

Depositional facies, climate and sediment load do not explain the rapid deflation on the east side of the weld. Based on the position of the ‘sag’ directly adjacent to the bend along the salt wall boundary, the most reasonable supposition is that rapid deflation in the Red Hills ‘sag’ is related to the bend in the salt wall, where either dissolution, structural flex (downward) or a combination of both generated the relatively rapid increased in accommodation space with respect to the west side of the weld and northeast flank of the salt wall. It is interesting to note, also, that the Cataract Lineament, (Fig. 5.1), intersects the north bend of the welded part of the Castle Valley salt wall.

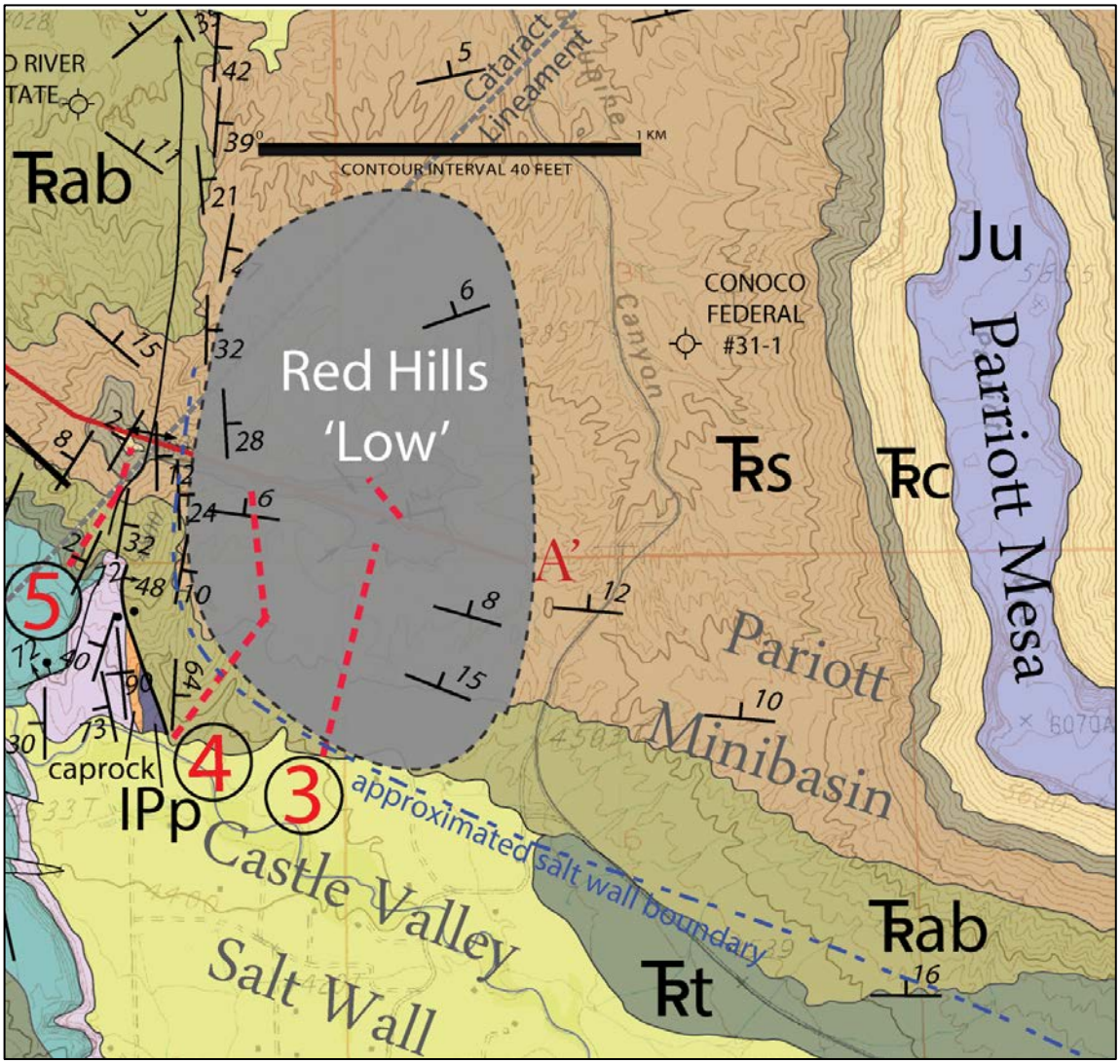

Figure 5.1: Part of the Moenkopi geologic map (see Plate 1 and Fig. 1.8 for symbol explanation) showing an approximated salt wall boundary that bends from a northeast trend to a northerly trend and an approximated extent (in gray) of thickened strata that parallels the bend in the salt wall.

Shoemaker and Newman (1959) observed that the Pariott Member resembles the overlying Chinle Formation with purple and orange sediments and arbitrarily assigned the strata to the Moenkopi Formation based on presence of mica and ripples and assigned a Middle Triassic age. The Pariott may be one of the few Middle Triassic units preserved because of preferential accommodation space created by the passive diapirism in the region. Despite detailed analysis of paleosol character in the Pariott by Prochnow and others (2006) while investigating the overlying Chinle Formation, the Pariott was not reassigned to the Chinle. However, based on the striking differences between the Pariott Member and

lower three Moenkopi members presented in this study, the Pariott is reclassified as a locally preserved formation of Early or Middle Triassic age and warrants further detailed study based on the following: (1) Contains much higher abundance of quartz-rich conglomerates than lower three Moenkopi members; (2) The Pariott Member has evidence of plant life (root traces) and animal life (burrows) while the lower three Moenkopi members do not; (3) the Pariott Member contains calcic paleosols indicating semi-arid climate while the lower three Moenkopi members contain gypsic paleosols, indicating arid to hyper-arid conditions; (4) detrital gypsum is absent or replaced by calcite in the Pariott and is present throughout lower three Moenkopi members; (5) Debris-flow deposits are not present in the Pariott Member while they are present throughout the lower three members of the Moenkopi Formation; (6) The mica content is less in the Pariott Member sandstones and fine-grained overbank deposits than the lower three members of the Moenkopi Formation;

Chapter 6

CONCLUSIONS

This study provides the first detailed map of the Moenkopi members in the Castle Valley area and possibly in the salt anticline region. This map aided in identifying the distribution of facies associations and better understanding stratal geometries.

1. Nine facies associations were recognized in the Moenkopi Formation in the Castle Valley region and seven corresponding depositional sub-environments were interpreted. These include (1) a channel-form sandstone and organized conglomerate association (FA1) in the Ali Baba and Pariott members, interpreted as fluvial channel-fill deposits in braided, ephemeral wadi streams; (2) a thinly interbedded siltstone and fine sandstone association (FA2) in the Ali Baba and Pariott members was defined and interpreted as suspension deposits from flooding related to FA1; (3) a tabular-to-lenticular siltstone and sandstone sheets association (FA3) was defined in the upper Tenderfoot and entire Sewemup. These are interpreted as deposits from ephemeral deposition in poorly confined channels by flash and sheet floods into an inland sabkha; (4) an indistinctly-bedded sandstone association (FA4) was defined in the lower portion of the Tenderfoot Member. These sediments are interpreted as being deposited in a distal wadi-fan system; (5) a disorganized conglomerate association (FA5) containing abundant clasts of gypsum and dolostone was defined and interpreted as debris-flows derived from the Castle Valley salt wall throughout Tenderfoot, Ali Baba and Sewemup deposition; (6) a well-sorted, well-rounded siliciclastic sandstone association (FA6) found within the Tenderfoot, Ali Baba and Sewemup members was defined and is interpreted as eolian dune and sheet deposits of reworked Moenkopi Formation siliciclastic material; (7) a gypsic sandstone association (FA7) was defined from deposits in the lower portion of the Tenderfoot Member and throughout the Sewemup Member. These are interpreted as reworked gypsum from the exposed salt wall and nearby playas that was deposited by wind in sand sheets and filling small channels running perpendicular to the salt wall; (8) a gypsic

paleosols association (FA8) was defined based on stage 2 calcic nodules from the Tenderfoot, Ali Ababa and Sewemup members and a calcic paleosols association (FA9) was defined from the Pariott Member. Gypsic paleosols are interpreted as stage I through incipient stage III soil development in sediments following deposition from flooding events during hype-arid climate and calcic paleosols are interpreted as mature soils forming in overbank flooding material during a cooler, semi-arid climate.

2. Gypsic sandstone, gypsum and dolostone clasts within debris-flow conglomerates, in combination with paleocurrent data and location of axial channel deposits, indicate that the Castle Valley salt wall was exposed, provided a source of sediment and that the salt wall had sufficient enough relief to influence fluvial facies distribution. This also reflects the prevailing hyperarid climate during Moenkopi deposition.

3. Based on the distribution of facies associations and corresponding depositional environments, the upper ~16 m originally assigned to Tenderfoot Member by Shoemaker and Newman (1959) is reassigned in this study to the lower Ali Baba Member.

4. Four stages of salt-sediment interaction were defined, one associated for each member in the study, that are characterized by distinct facies associations and distributions as well as stratal geometries. Each member represents individual halokinetic sequences and should be grouped into composite halokinetic sequences.

5. Composite halokinetic sequences (CHS) were identified within the Moenkopi Formation, but the type differs from the western side to eastern side of the weld/diapir; 1) a northeast flank tapered CHS, 2) a western Red Hills tapered CHS and 3) an eastern Red Hills tabular CHS. These CHS indicate that sediment accumulation rates were greater than diapiric rise for most of salt wall flanks, with the exception of the hook HS on the east side of the weld where stratal geometries and abrupt facies changes indicate the area experienced higher diapiric rise rate relative to sediment accumulation rate, most likely due to deflation related to the sharp bend in the salt wall.

6. An outcome of this study is that Pariott strata is removed from Moenkopi Member status based on several striking differences between the Pariott and underlying Moenkopi Members, placement in the Moenkopi Formation is unsuitable and it evaluated for reassignment to formation status or be included with the overlying Chinle Formation. The differences include the Pariott member contains 1) a higher abundance of quartz clasts in conglomerates; 2) lacks detrital gypsum and paleosols are calcic, in contrast with the gypsic paleosols within the underlying Moenkopi members; 3) lacks gypsic beds, clasts and veins which are abundant in the lower three Moenkopi members; 4) lacks debris-flow deposits, which are present in the underlying Sewemup and Ali Baba members; 5) has lower mica content is much less in sandstone and fine-grained overbank sediments than in the lower three members 6) is also the only member of the Moenkopi Formation in the study area with root traces and burrows. The root traces and burrows are on the mm-scale.

REFERENCES

Allen, J.R.L., 1970, A quantitative model of climbing ripples and their cross-laminated deposits: Sedimentology, v. 14, p. 5-26.

Ashley G.M., Southard, J.B. and Boothroyd, J.C., 1982, deposition of climbing-ripple beds: A flume simulation: Sedimentology, v. 29, p. 67-79.

Baars, D. L., 2000, Geology of Canyonlands National Park: In Geology of Utah's Parks and Monuments, Sprinkel, D.A., Chidsey, T. C., and Anderson, P. B., eds., Utah Geological Association Publication 28, p. 61-83.

Baars, D.L., and Stevenson, G.M., 1981, Tectonic evolution of the Paradox basin, Utah and Colorado, *in* Weigand, D.L., ed., Geology of the Paradox basin: Rocky Mountain Association of Geologists Guidebook, p. 23-31.

Baker, A.A., Dobbin, C.E., McKnight, E.T. and Reeside, J.B., 1927, Notes on the stratigraphy of the Moab region, Utah: American Association of Petroleum Geologists Bulletin, v. 11, no. 8, p. 785-808.

Baker, A.A. and Reeside, J.B., Jr., 1929, Correlation of the Permian of southern Utah, northern Arizona, northwestern New Mexico, and southwestern Colorado: American Association of Petroleum Geologists Bulletin, v. 13, no. 11, p. 1413-1448.

Banbury, N. J., 2005, The role of salt mobility in the development of supra-salt sedimentary depocentres and structural styles: Ph.D. thesis, University of Edinburgh, Edinburgh, United Kingdom, 298 p.

Banham, S.G. and Mountney, N.P., 2013, Controls on fluvial sedimentary architecture and sediment-fill state in salt-walled mini-basins: Triassic Moenkopi Formation, Salt Anticline Region, SE Utah, USA, Basin Research, v. 25, p. 1-29.

Barbeau, D.L., 2003, A flexural model for the Paradox basin: Implications for the tectonics of the Ancestral Rocky Mountains: Basin Research, v. 15, p. 97–115.

Blakey, R.C., 1973, Stratigraphy and origin of the Moenkopi Formation (Triassic) of southeastern Utah: Mountain Geologist, v. 10, p. 1–17.

Blakey, R.C., 1974, Stratigraphic and depositional analysis of the Moenkopi Formation, southeastern Utah: Utah Geological and Mineral Survey Bulletin 194, p. 1–85.

Blakey, R. C. and Gubitosa, R., 1984, Controls of sandstone body geometry and architecture in the Chinle Formation (Upper Triassic), Colorado Plateau: Sedimentary Geology, v. 38, p. 51–86.

Blakey, R.C. and Ranney, W., 2008, Ancient Landscapes of the Colorado Plateau. Grand Canyon Association, Grand Canyon, Arizona.

Bowen, B.B., Benison, K.C., Oboh-Ikuenobe, F.E., Story, S. and Mormile, M.R., 2008, Active hematite concretion formation in modern acid saline lake sediments, Lake Brown, Western Australia: Earth and Planetary Science Letters, v. 268, p. 52-63.

Bromley, M.H., 1991, Architectural features of the Kayenta Formation (Lower Jurassic), Colorado Plateau, USA: relationship to salt tectonics in the Paradox Basin: Sedimentary Geology, v. 73, p. 77-84.

Buck, B.J., and Van Hoesen, J., 2002, Snowball morphology and SEM analysis of pedogenic gypsum, southern New Mexico, USA: Journal of Arid Environments, v. 51, p. 469–487.

Buller, C.D., 2009, The influence of salt on stratigraphy and depositional environments in the Pennsylvanian-Permian Honaker Trail and Cutler formations, Paradox Basin, Utah [M.S. thesis]: Las Cruces, New Mexico State University, 91.p.

Cadigan, R.A., 197, Petrology of the Triassic Moenkopi Formation and related strata, *in* the Colorado Plateau region, with a section on stratigraphy, by J.H. Stewart: USGS Professional Paper 692, 70 p.

Case, J.E., and Joesting, H.R., 1972, Regional geophysical investigations in the central Colorado Plateau: U.S. Geological Survey Professional Paper 736, 31 p.

Case, J.E., Joesting, H.R., and Byerly, P.E., 1963, Regional geophysical investigations in the La Sal Mountain area, Utah and Colorado: USGS Professional Paper 316-F, 25 p.

Cater, F.W., 1970, Geology of the Salt Anticline region in southwest Colorado: United States Geological Survey Professional Paper 637, 80 p.

Cater, F.W. and Elston, D.P., 1963, Structural development of salt anticlines of Colorado and Utah: American Association of Petroleum Geologists Memoir 2, Backbone of the Americas, p. 152-159.

Carter, W. D. and Gualtieri, J. L., 1969, Geology of the Uravan vanadium deposits of the La Sal quadrangle, San Juan County, Utah, and Montrose County, Colorado: U.S. Geological Survey Professional Paper 508, 82 p.

Condon, S.M., 1997, Geology of the Pennsylvanian and Permian Cutler Group and Permian Kaibab Limestone in the Paradox basin, southeastern Utah and southwestern Colorado: U.S. Geological Survey Bulletin 2000-P, 55 p.

Dane, C.H., 1935, Geology of the Salt Valley anticline and adjacent areas, Grand County, Utah, US Department of the Interior, US Geological Survey Bulletin, 863, 184pp.

Doelling, H. H., 1988, Geology of Salt Valley anticline and Arches National Park, Grand County, Utah, in H. H. Doelling, C. G. Oviatt, and P. W. Huntoon, eds., Salt deformation in the Paradox region: Utah Geological and Mineral Survey Bulletin, v. 122, p. 1– 58

Doelling, H. H., 2001, Geologic map of the Moab and eastern part of the San Rafael Desert 300 x 600 quadrangles, Grand and Emery counties, Utah and Mesa County, Colorado: Utah Geological Survey Map 180, scale 1:100,000, 3 sheets.

Doelling, H. H., 2002, Geologic map of the Fisher Towers quadrangle, Grand County, Utah: Utah Geological Survey Map 183, scale 1:24,000, 22 sheets.

Doelling, H. H., and Ross, M. L., 1998, Geologic map of the Big Bend quadrangle, Grand County, Utah: Utah Geological Survey Map 171, scale 1:24,000, 29 sheets.

Doelling, H. H., Ross, M. L., and Mulvey, W. L., 2002, Geologic map of the Moab quadrangle, Grand County, Utah: Utah Geological Survey Map 181, scale 1:24,000, 34 sheets.

Fielding, C.R., 2006, Upper flow regime sheets, lenses and scour fills: Extending the range of architectural elements for fluvial sediment bodies: Sedimentary Geology, v. 90, p. 227-240.

Fillmore, R.P., 2006, A salt anticline-controlled fluvial system: A preliminary study of the Ali Baba Member of the Triassic Moenkopi Formation, eastern Utah and western Colorado (abs.): Geological Society of America Abstracts with Programs, v. 38, no. 6, p. 7.

Friedman, J.D., Case, J.E. & Simpson, S.L., 1994, Tectonic trends of the northern part of the Paradox Basin, southeastern Utah and southwestern Colorado, as derived from landsat multispectral scanner imaging and geophysical and geologic mapping. US Department of the Interior, US Geological Survey Bulletin, 2000-C, p. 34.

Fryberger, S.G., Ahlbrandt, T.S., and Andrews, S., 1979, Origin, sedimentary features, and significance of low-angle eolian 'sand sheet' deposits, Great Sand Dunes National Monument and vicinity, Colorado: Journal of Sedimentary Petrology, v. 49, p. 733-746. Fryberger, S.G., Al-Sari, A.M. and Clisham, T.J., 1983, Eolian dune, interdune, sand sheet, and siliciclastic sabkha sediments of an offshore prograding sand sea, Dhahran Area, Saudi Arabia: American Association of Petrology Bulletin, v. 67, p. 280-312.

Giles, K.A. and T.F. Lawton, 2007, Halokinetic sequence stratigraphy adjacent to the El Papalote diapir, northeastern Mexico: AAPG Bulletin, v. 86, p. 823-840.

Giles, K.A. & Rowan, M.G., 2012, Concepts in halokinetic-sequence deformation and stratigraphy, *In.* Alsop, G.I. et al. (eds), Salt Tectonics, Sedimentation and Prospectivity, Geological Society, London, Special Publication.

Gilluly, J. and Reeside, J. B., 1928, Sedimentary rocks of the San Rafael swell and some adjacent areas in eastern Utah: U. S. Geol. Survey Prof. Paper 150-D, p. 61-110.

Glennie, K.W., 1970, Desert sedimentary environments: New York, Elsevier Publishing Co.

Glennie, K.W., 1972, Permian Rotliegendes of north-west Europe interpreted in light of modern desert sedimentation: AAPG Bulletin, v. 56, p. 1048-1071.

Glennie, K. W., 1987, Desert sedimentary environments, present and past— A summary: Sedimentary Geology, v. 50, p. 135– 166.

Gregory, H.E., 1917, Geology of the Navajo country: USGS Professional Paper 93, 161 p.

Grout, M.A. and Verbeek, E.R., 1997, Tectonic and paleostress significance of the regional joint network of the Central Paradox Basin, Utah and Colorado, In: Friedman, J.D. and Huffman, A.C. (eds.), Laccolith complexes of southeastern Utah: tectonic control and time of emplacement-workshop proceedings: USGS Bulletin 2158, p. 151-166.

Hazel, J.E, Jr., 1994, Sedimentary response to intrabasinal salt tectonism in the Upper Triassic Chinle Formation, Paradox Basin, Utah: USGS Bull., 2000-F, 34 p.

Hite, R.J., 1968, Salt deposits of the Paradox Basin, southeast Utah and southwest Colorado, *in* R. B. Mattox, ed., Saline deposits: A symposium based on papers from the international conference on saline deposits, Houston, Texas, 1962, Geological Society of America Special Papers 88, pages 319-330.

Hogg, S.E., 1982, Sheetfloods, sheetwash, sheetflow, or …?: Earth Science Review, v. 18, p. 59-76.

Horne, R.R., 1975, The association of alluvial fan, aeolian and fluviatile facies in the Caherbla Group (Devonian), Dingle Peninsula, Ireland: Journal of sedimentary Petrology, v. 45, p. 535-540.

Huntoon, J.E., Dubiel, R.F., Stanesco, J.D., Mickelson, D.L., and Condon, S.M., 2002, Permian-Triassic depositional systems, paleogeography, paleoclimate, and hydorcarbon resources in Canyonlands and Monument Valley, Utah: Geological Society of America Field Guide 3, 26 p.

Jones, R.W., 1959, Origin of salt anticlines of Paradox Basin: American Association of Petroleum Geologists Bulletin, v. 43, no. 8, p. 1869-1885.

Jutson, J.T., 1919, Sheet flows, or sheet floods, and their associated phenomena in the Niagara district of sub-arid south-central Western Australia: American Journal of science, Series 4, v. 48, p. 435-439.

Karcz, I., 1970, Possible significance of transition flow patterns in interpretation of origin of some natural bedforms: Journal of Geophysical Research, v. 75, p. 2869-2873.

Kelley, V.C., 1958, Tectonics of the region of the Paradox Basin, in Sanborn, A.F., ed., Guidebook to the Geology of the Paradox Basin: Intermountain Association of Petroleum Geologists, p. 31–38.

Lawton, T.F., and Buck, B.J., 2006, Implications of diapir-derived detritus and gypsic paleosols in Lower Triassic strata near the Castle Valley salt wall, Paradox basin, Utah: Geology, v. 34, p. 885–888.

Longwell, C.R., Miser, H.D., Moore, R.C., Bryan, K. and Paige, S., 1923, Rock formations in the Colorado Plateau of southern Utah and northern Arizona: United States Geological Survey Professional Paper 132-A, p. 1-22.

Lucas, S.P., Kietzke, K.K., and Goodspeed, T.H., 1997, Paleontology of nonmarine Cretaceous-not marine Triassic-limestone in the Salt anticline, Southern Utah: New Mexico Geological Society Guidebook, 48th Field Conference, Mesozoic geology and paleontology of the Four Corners Region: p. 157-162.

Mack, G. H., and K. A. Rasmussen, 1984, Alluvial-fan sedimentation of the Cutler Formation (Permo-Pennsylvanian), near Gateway, Colorado: Geological Society of America Bulletin, v. 95, p. 109–116.

Marren, P.M., 2002, Criteria for identifying high magnitude flood events in the proglacial fluvial sedimentary record. In: Snorrason, A´., Finnsdo´ ttir, H.P., Moss, M. (Eds.), The Extremes of the Extremes: Extraordinary Floods. IAHS Publication, vol. 271, pp. 237–241.

Matthews, W.J., Hampson, G.J., Trudgill, B.D., and Underhill, J.R., 2004, Impact of salt movement on fluvio-lacustrine stratigraphy and facies architecture: late Triassic Chinle Formation, northern Paradox Basin, southeastern Utah, USA: Houston, Texas, Proceedings of the Gulf Coast Section of the Society of Economic Paleontologists and Mineralogists Foundation 24th Annual Bob F. Perkins Research Conference.

Matthews, W.J., Hampson, G.J., Trudgill, B.D., and Underhill, J.R., 2007, Controls on fluviolacustrine distribution and architecture in passive salt-diapir provinces: Insights from outcrop analogs: American Association of Petroleum Geologists Bulletin, v. 91, no. 10, p. 1367-1403.

McKee, E.D., 1954, Stratigraphy and history of the Moenkopi Formation of Triassic age: Geological Society of America Memoir 61, 133 p.

McKee, E.D., Crosby, E,J., and Berryhill Jr., H.L., 1967, Flood deposits, Bijou Creek, Colorado, 1965: Journal of Sedimentary Petrology, v. 37, p. 829-851.

Miall, A.D., 1978, Facies types and vertical profile models in braided river deposits: A summary *in* Miall, A.D., ed., Fluvial Sedimentology: Canadian Society of Petroleum Geologists Memoir, v. 5, p. 597-604.

Miall, A. D., 1996, The geology of fluvial deposits: Sedimentary facies, basin analysis, and petroleum geology: Berlin, Springer-Verlag.

Miall, A.D., and M. Arush, 2001, Cryptic sequence boundaries in braided fluvial successions: Sedimentology, v. 48, p. 971-985.

Molenaar, C. M., 1981, Mesozoic stratigraphy of the Paradox basin: An overview, *in* Wiegand, D. L., ed., Geology of the Paradox basin: Rocky Mountain Association of Geologists Field Conference, p. 119–127

Nelson, S.T., 1998, Reevaluation of the central Colorado Plateau laccoliths in the light of new age determinations: U.S. Geological Survey Bulletin, v. 2158, p. 37-39.

Newberry, J.S., 1861, Geological report, In: Report upon the Colorado River of the West: U.S. 36th Cong. 1st Sess. (Ed. By J.C Ives) Senate and House Ex. Doc., 90 (Pt. 3), 154.

North, C.P., Nanson, G.C., and Fagan, S.D., 2007, Recognition of the sedimentary architecture of dryland anabranching (anastamosing) rivers: Journal of Sedimentary Research, v. 77, p. 925–938.

Nuccio, V. F., and S. M. Condon, 1996, Burial and thermal history of the Paradox Basin, Utah and Colorado, and petroleum potential of the middle Pennsylvanian Paradox Formation: U.S. Geological Survey Bulletin, v. 2000-O, 41 p.

Parr, T., 2012, Correlation of the Castle Valley Eolianite, Castle Valley, Utah, and the influence of the Castle Valley salt diapir on depositional setting and stratigraphic geometry [M.S. thesis]: Las Cruces, New Mexico State University, 234 p.

Peterson, J.A. & Hite, R.J., 1969, Pennsylvanian evaporite-carbonate cycles and their relation to petroleum occurrence, southern Rocky Mountains. Am. Assoc. Petrol. Geol. Bull., v. 53, 884-908.

Pipiringos, G.N. and O'Sullivan, R.B., 1978, Principle unconformities in Triassic and Jurassic rocks, Western Interior United States - a preliminary survey; United States Geological Survey Professional Paper, v. 1035-A, 29 p.

Prochnow, S. J., L. C. Nordt, S. C. Atchley, M. R. Hudec, and T. E. Boucher, 2005, Triassic paleosol catenas associated with a salt-withdrawal minibasin in southeastern Utah, U.S.A.: Rocky Mountain Geology, v. 40, p. 25– 49.

Prochnow, S. J., L. C. Nordt, S. C. Atchley, and M. R. Hudec, 2006, Multi-proxy paleosol evidence for Middle and Late Triassic climate trends in eastern Utah: Palaeogeography, Palaeoclimatology, Palaeoecoloy, v. 232, p. 53– 72.

Prommel, H. W. C., 1923, Geology and structure of portions of Grand and San Juan counties, Utah: American Association of Petroleum Geologists Bulletin, v. 7, p. 384– 399.

Ross, M. L., 1998, Geology of the tertiary intrusive centers of the La Sal Mountains, Utah: influence of preexisting structural features on emplacement and morphology: Proceedings of the Workshop on Laccolith Complexes of Southeastern Utah, Utah Geological Survey, p. 61-81.

Sharp, Robert P. 1978. The Kelso dune complex, in Greely, R., Womar, M.B., Papson, R.P., and Spudis, P.D., eds., Aeolian Features of Southern California: A Comparative Planetary Geology Guidebook. Washington, D.C., NASA Office of Planetary Geology, pp. 54-63.

Shock, A.L., 2012, Origin and implications of Permian and Triassic diagenetic carbonate caprock adjacent to diapiric salt walls, Paradox Basin, Utah [M.S. thesis]: Las Cruces, New Mexico State University, 91 p.

Shoemaker, E. M., Case, J. E., and Elston, D. P., 1958, Salt anticlines of the Paradox basin, in Intermountain Assoc. Petroleum Geologists Guidebook 9th Ann. Field Conf., Geology of the Paradox basin: p. 39-59.

Shoemaker, E.M., and Newman, W.L., 1959, Moenkopi Formation (Triassic? and Triassic) in salt anticline region, Colorado and Utah: American Association of Petroleum Geologists Bulletin, v. 43, p. 1835–1851.

Stear, W.M., 1985. Comparison of the bedform distribution and dynamics of modern and ancient sandy ephemeral flood deposits in the southwestern Karoo region, South Africa: Sedimentary Geology, v. 45, p. 209–230.

Stewart, J.H., 1959, Stratigraphic relations of Hoskinnini Member (Triassic?) of Moenkopi Formation on Colorado Plateau: American Association of Petroleum Geologists Bulletin, v. 43, no. 8, p. 1852-1868.

Stewart, J. H., 1969, Major Upper Triassic lithogenetic sequences in the Colorado Plateau region: AAPG Bulletin, v. 53, p. 1866– 1879.

Stewart, J.H., Poole, F.G., and Wilson, R.F., 1972, Stratigraphy and origin of the Triassic Moenkopi Formation and related strata in the Colorado Plateau region: U.S. Geological Survey Professional Paper 691, 195 p.

Stevenson, G.M. and Baars, D.L., 1986, The Paradox: a pull-apart basin of Pennsylvanian age, in Peterson, J.A., ed., Paleotectonics and sedimentation in the Rocky Mountain region: American Association of Petroleum Geologists Memoir 41, p. 513-540.

Szabo, E. and Wengerd, S.A., 1975, Stratigraphy and tectogenesis of the Paradox Basin: Durango, Colorado, Four Corners Geological Society Guidebook 8, p. 193-210.

Talmage, S.B. and Wootton, T.P., 1937, The non-metallic mineral resources of New Mexico and their economic features (exclusive of fuels): New Mexico Geological Society Bulletin 12, 159 p.

Trudgill, B.D., 2010, Evolution of salt structures in the Paradox Basin: Controls on evaporite deposition, salt wall growth and supra-salt stratigraphic architecture: Basin Research, v. 23, p. 208-238.

Trudgill, B. D., N. Banbury, and J. R. Underhill, 2004, Salt evolution as a control on structural and stratigraphic systems: Northern Paradox foreland basin, SE Utah, U.S.A., in P. J. Post, D. L. Olson, K. T. Lyons, S. L. Palmes, P. F. Harrison, and N.C. Rosen, eds., Salt-sediment interactions and hydrocarbon prospectivity: Proceedings of 24th Annual Gulf Coast Section SEPM Foundation Bob F. Perkins Research Conference, p. 669–700.

Trudgill, B.D. and Paz, M., 2009, Restoration of mountain front and salt structures in the northern Paradox Basin, SE Utah, in W.S. Houston, L.L. Wray and P.G. Moreland, eds., The Paradox Basin Revisited-New Developments in Petroleum Systems and Basin Analysis: Rocky Mountain Association of Geologists, pp. 132-177.

Tyler, N., and F. G. Etheridge, 1993, Depositional setting of the Salt Wash Member of the Morrison Formation, southwest Colorado: Journal of Sedimentary Petrology, v. 53, p. 67– 82.

Ward, L.F., 1901, Geology of the Little Colorado River Valley: American Journal of Science, v. 12, p. 401-413.

Wengerd, S.A., 1950, Triassic rocks of northwestern New Mexico and southwestern Colorado, in New Mexico Geological Society Guidebook 1st Field Conference, San Juan Basin, New Mexico and Colorado; p. 67-75.

White, M.A., and Jacobson, M.I., 1983 Structures associated with southwest margin of the Ancestral Uncompahgre uplift, in Averett, W.R., ed., Northern Paradox basin – Uncompahgre uplift: Grand Junction Geological Society Guidebook, p. 33-39.

Wilson, R.F., and Stewart, J.H., 1967, Correlation of Upper Triassic and Triassic (?) formations between southwestern Utah and southern Nevada, In Contributions to stratigraphy, 1966: USGS Bulletin 1244-D, 20 p.

APPENDIX

Paleocurrent Data

Ali Baba Member

East of Pariott Mesa, west of "saddle trail"

Trough cross-bedded sandstone

294	283
289	290
275	296
300	

East of Pariott Mesa, west of "saddle trail"

Current ripples

275	300
284	275
292	225
310	255
273	352

Central Red Hills

Trough cross-bedded sandstone

345	2
350	337
345	330

Climbing ripples near base

298	315
345	

Western Red Hills

Trough cross-bedded conglomerate at base of measured section 5, Red Hills

330	328
325	

Trough cross-bedded fluvial sandstone

335	337
342	

Low angle cross-bedded sandstone

355	5

Northern Red Hills, just south of Red Cliffs Lodge

Trough cross-bedded sandstone

300	330
315	

Current ripples

312 310
Base of member, Castleton Tower measured section 1
Trough cross-bedded sandstone
296 305

Sewemup Member
Eastern Red Hills
Current ripples
316 305
319 295
320 302
305

Pariott Member
Castleton Tower, along measured section 1
Trough cross-bedded sandstone
282 290
286 320
282 293

Red Hills, along measured section 3
Trough cross-bedded sandstone
340 320
324

CURRICULUM VITA

Ann Marie Foster was born Ann Marie Kline in Santa Barbara, California to Thomas and Colby Kline. She graduated from Santa Barbara High School in the spring of 1997 and began attending Santa Barbara City College in the fall of 1997. It was there that she declared geology as her major and received the Karen Armstrong Summer Field Scholarship and was awarded the Coast Geological Society top student award with a Brunton compass. She transferred to Sonoma State University in Rohnert Park, California in the fall of 2001 and completed a Bachelor of Science in Geology in May of 2004. In the fall of 2004 she began taking courses toward a Master's of Science at New Mexico State University in Las Cruces, New Mexico where she was a graduate teaching assistant and was awarded the Russell Clemons Field Research Scholarship. During her studies there she presented a poster on her research at the 2006 Geological Society of America annual conference in Philadelphia, Pennsylvania. After starting a family and moving to Houston, Texas, she was a lecturer on a geologic field course of the Colorado Plateau with Santa Barbara City College during the summer of 2009. She transferred to The University of Texas at El Paso in the spring of 2013 to continue her Master's degree and completed her Master's of Science in Geological Sciences in May of 2015.

Permanent address: 2315 Oak Sand Dr.
Katy, TX 77450